

NAVAL POSTGRADUATE SCHOOL MONTEREY, CALIFORNIA



THESIS

**A METHODOLOGY FOR DESIGN OF PASSIVE
ISOLATION FOR SHIP/BARGE CONNECTION**

by

Scott R. Barry

September 1999

Thesis Advisor:

Fotis A. Papoulias

Approved for public release; distribution is unlimited.

19991126 110

REPORT DOCUMENTATION PAGE			Form Approved OMB No. 0704-0188	
Public reporting burden for this collection of information is estimated to average 1 hour per response, including the time for reviewing instruction, searching existing data sources, gathering and maintaining the data needed, and completing and reviewing the collection of information. Send comments regarding this burden estimate or any other aspect of this collection of information, including suggestions for reducing this burden, to Washington Headquarters Services, Directorate for Information Operations and Reports, 1215 Jefferson Davis Highway, Suite 1204, Arlington, VA 22202-4302, and to the Office of Management and Budget, Paperwork Reduction Project (0704-0188) Washington DC 20503.				
1. AGENCY USE ONLY (Leave blank)		2. REPORT DATE September 1999		3. REPORT TYPE AND DATES COVERED Master's Thesis
4. TITLE AND SUBTITLE: A METHODOLOGY FOR DESIGN OF PASSIVE ISOLATION FOR SHIP/BARGE CONNECTION			5. FUNDING NUMBERS	
6. AUTHOR(S) Barry, Scott R.				
7. PERFORMING ORGANIZATION NAME(S) AND ADDRESS(ES) Naval Postgraduate School Monterey, CA 93943-5000			8. PERFORMING ORGANIZATION REPORT NUMBER	
9. SPONSORING/MONITORING AGENCY NAME(S) AND ADDRESS(ES)			10. SPONSORING/MONITORING AGENCY REPORT NUMBER	
11. SUPPLEMENTARY NOTES The views expressed here are those of the authors and do not reflect the official policy or position of the Department of Defense or the U.S. Government.				
12a. DISTRIBUTION/AVAILABILITY STATEMENT Approved for public release; distribution is unlimited.			12b. DISTRIBUTION CODE	
13. ABSTRACT (maximum 200 words) Current ramp designs used in RORO operations have been determined to be structurally inadequate in Sea-State 3. The main reason for this is that when the ramp is loaded with two vehicles, the relative motions between the ship and the discharge facility induce stresses above yield. The objective of this thesis is to formulate the problem and present results that will enable the design of proper isolators. The problem is formulated in terms of the hydrodynamic interaction between adjacent bodies along with structural coupling. The applicability and limitations of strip theory approaches are established through comparisons with three dimensional hydrodynamic analysis data. An analytic model of the ship-ramp-barge system is developed and tested. The results indicate the validity of the approach and establish a procedure that may be utilized for the design of passively controlled isolators.				
14. SUBJECT TERMS Hydrodynamic Modeling, Roll-On, Roll-Off, Hydrodynamic Interactions, Strip Theory			15. NUMBER OF PAGES 122	
			16. PRICE CODE	
17. SECURITY CLASSIFICATION OF REPORT Unclassified	18. SECURITY CLASSIFICATION OF THIS PAGE Unclassified	19. SECURITY CLASSIFICATION OF ABSTRACT Unclassified	20. LIMITATION OF ABSTRACT UL	

NSN 7540-01-280-5500

Standard Form 298 (Rev. 2-89)
Prescribed by ANSI Std. Z39-18 298-102

THIS PAGE INTENTIONALLY LEFT BLANK

Approved for public release; Distribution is unlimited

**A METHODOLOGY FOR DESIGN OF PASSIVE ISOLATION FOR
SHIP/BARGE CONNECTION**

Scott R. Barry
Lieutenant, United States Navy
B.A. History, University of Washington, 1992


Submitted in partial fulfillment of the
requirements for the degree of

MASTER OF SCIENCE IN MECHANICAL ENGINEERING

from the


**NAVAL POSTGRADUATE SCHOOL
September 1999**

Author:


 **LTJUN**

Scott R. Barry

Approved by:



Fotis A. Papoulas, Thesis Advisor



Matthew Kelleher, Acting Chairman
Department of Mechanical Engineering

THIS PAGE INTENTIONALLY LEFT BLANK

ABSTRACT

Current ramp designs used in RORO operations have been determined to be structurally inadequate in Sea-State 3. The main reason for this is that when the ramp is loaded with two vehicles, the relative motions between the ship and the discharge facility induce stresses above yield. The objective of this thesis is to formulate the problem and present results that will enable the design of proper isolators. The problem is formulated in terms of the hydrodynamic interaction between adjacent bodies along with structural coupling. The applicability and limitations of strip theory approaches are established through comparisons with three dimensional hydrodynamic analysis data. An analytic model of the ship-ramp-barge system is developed and tested. The results indicate the validity of the approach and establish a procedure that may be utilized for the design of passively controlled isolators.

THIS PAGE INTENTIONALLY LEFT BLANK

TABLE OF CONTENTS

I.	INTRODUCTION	1
II.	BACKGROUND	3
	A. MOTIVATION	3
	B. OBJECTIVE	3
	C. BACKGROUND	4
	D. CONTENTS	7
III.	PROBLEM FORMULATION	9
	A. INTRODUCTION.....	9
	B. HYDRODYNAMIC EQUATIONS OF MOTION.....	9
	C. RAMP EQUATIONS OF MOTION.....	17
	1. Introduction	17
	2. Derivation of the Equation of Motion	17
IV.	RESULTS	23
	A. LARGE MEDIUM SPEED ROLL-ON ROLL-OFF VESSEL ANALYSIS	23
	1. Introduction	23
	2. Data Analysis	23
	3. Figures	26
	B. ROLL-ON, ROLL-OFF DISCHARGE FACILITY (BARGE) ANALYSIS.....	56
	1. Introduction	56
	2. Data Analysis	56
	a. Proximity Induced Exciting Force	57
	b. Sheltering/Magnification Effect	57
	3. Figures	59
	C. RAMP ANALYSIS	82
	1. Introduction	82
	2. Data Analysis	82
	3. Figures	84
V.	CONCLUSIONS	103
VI.	RECOMMENDATIONS	105
	APPENDIX A	107
	LIST OF REFERENCES	109
	INITIAL DISTRIBUTION LIST	111

THIS PAGE INTENTIONALLY LEFT BLANK

ACKNOWLEDGMENT

The author would like to thank Mr. Frank Leban and Mr. John O'Dea for all of their assistance during the writing of this thesis. The author would also like to thank Professor Fotis A. Papoulias for all of his guidance, patience, and assistance while this thesis was completed. Finally, the author would like to thank his family, Julie, Nicholas, and Danielle for all of their patience and understanding.

THIS PAGE INTENTIONALLY LEFT BLANK

I. INTRODUCTION

Over the years, there has been very little research conducted on vessels with objects in the vicinity. Of the research conducted, most of it was centered on the analysis of supply ships mooring alongside oil platforms. With the increased emphasis on littoral warfare, it is becoming more important to be able to discharge supplies from ships to shore without a readily available port facility. Therefore, it is desired to develop supply ships with the ability to offload cargo to a roll-on, roll-off discharge facility (RRDF) in the open ocean.

To accomplish this, a ramp is mounted from the ship to the RRDF. However, due to hydrodynamic forces on the ship and barges, the mounting connections are exceeding their design limitations. Therefore, it has become necessary to develop a method to minimize these forces on the pinned connections. To accomplish this, the hydrodynamic forces on the ship and barge must be accurately modeled. Then, these hydrodynamic forces must be adapted to determine the magnitude of the forces that act on the pinned connection so that a passive damping system may be produced in the future.

THIS PAGE INTENTIONALLY LEFT BLANK

II. BACKGROUND

A. MOTIVATION

In recent years, the United States military has taken an increasing interest in developing the ability to offload equipment and machinery from roll-on, roll-off (RORO) vessels in the open seas. Operational requirements for equipment transfer are set at sea state three while maintaining a total dynamic acceleration of no more than 25% of the static gravitational constant. In order to accomplish equipment transfer, a connected ramp system has been established between the RORO and a transport barge. The operational requirements stated above should hold in the case of two tanks located in the middle point of the ramp. This corresponds to an envisioned worse case scenario of one tank breaking down in the middle of the ramp and the second tank providing assistance. This coupled problem of multiple rigid bodies combines elements of hydrodynamic interactions and structural response. The philosophy of a design and analysis strategy is how to ensure proper connectivity between the different bodies such that cargo motions and ramp stress levels are minimized.

B. OBJECTIVE

The objective of this thesis is to formulate and present preliminary results for the problem of reducing ramp stress levels via reductions in ramp motion inputs. This will be done by coupling the hydrodynamic analysis of the adjacent floating bodies to a structural model of the ramp. Passive/semi-active isolator design will then be used as the basis for the synthesis of the entire model in the frequency domain.

C. BACKGROUND

A great deal of the analysis of hydrodynamic study of multiple body systems revolves around the wave effects upon vertical cylinders in waves. Most of this research surrounds the desire to accurately predict the affects of waves on different parts of a structure to ensure geometric stability. Much of this research is motivated to produce continued stability in offshore oil producing stations during drilling operations. However, there has not been significant analysis performed when two independent bodies are in close proximity to one another. [Ref. 9: p. 725]

Developing the equations of motion of a solitary vessel in various incident wave conditions is fairly routine. It simply involves defining the added mass characteristics and associated stiffness and damping matrices, which the ship will possess due to its design. However, the effects that waves will have on ships in close proximity to one another are very different. This is because the diffracted and radiated waves and their respective hydrodynamic forces will affect the adjacent vessels.

The equations of motion of vessels in close proximity to one another are derived in much the same manner as independent vessels. However, when multiple vessels are close to one another, additional terms must be incorporated into the equations of motion to ensure validity. The importance of these additional terms depends on relative size of each vessel, how each vessel is positioned with respect to the other, and overall distances between them. [Ref. 9] Taking these criteria into account, an additional added mass term

and an additional damping term must be utilized to accurately predict the hydrodynamic response of each vessel.

Research has indicated that there are multiple techniques that could, in principle, predict the numerical values of the additional terms necessary to accurately predict the hydrodynamic motion of a vessel. One of these techniques is the use of what is known as the macroelement technique. This method approximates each of the vessel's cross-sectional areas with a step curve. The flow field around each area is then subdivided into macroelements and approximated. This technique uses the method of separation of variables and Laplace's differential equations for the flow field. Once the velocity potentials for the diffraction and radiation features for each element are established, a Fourier series is developed that meets the free surface and ship body boundary conditions. To obtain the remaining coefficients, the Galerkin method is utilized. This method is effective as it does not produce many numerical irregularities and saves in computer processing time. [Ref. 1] Due to its approximations, this method may be inaccurate for certain cases and it suffers from the basic limitations of a two-dimensional analysis, most notably end effects and the existence of standing waves.

Another technique that is widely studied is that of finite element approximations. In this approach, the area around the vessel is modeled using boundary dampers/infinite elements or eigenfunction expansion/boundary integral techniques. [Ref 5: p 358] Using standard assumptions that wave and body motions are small, the complex velocity potential is obtained for the diffracted and radiated wave potentials. Using data regarding complex velocity potentials; information about linearized free surface, bottom, radiation,

and body boundary conditions; and hydrodynamic forces and coefficients, a final equation is developed. This equation integrates and sums the added mass, damping, and stiffness matrices of each vessel and its effects on the other vessel. Furthermore, it solves for the forces on each vessel due to waves and any associated hydrodynamic effects from the other vessel. This method is effective for various wave conditions as long as the problem assumptions are met. However, proper nodal placement and meshing is essential for accurate results. Due to the requirement for very fine meshing in some problems, computer resources may restrict the determination of accurate results. [Ref 5]

Techniques based on strip theory formulations are easier to solve than the previous methods while producing an accurate wave force and linked body prediction. In this approach, there are two floating vessels attached alongside one another. The equations of motion are generated using known data for each vessel and coupled together. When coupled, each equation of motion from one vessel effects that of the other. Vessel interaction is approximated by assuming that as a wave strikes a vessel, the wave is reflected an infinite number of times between vessels. This produces two additional equations for the wave interaction forces on each vessel. To determine the wave interaction forces, strip theory, which assumes that changes in the longitudinal gradients of the flow field around a vessel are much smaller than corresponding changes in the transverse direction, is utilized. The wave forces are a combination of the Froude-Krylov force and the diffraction wave force. Additional equations for added mass, damping, and stiffness for each vessel are needed to represent the interaction effects. Taking the equations generated by wave interaction between the vessels and those equations for

added mass, damping, and stiffness and placing them back into the original equation of motions for each vessel, a new equation of motion is developed which will depict the motion of the vessel to various wave loading. This technique has shown to be effective in all sea directions as long as the assumptions of linearized motions and slender bodies are accurate. [Ref 2]

Another related technique that is commonly used to solve for the additional terms is that of the boundary integral method. This method first divides the vessels into sections. The radiation velocity potential function is determined using Green's theorem and the Fredholm integral equation of the second kind, which is then applied to each of the divided sections. Once the radiation velocity potential function is developed, an interpolating shape function can be formed. Finally, a set of linear equations are developed which produce a set of algebraic equations for each of the radiation velocity potential equations throughout the vessels. This method produced accurate results in all types of wave loading directions at varying frequencies. [Ref 3]

D. CONTENTS

The boundary integral technique is the method that most researches utilize when obtaining the numerical solution to the added mass, damping, and stiffness terms in the equation of motion of a vessel. For this reason, it was adopted as the method of choice for this study. Chapter III presents the theoretical foundation for the hydrodynamic equations of motion. This is followed by the development of the algebraic constraint equations that were incorporated in the original differential equations of motion in order to model the structural coupling between the bodies. Modeling of the connecting ramp is also

included in Chapter III, followed by the results of this work in Chapter IV. Finally, the conclusions from this research and some recommendations for follow-up work are summarized in Chapters V and VI.

III. PROBLEM FORMULATION

A. INTRODUCTION

When examining the connection between the ship and the barge, the points where the ramp attached to the barge and the ship exhibit induced forces on the pinned connection. The equations to develop these forces are formulated by considering heave, pitch, and roll forces upon the ship and the barge.

B. HYDRODYNAMIC EQUATIONS OF MOTION

To obtain the force equations, it was necessary to define a standard coordinate system. The system used was the same one utilized in the reference 14, *Principles of Naval Architecture*, in which η_1 =surge; η_2 =sway; η_3 =heave; η_4 =roll; η_5 =pitch; and η_6 =yaw. The three principle motions that affect the problem were heave, roll, and pitch. Relative surge, sway, and yaw motions were considered negligible and were not analyzed further.

The other assumption that was made at this point was that the only appreciable affect upon ship movement would be in the vertical direction. Therefore, the equation for absolute vertical motion of a vessel at a given point was found to be

$$\bar{\xi}_3 = \bar{\eta}_3 + \bar{\eta}_4 \bar{y} - \bar{x} \bar{\eta}_5 \quad (1)$$

Where \bar{y} and \bar{x} is the motion at any point on the body in the x and y planes. ξ_3 is the complex local amplitude at \bar{x} , and \bar{y} in heave.

After defining the governing equation that would control the motion of each vessel, a free-body diagram was produced of the ramp. This diagram assumed that there

are three spring connections mounting the ramp to the ship and barge. Each connection produces a displacement at the pinned joint defined as ξ_1 , ξ_2 , and ξ_3 . The first ξ represents the connection for the ship and the last two ξ 's are for the barge connections. The next assumption was that each spring would exert a force at the connection as a force-couple system. This force-couple system represents a single force at each pinned location. Therefore, the equation given for the force at each location is defined as

$$F_i = G_{ij} \xi_j \quad (2)$$

where the subscripts i and j reference the particular force-couple system at a given location. G is the matrix of influence coefficients, which is a transfer function. From (2), the following matrix was obtained:

$$\begin{bmatrix} F_1 \\ F_2 \\ F_3 \end{bmatrix} = \begin{bmatrix} G_{11} & G_{12} & G_{13} \\ G_{21} & G_{22} & G_{23} \\ G_{31} & G_{32} & G_{33} \end{bmatrix} \begin{bmatrix} \xi_1 \\ \xi_2 \\ \xi_3 \end{bmatrix} \quad (3)$$

Using this process, it was then necessary to find the equations of motion for heave, roll, and pitch. This was done using (4) where A, B, and C are the added mass, damping, and stiffness matrices for the ship and barge. The j terms are for the 6 directions of motion in which only heave, roll, and pitch were considered. F_j^I and F_j^D are the complex amplitude of the exciting force components due to incident and diffracted waves, and F_j^r are the connection forces at the ramp, to be determined.

$$\sum_{k=1}^6 \left[-\omega_e^2 (\Delta_{jk} + A_{jk}) + i\omega_e B_{jk} + C_{jk} \right] \eta_k = F_j^I + F_j^D + F_j^r \quad (4)$$

Solving these equations for the three relevant motions to this problem, the final equations of motion were found to be:

$$\bar{A}_{33}\bar{\eta}_3 + \bar{A}_{35}\bar{\eta}_5 = F_3 \text{ in Heave} \quad (5)$$

$$\bar{A}_{44}\bar{\eta}_4 = F_4 \text{ in Roll} \quad (6)$$

$$\bar{A}_{53}\bar{\eta}_3 + \bar{A}_{55}\bar{\eta}_5 = F_5 \text{ in Pitch} \quad (7)$$

The various terms in these equations are defined as:

$$\bar{\eta}_3(t) = \eta_3 e^{i\omega_e t} \Rightarrow \text{Heave} \quad (8)$$

$$\bar{\eta}_4(t) = \eta_4 e^{i\omega_e t} \Rightarrow \text{Roll} \quad (9)$$

$$\bar{\eta}_5(t) = \eta_5 e^{i\omega_e t} \Rightarrow \text{Pitch} \quad (10)$$

Each of the internal terms in the equations of motion are all matrices. These matrices are characterized as A, B and C and represent the added mass of the vessel, the damping coefficient, and the stiffness. This implies that each vessel's hydrodynamic properties are modeled as a spring-mass-damper system. The first number in the following equation's subscripts refers to the direction (heave, pitch, or roll) and the second number is with respect to a particular direction. For example, A_{35} in (12) would be the heave added mass due to pitch.

$$\bar{A}_{33} = -\omega_e^2 (\Delta + A_{33}) + i\omega_e B_{33} + C_{33} \quad (11)$$

$$\bar{A}_{35} = -\omega_e^2 (\Delta x_c + A_{35}) + i\omega_e B_{35} + C_{35} \quad (12)$$

$$\bar{A}_{55} = -\omega_e^2 (I_{55} + A_{55}) + i\omega_e B_{55} + C_{55} \quad (13)$$

$$\bar{A}_{53} = -\omega_e^2 (\Delta x_c + A_{53}) + i\omega_e B_{53} + C_{53} \quad (14)$$

$$\bar{A}_{44} = -\omega_e^2 (I_{44} + A_{44}) + i\omega_e B_{44} + C_{44} \quad (15)$$

The terms in the added mass equations are the specific equations of mass, damping, and stiffness for the particular vessel. Due to inherent symmetrical relations within the vessel, the following additional assumptions are utilized:

$$C_{53} = C_{35} \quad (16)$$

$$B_{35} = B_{53} \quad (17)$$

$$A_{35} = A_{53} \quad (18)$$

The force terms in the equations of motion are simplified to make individual force calculations easier. This leads to the following equations that produce the resultant heave, roll, and pitch forces:

$$F_3 = F_3^I + F_3^D + F_3^r \quad (19)$$

$$F_4 = F_4^I + F_4^D + F_4^r \quad (20)$$

$$F_5 = F_5^I + F_5^D + F_5^r \quad (21)$$

The F_3^r , F_4^r , and F_5^r terms are the heave, roll, and pitch forces that act on the ship or barge from the motion of the ramp.

The equations of motion in (5) through (7) are body independent. Consequently, they are used to describe the motions of the ship and barge. Therefore, a subscript 'S' or 'B' is used to distinguish the motions of each vessel. Furthermore, equations (5) through (7) fail to recognize that as two objects are in close proximity to one another, there will exist a radiative effect between the two vessels. This results from waves striking one vessel, bouncing off the hull and then striking the vessel alongside. These reflected waves effect heave, pitch and roll of the adjacent vessel. Combining the vessel distinguishing subscripts and the radiative matrices yielded the following equations.

$$\text{Heave, ship} \Rightarrow \bar{A}_{33,S} \bar{\eta}_{3,S} + \bar{A}_{35,S} \bar{\eta}_{5,S} + \bar{B}_{33,B} \bar{\eta}_{3,B} + \bar{B}_{35,B} \bar{\eta}_{5,B} + \bar{B}_{34,B} \bar{\eta}_{4,B} = F_{3,S} \quad (22)$$

$$\text{Pitch, ship} \Rightarrow \bar{A}_{53,S} \bar{\eta}_{3,S} + \bar{A}_{55,S} \bar{\eta}_{5,S} + \bar{B}_{53,B} \bar{\eta}_{3,B} + \bar{B}_{55,B} \bar{\eta}_{5,B} + \bar{B}_{54,B} \bar{\eta}_{4,B} = F_{5,S} \quad (23)$$

$$\text{Roll, ship} \Rightarrow \bar{A}_{44,S} \bar{\eta}_{4,S} + \bar{B}_{43,B} \bar{\eta}_{3,B} + \bar{B}_{45,B} \bar{\eta}_{5,B} + \bar{B}_{44,B} \bar{\eta}_{4,B} = F_{4,S} \quad (24)$$

$$\text{Heave, barge} \Rightarrow \bar{A}_{33,B} \bar{\eta}_{3,B} + \bar{A}_{35,B} \bar{\eta}_{5,B} + \bar{B}_{33,S} \bar{\eta}_{3,S} + \bar{B}_{35,S} \bar{\eta}_{5,S} + \bar{B}_{34,S} \bar{\eta}_{4,S} = F_{3,B} \quad (25)$$

$$\text{Pitch, barge} \Rightarrow \bar{A}_{53,B} \bar{\eta}_{3,B} + \bar{A}_{55,B} \bar{\eta}_{5,B} + \bar{B}_{53,S} \bar{\eta}_{3,S} + \bar{B}_{55,S} \bar{\eta}_{5,S} + \bar{B}_{54,S} \bar{\eta}_{4,S} = F_{5,B} \quad (26)$$

$$\text{Roll, barge} \Rightarrow \bar{A}_{44,B} \bar{\eta}_{4,B} + \bar{B}_{43,S} \bar{\eta}_{3,S} + \bar{B}_{45,S} \bar{\eta}_{5,S} + \bar{B}_{44,S} \bar{\eta}_{4,S} = F_{4,B} \quad (27)$$

The \bar{B} terms are the radiative matrices between the barge and ship while the subscript S and B designate the ship or barge. The radiative matrices are defined with the following equations:

$$\bar{B}_{33,B} = -\omega^2 D_{33,B} + i\omega E_{33,B} \quad (28)$$

$$\bar{B}_{34,B} = -\omega^2 D_{34,B} + i\omega E_{34,B} \quad (29)$$

$$\bar{B}_{35,B} = -\omega^2 D_{35,B} + i\omega E_{35,B} \quad (30)$$

$$\bar{B}_{43,B} = -\omega^2 D_{43,B} + i\omega E_{43,B} \quad (31)$$

$$\bar{B}_{44,B} = -\omega^2 D_{44,B} + i\omega E_{44,B} \quad (32)$$

$$\bar{B}_{45,B} = -\omega^2 D_{45,B} + i\omega E_{45,B} \quad (33)$$

$$\bar{B}_{53,B} = -\omega^2 D_{53,B} + i\omega E_{53,B} \quad (34)$$

$$\bar{B}_{54,B} = -\omega^2 D_{54,B} + i\omega E_{54,B} \quad (35)$$

$$\bar{B}_{55,B} = -\omega^2 D_{55,B} + i\omega E_{55,B} \quad (36)$$

D and E are the added mass and damping influence coefficients due to the radiated waves from one vessel to another. Similar equations for the radiative matrices are obtained for the ship. Due to symmetry $E_{jk}^{(1)} = E_{kj}^{(2)}$ and $D_{jk}^{(1)} = D_{kj}^{(2)}$. An example of one of these symmetric equations is the following:

$$D_{35,B} = D_{53,S} \quad (37)$$

Using a free-body diagram, (5) through (7) were expanded allowing the hydrostatic and ramp forces on each vessel to be separated. The terms F_1^r , F_2^r , and F_3^r were defined as f_1 , f_2 , and f_3 respectfully. The following revised equations of motion are:

$$\text{Heave, ship} \Rightarrow \bar{A}_{33,S} \bar{\eta}_{3,S} + \bar{A}_{35,S} \bar{\eta}_{5,S} + \bar{B}_{33,B} \bar{\eta}_{3,B} + \bar{B}_{34,B} \bar{\eta}_{4,B} + \bar{B}_{35,B} \bar{\eta}_{5,B} = F_{3,S}^H + f_1 \quad (38)$$

$$\text{Pitch, ship} \Rightarrow \bar{A}_{53,S} \bar{\eta}_{3,S} + \bar{A}_{55,S} \bar{\eta}_{5,S} + \bar{B}_{53,B} \bar{\eta}_{3,B} + \bar{B}_{54,B} \bar{\eta}_{4,B} + \bar{B}_{55,B} \bar{\eta}_{5,B} = F_{5,S}^H - f_1 x_1 \quad (39)$$

$$\text{Roll, ship} \Rightarrow \bar{A}_{44,S} \bar{\eta}_{4,S} + \bar{B}_{43,B} \bar{\eta}_{3,B} + \bar{B}_{44,B} \bar{\eta}_{4,B} + \bar{B}_{45,B} \bar{\eta}_{5,B} = F_{4,S}^H + f_1 y_1 \quad (40)$$

$$\text{Heave, barge} \Rightarrow \bar{A}_{33,B} \bar{\eta}_{3,B} + \bar{A}_{35,B} \bar{\eta}_{5,B} + \bar{B}_{33,S} \bar{\eta}_{3,S} + \bar{B}_{34,S} \bar{\eta}_{4,S} + \bar{B}_{35,S} \bar{\eta}_{5,S} = F_{3,B}^H + f_2 + f_3 \quad (41)$$

$$\text{Roll, barge} \Rightarrow \bar{A}_{44,B} \bar{\eta}_{4,B} + \bar{B}_{43,S} \bar{\eta}_{3,S} + \bar{B}_{44,S} \bar{\eta}_{4,S} + \bar{B}_{45,S} \bar{\eta}_{5,S} = F_{4,B}^H + f_2 y_2 + f_3 y_3 \quad (42)$$

$$\text{Pitch, barge} \Rightarrow \bar{A}_{53,B} \bar{\eta}_{3,B} + \bar{A}_{55,B} \bar{\eta}_{5,B} + \bar{B}_{53,S} \bar{\eta}_{3,S} + \bar{B}_{54,S} \bar{\eta}_{4,S} + \bar{B}_{55,S} \bar{\eta}_{5,S} = F_{5,B}^H - f_2 x_2 - f_3 x_3 \quad (43)$$

This allowed for the effects on the ship and barge at the pinned connections due to the direct forces from the ramp as well as moment forces due to ramp movement. The superscript H is to show the force acting on the hull of the respective vessel.

Once the above hydrodynamic equations of motion are solved, the values for f_1 , f_2 , and f_3 can be established. However, all of the η terms in the above equations are unknown and all the f terms are also unknown. Therefore, the values for the η terms are determined by defining additional equations. η is thus defined as a function of f_1 , f_2 , and f_3 for the ship and barge as:

$$\bar{\eta}_{3,S} = \mu_{31} f_1 + \mu_{30} \quad (44)$$

$$\bar{\eta}_{4,S} = \mu_{41} f_1 + \mu_{40} \quad (45)$$

$$\bar{\eta}_{5,S} = \mu_{51} f_1 + \mu_{50} \quad (46)$$

$$\bar{\eta}_{3,B} = \nu_{32} f_2 + \nu_{33} f_3 + \nu_{30} \quad (47)$$

$$\bar{\eta}_{4,B} = \nu_{42} f_2 + \nu_{43} f_3 + \nu_{40} \quad (48)$$

$$\bar{\eta}_{5,B} = \nu_{52} f_2 + \nu_{53} f_3 + \nu_{50} \quad (49)$$

From these equations, it is possible to solve the six linear equations for each respective μ and ν in terms of various known added mass matrices, known physical positions on the vessel, and the forces acting on the pinned connections as well as the hydrodynamic wave forces.

Once each μ and ν term is solved, every η is considered a known value in terms of f_1 , f_2 , and f_3 . Each η term has a contribution to the total force acting where the ramp attaches to the barge or the ship. Therefore, the total force acting on a pinned joint includes forces from heave, roll, and pitch. This produces three combined displacement equations for each connection that are:

$$\xi_1 = \bar{\eta}_{3,S} + \bar{\eta}_{4,S} y_1 - x_1 \bar{\eta}_{5,S} = k_{11} f_1 + k_{10} \quad (50)$$

$$\xi_2 = \bar{\eta}_{3,B} + \bar{\eta}_{4,B} y_2 - x_2 \bar{\eta}_{5,B} = k_{22} f_2 + k_{23} f_3 + k_{20} \quad (51)$$

$$\xi_3 = \bar{\eta}_{3,B} + \bar{\eta}_{4,B} y_3 - x_3 \bar{\eta}_{5,B} = k_{32} f_2 + k_{33} f_3 + k_{30} \quad (52)$$

It was stated previously that ξ_1 , ξ_2 , and ξ_3 are the combined displacements that act at each of the pinned connections. Now the equations are defined by relating the forces

acting on the pinned connections from the above k terms using the known formulas for η and equating portions of the ξ equations that correspond to the respective x or y terms.

Thus, the k terms become:

$$k_{11} = \mu_{31} + \mu_{41}y_1 - \mu_{51}x_1 \quad k_{10} = \mu_{30} + \mu_{40}y_1 - \mu_{50}x_1 \quad (53)$$

$$k_{22} = \nu_{32} + \nu_{42}y_2 - \nu_{52}x_2 \quad k_{23} = \nu_{33} + \nu_{43}y_2 - \nu_{53}x_2 \quad k_{20} = \nu_{30} + \nu_{40}y_2 - \nu_{50}x_2 \quad (54)$$

$$k_{32} = \nu_{32} + \nu_{42}y_3 - \nu_{52}x_3 \quad k_{33} = \nu_{33} + \nu_{43}y_3 - \nu_{53}x_3 \quad k_{30} = \nu_{30} + \nu_{40}y_3 - \nu_{50}x_3 \quad (55)$$

These k terms are then set equal to the transfer functions that relate the forces at one pinned connection to the other forces from each pinned connection, and how the various forces interact through the ramp system. This leads to the equations:

$$k_{10} + k_{11} f_1 = G_{11} f_1 + G_{12} f_2 + G_{13} f_3 \quad (56)$$

$$k_{20} + k_{22} f_2 + k_{23} f_3 = G_{21} f_1 + G_{22} f_2 + G_{23} f_3 \quad (57)$$

$$k_{30} + k_{32} f_2 + k_{33} f_3 = G_{31} f_1 + G_{32} f_2 + G_{33} f_3 \quad (58)$$

Rearranging equations (56) through (58) and placing into matrix for yields:

$$\begin{bmatrix} k_{11}-G_{11} & -G_{12} & -G_{13} \\ -G_{21} & k_{22}-G_{22} & k_{23}-G_{23} \\ -G_{31} & k_{32}-G_{32} & k_{33}-G_{33} \end{bmatrix} \begin{bmatrix} f_1 \\ f_2 \\ f_3 \end{bmatrix} = \begin{bmatrix} -k_{10} \\ -k_{20} \\ -k_{30} \end{bmatrix} \quad (59)$$

This first matrix is labeled as matrix $[G_k]$. Solving for the forces yields:

$$\begin{bmatrix} f_1 \\ f_2 \\ f_3 \end{bmatrix} = [G_k]^{-1} \begin{bmatrix} -k_{10} \\ -k_{20} \\ -k_{30} \end{bmatrix} \quad (60)$$

The three forces are easily solved using Matlab or any other engineering computational program given the numerical values of the added mass, damping, and stiffness matrices.

C. RAMP EQUATION OF MOTION

1. Introduction

To accurately model the ship barge combination, it is important to incorporate the ramp connecting the two vessels because there will be interaction effects between the two vessels transmitted through the ramp. The ramp is modeled here as a rigid body, although the procedure is general enough so that it can be generalized to include flexibility effects.

2. Derivation of the Equation of Motion

To obtain the equations of motion for the ramp, it was first necessary to examine the ramp as a separate entity. First, the ramp is a three-degree of freedom system in the heave, pitch, and roll directions. The ramp is assumed to be connected to the ship and barge at three locations. See appendix A for figure of LMSR/barge connection. Each of these locations has a spring connection and the overall ramp has a mass of M . It was further assumed that the ramp is a homogenous device with uniform properties throughout. Using these assumptions, the equations of motion were derived using the method of summing kinetic and potential energies of the ramp and then using Lagrange's Equations to derive the equations of motion.

First, it is necessary to define Lagrange's equations. The Lagrangian is defined as

$$L = T - U \quad (61)$$

where L is the Lagrangian, T is kinetic energy, and U is the potential energy of the ramp.

The Lagrangian is then used to find the value of the forces at each degree of freedom.

The equation for this is written below as equation (62). This equation takes the partial derivative of the Lagrangian with respect to the velocity of one of the degrees of freedom. The partial derivative of the Lagrangian with respect to position is then taken and subtracted from the time derivative of the first value. This produces the force at one of the degrees of freedom.

$$\frac{d}{dt} \left(\frac{\partial L}{\partial \dot{q}_i} \right) - \frac{\partial L}{\partial q} = F_i \quad (62)$$

After the Lagrangian is defined, the kinetic and potential energies for the ramp are found. Looking at the ramp from a view approximately 45 degrees above the horizontal, it was assumed that there are three pinned connections. These are at the two corners that would attach the ramp to the barge and the third connection is from a kingpin in the center of the ramp that attaches the ramp to the ship. These connections produce a force upward due to the associated springs. Visualizing the ramp in some deformed state, it is possible to define the change in position due to heave, pitch, and roll. The heave is simply the distance y upward from the original axis. The pitch is defined as a positive upward angle from the new horizontal axis on the ship side of the ramp. Roll is the rotation about the x -axis from the new pitch angled ramp. Kinetic energy is defined as

$$T = .5 M \dot{y}^2 + .5 M \dot{\theta}^2 + .5 M \dot{\psi}^2 \quad (63)$$

In this equation, M is the mass of the ramp and y , θ , and ψ are the three individual displacements which act on the ramp throughout the ramp motion.

Potential energy is defined as the stored energy of the springs throughout the system. Damping of the ramp was not included in the determination of the potential energy as proportional damping was considered to be in effect. Therefore, the value of the damping coefficients will be proportional to the spring coefficients by some set amount. This allows easier calculation of the potential energy. In the potential energy equation, U is the potential energy, k is the spring coefficient, A is the length of the ramp, and B is the width of the ramp. Y , θ , and Ψ are the same as previously defined.

$$U = .5k_1 \left(y + \frac{A}{2} \sin \Theta \right)^2 + .5k_2 \left(y - \frac{A}{2} \sin \Theta + \frac{B}{2} \sin \Psi \right)^2 + .5k_3 \left(y - \frac{A}{2} \sin \Theta - \frac{B}{2} \sin \Psi \right)^2 \quad (64)$$

Once the kinetic and potential energies are defined, the determination of the equations of motion of the system is fairly straightforward. Set up the Lagrangian, take derivatives, and equate terms and place in matrix form. The force equations were found to be

$$M \ddot{y} - k_1 \left(y + \frac{A}{2} \sin \Theta \right) - k_2 \left(y - \frac{A}{2} \sin \Theta + \frac{B}{2} \sin \Psi \right) - k_3 \left(y - \frac{A}{2} \sin \Theta - \frac{B}{2} \sin \Psi \right) = F_y \quad (65)$$

$$M \ddot{\Theta} - \frac{A}{2} \cos \Theta k_1 \left(y + \frac{A}{2} \sin \Theta \right) - \frac{A}{2} \cos \Theta k_2 \left(y - \frac{A}{2} \sin \Theta + \frac{B}{2} \sin \Psi \right) - \frac{A}{2} \cos \Theta k_3 \left(y - \frac{A}{2} \sin \Theta - \frac{B}{2} \sin \Psi \right) = F_\Theta \quad (66)$$

$$M \ddot{\Psi} - \frac{B}{2} \cos \Psi k_2 \left(y - \frac{A}{2} \sin \Theta + \frac{B}{2} \sin \Psi \right) - \frac{B}{2} \cos \Psi k_3 \left(y - \frac{A}{2} \sin \Theta - \frac{B}{2} \sin \Psi \right) = F_\Psi \quad (67)$$

It should be noted that there is not a term for Ψ in the k_1 part of the equation. This is because as the ramp rolls, the changes in the Ψ angle for the spring on the centerline is zero. This also causes the F_Ψ force to not have a k_1 term as the derivative does not have a Ψ term in it.

$$\begin{bmatrix} F_y \\ F_\Theta \\ F_\Psi \end{bmatrix} = \begin{bmatrix} M & 0 & 0 \\ 0 & M & 0 \\ 0 & 0 & M \end{bmatrix} \begin{bmatrix} \ddot{y} \\ \ddot{\Theta} \\ \ddot{\Psi} \end{bmatrix} + \begin{bmatrix} -C_1 - C_2 - C_3 & \frac{A}{2}C_1 + \frac{A}{2}C_2 + \frac{A}{2}C_3 & \frac{B}{2}C_2 + \frac{B}{2}C_3 \\ -\frac{A}{2}C_1 - \frac{A}{2}C_2 + \frac{A}{2}C_3 & \frac{A^2}{4}C_1 - \frac{A^2}{4}C_2 - \frac{A^2}{4}C_3 & \frac{AB}{4}C_2 - \frac{AB}{4}C_3 \\ \frac{B}{2}C_2 + \frac{B}{2}C_3 & \frac{AB}{4}C_2 - \frac{AB}{4}C_3 & \frac{B^2}{4}C_2 + \frac{B^2}{4}C_3 \end{bmatrix} \begin{bmatrix} y \\ \Theta \\ \Psi \end{bmatrix} + \begin{bmatrix} -K_1 - K_2 - K_3 & \frac{A}{2}K_1 + \frac{A}{2}K_2 + \frac{A}{2}K_3 & \frac{B}{2}K_2 + \frac{B}{2}K_3 \\ \frac{A}{2}K_1 - \frac{A}{2}K_2 + \frac{A}{2}K_3 & \frac{A^2}{4}K_1 - \frac{A^2}{4}K_2 - \frac{A^2}{4}K_3 & \frac{AB}{4}K_2 - \frac{AB}{4}K_3 \\ \frac{B}{2}K_2 + \frac{B}{2}K_3 & \frac{AB}{4}K_2 - \frac{AB}{4}K_3 & \frac{B^2}{4}K_2 + \frac{B^2}{4}K_3 \end{bmatrix} \begin{bmatrix} y \\ \Theta \\ \Psi \end{bmatrix}$$

(68)

Equation (68) above shows the end result matrix for the three directional forces on the ramp. This matrix is produced after deriving the equations of motion for the ramp, adding the proportional damping values and linearizing the all three equations using the small angle approximation. This allowed $\sin\theta$ and $\sin\Psi$ to be approximated as simply θ and Ψ and $\cos\theta$ and $\cos\Psi$ to be approximated as 1.

Once the final matrix for the ramp equations of motion was derived, these forces representing the position of the ramp in terms of y , θ , and Ψ had to be correlated to be in terms of F_1 , F_2 , and F_3 , the forces at each of the connecting locations and their associated changes in absolute vertical motion. First, the forces on the ramp were written in terms of F_1 , F_2 , and F_3 . This produced the following matrix where all symbols are as previously stated.

$$\begin{bmatrix} F_y \\ F_\theta \\ F_\Psi \end{bmatrix} = \begin{bmatrix} \frac{1}{2} & \frac{1}{2} & \frac{1}{2} \\ \frac{A}{2} & \frac{-A}{2} & \frac{-A}{2} \\ 0 & \frac{B}{2} & \frac{-B}{2} \end{bmatrix} \begin{bmatrix} F_1 \\ F_2 \\ F_3 \end{bmatrix} \quad (69)$$

The next step was to state the changes in position of the ramp connecting locations in terms of y , θ , and Ψ .

$$\begin{bmatrix} x_1 \\ x_2 \\ x_3 \end{bmatrix} = \begin{bmatrix} 1 & \frac{A}{2} & 0 \\ 1 & \frac{-A}{2} & \frac{B}{2} \\ 1 & \frac{-A}{2} & \frac{-B}{2} \end{bmatrix} \begin{bmatrix} y \\ \theta \\ \Psi \end{bmatrix} \quad (70)$$

In this matrix, x_1 , x_2 , and x_3 are the vertical displacements for each of the pinned connections. The final relation must be to have F_y , F_θ , and F_Ψ in terms of only the displacements. The resulting equation is as follows:

$$\begin{bmatrix} F_y \\ F_\theta \\ F_\Psi \end{bmatrix} = \left[-\omega^2 [M] + j\omega [C] + [K] \right] \begin{bmatrix} y \\ \theta \\ \Psi \end{bmatrix}$$

(71)

In this matrix, the M, C, and K matrices are the mass, damping, and spring stiffness matrices defined earlier. Frequency is defined as ω and is the frequency of wave impact from the hydrodynamic information.

Once the relations are made between the pinned connections and the equations of motion, a relation can be established to relate the displacements of the connections to the ramp equations of m

$$\begin{bmatrix} x_1 \\ x_2 \\ x_3 \end{bmatrix} = \begin{bmatrix} 1 & \frac{A}{2} & 0 \\ 1 & -\frac{A}{2} & \frac{B}{2} \\ 1 & -\frac{A}{2} & -\frac{B}{2} \end{bmatrix} [F_{total}]^{-1} \begin{bmatrix} \frac{1}{2} & \frac{1}{2} & \frac{1}{2} \\ \frac{A}{2} & -\frac{A}{2} & -\frac{A}{2} \\ 0 & \frac{B}{2} & -\frac{B}{2} \end{bmatrix} \begin{bmatrix} F_1 \\ F_2 \\ F_3 \end{bmatrix} \quad (72)$$

Known values are the length and width of the ramp, the M, C, and K matrices, and the hydrodynamic forces on the pinned connection. Placing all this information together results in the final matrix describing the change in vertical displacement of the pinned connection.

THIS PAGE INTENTIONALLY LEFT BLANK

IV. RESULTS

A. LARGE MEDIUM-SPEED ROLL-ON ROLL-OFF VESSEL ANALYSIS

1. Introduction

The comparison between the strip theory and full three-dimensional (WAMIT) program solvers are presented in Figures 1 through 48. Each of the values in the figures has been non-dimensionalized in a consistent manner displayed in Table 1. Furthermore, all pertinent ship parameters are shown in Table 3. All symbols used are identified in Table 2.

Ship/Barge Coefficient	WAMIT Non-dimensionalization
A33, Heave Added Mass	$A_{33}/\rho L^3$
B33, Heave Damping	$B_{33}/\omega \rho L^3$
A55, Pitch Added Mass	$A_{55}/\rho L^3$
B55, Pitch Damping	$B_{55}/\omega \rho L^3$
A35, Heave to Pitch Added Mass	$A_{35}/\rho L^4$
B35, Heave to Pitch Damping	$B_{35}/\omega \rho L^4$
A53, Pitch to Heave Added Mass	$A_{53}/\rho L^4$
B53, Pitch to Heave Damping	$B_{53}/\omega \rho L^4$
C33, Heave Stiffness	$C_{33} * \rho g A_w / \rho g L^2$
F3, Heave Exciting Force	$F_3 / \rho g A L^2$
F5, Pitch Exciting Moment	$F_5 / \rho g A L^3$
Phase Angle	None

Table 1. Table of Various Non-Dimensionalizations

2. Data Analysis

Figures 1 through 28 display the added mass and damping results for the large medium speed roll-on roll-off vessel (LMSR) data. The first 8 figures portray data obtained from the strip theory solver and WAMIT when over 2000 panels were used in the 3-D analysis. The next 8 figures show the same added mass and damping curves comparing strip theory and WAMIT but in these curves, there were only about 1000

panels for the ship and barges. Figures 21 through 28 show the effects due to wave radiation effects from the barge on the LMSR. Overall, the results show that relatively good agreement is obtained between the two computer solving techniques, especially in the heave mode. However, oscillatory behavior is observed for the WAMIT program at high frequencies (low periods), especially when fewer panels are utilized. This is due to discretization effects in the solver. To overcome these problems, a relatively high number of panels are required to accurately represent the hydrodynamic interactions between the LMSR and the small Roll-on, Roll-off Discharge Facility (RRDF). The strip theory solver does not take such interactions into consideration. Therefore, it is not susceptible to high frequency “chattering”, unlike the 3-D solver.

SYMBOL	DEFINITION
M	Mass of the ship or barge in pounds.
L	Length of the ship in feet.
g	Force due to gravity in pounds-force per second-squared.
A_w	Waterplane area produced by the strip theory solver in square feet.
A	Wave amplitude.
ω	Frequency of wave impact upon the ship or barge in Hertz.
∇	Ship's displacement in cubic feet.
ρ	Density of Seawater in pounds-mass per cubic feet. Considered to be 1.9904 lb/ft ³ .

Table 2. List of Applicable Symbols and Their Definitions

As mentioned, the 3-D solver can overcome the high frequency oscillations by utilizing a more refined panel scheme. However, the very large number of panels that is required by the 3-D solver incurs a significant cost in both computational time (more than 16 hours for the 2000 panel case on a high-end CPU) as well as the time needed to

prepare the data file. By contrast, the strip theory solver results were obtained after only a few seconds of execution time on an older generation Pentium CPU. Of course, the limitations of the strip theory solver are that the interaction effects are not capable of being modeled. By comparing the strip theory and WAMIT solvers, it was clear that modeling of the added mass and damping characteristics of the main ship could be achieved both accurately and efficiently through a combination of the two-dimensional and three-dimensional hydrodynamic solvers.

The results for the hydrodynamic wave excitation forces and phase angles for the LMSR are presented in Figures 25 through 60. These wave forces range from zero degrees (head seas) through 315 degrees at 45-degree intervals. This provides complete 360-degree coverage for wave force analysis for the LMSR. In these plots, overall agreement between the strip theory solver and WAMIT is outstanding. As will be noted in more detail when the barge data is analyzed, there are some slight differences between the port and starboard wave directions in the 3-D results. These deviations are due to interactions between the barge and the LMSR.

Dimension	LMSR	Barge
Length (in Feet)	894.53	79.2
Beam (in Feet)	105.8	72.6
Depth (in Feet)	None Given	4.7
Draft (in Feet)	27.5(FWD), 32.27(AFT)	1.3
Displacement	45,211 Long Tons	402,783 Pounds
Ramp Location (Feet From FP)	X=301.2, Y=71.3	39.5 (From Hinged Side Edge) 8.8(From Centerline of Causeway to Port)

Table 3. Applicable Ship, Barge, and Ramp Dimensions

3. Figures

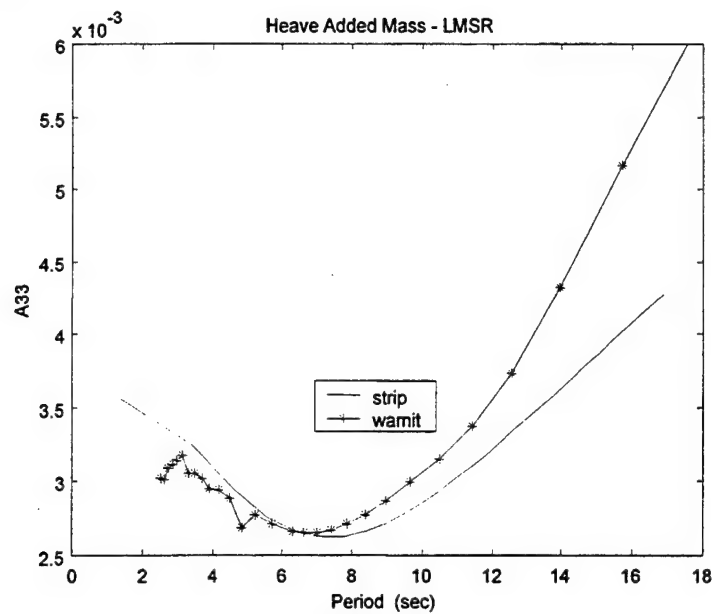


Figure 1. Plot of Strip Theory and Wamit Program Comparisons for Heave Added Mass for the LMSR.

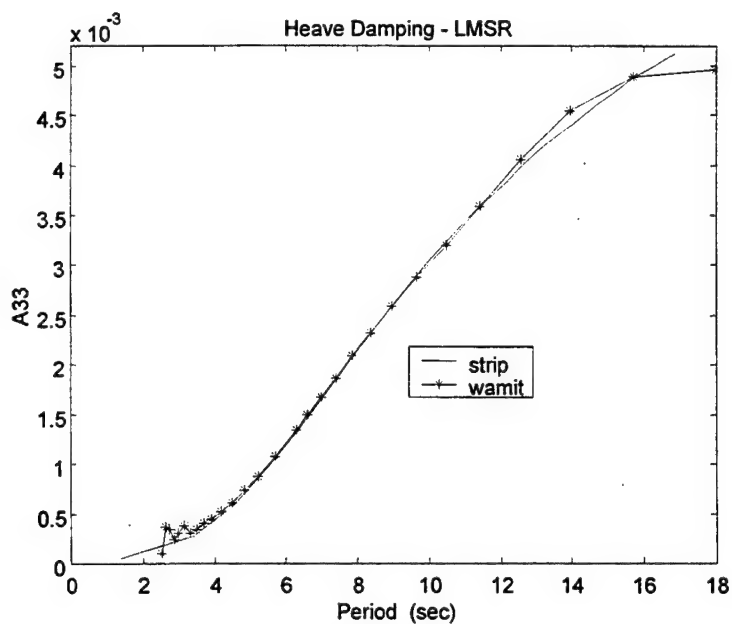


Figure 2. Plot of Strip Theory and Wamit Program Comparisons for Heave Damping for the LMSR.

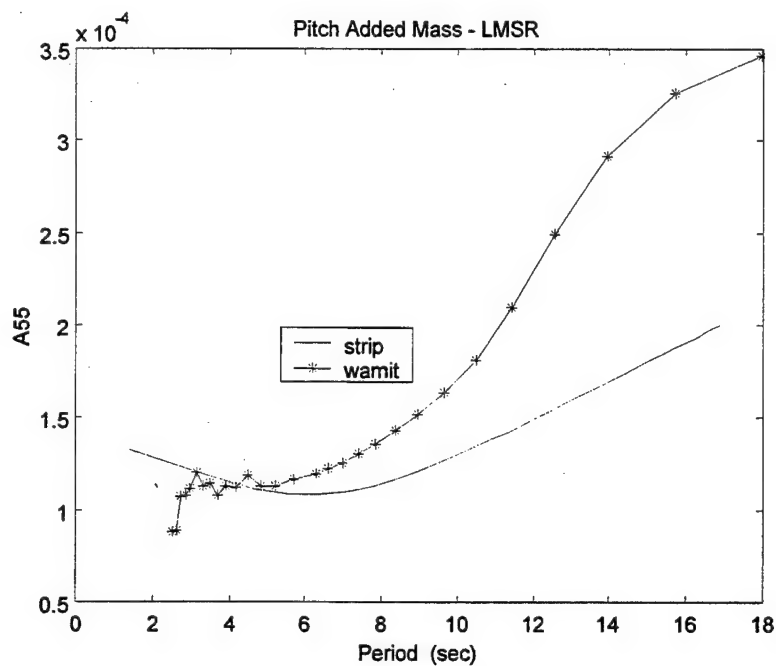


Figure 3. Plot of Strip Theory and Wamit Program Comparisons for Pitch Added Mass for the LMSR.

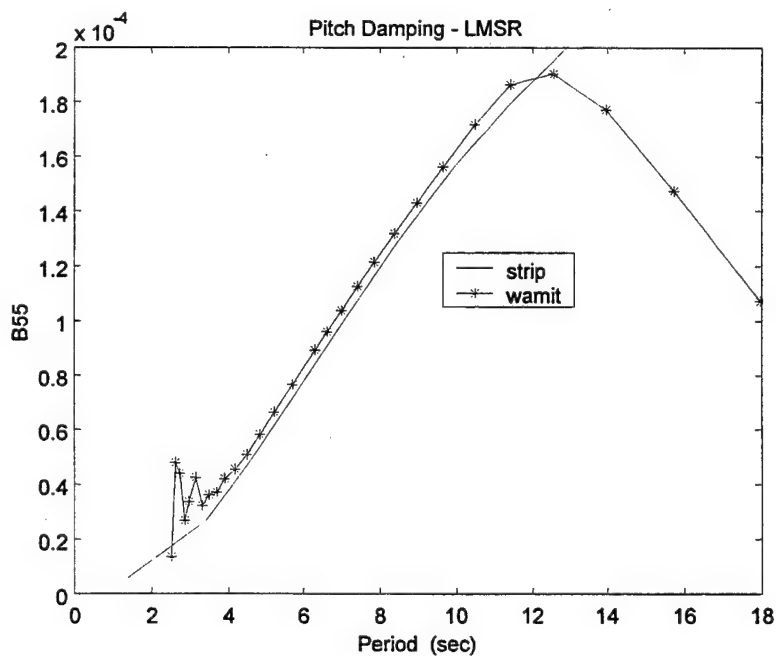


Figure 4. Plot of Strip Theory and Wamit Program Comparisons for Pitch Damping for the LMSR.

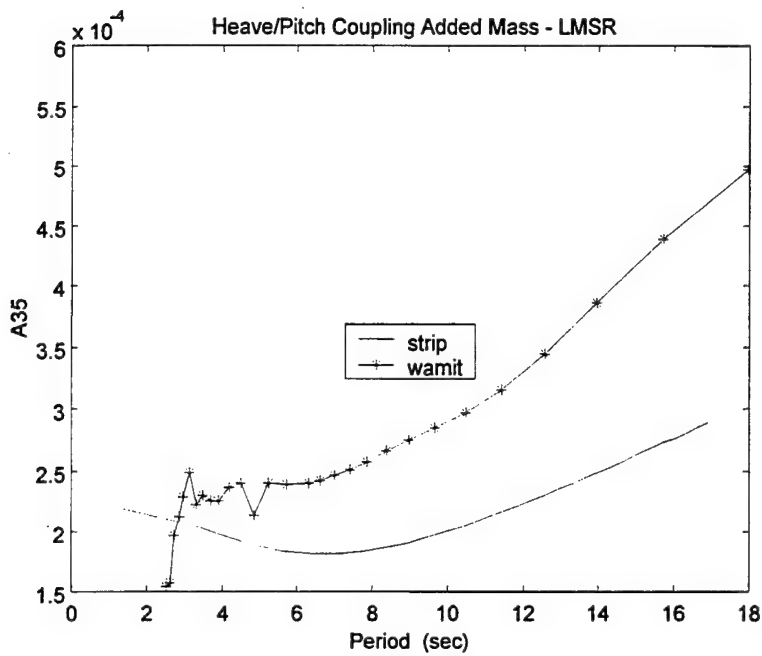


Figure 5. Plot of Strip Theory and Wamit Program Comparisons for Heave/Pitch Added Mass for the LMSR.

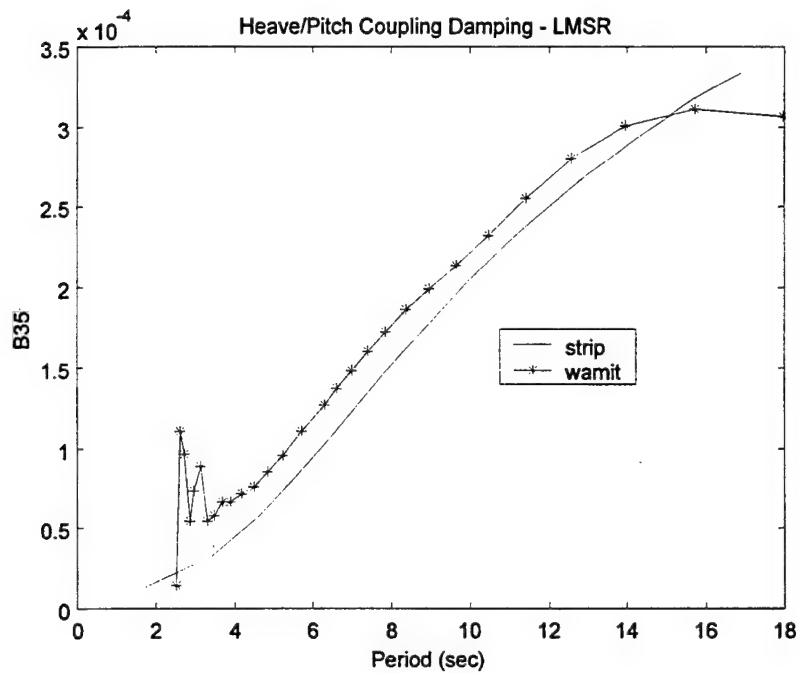


Figure 6. Plot of Strip Theory and Wamit Program Comparisons for Heave/Pitch Damping for the LMSR.

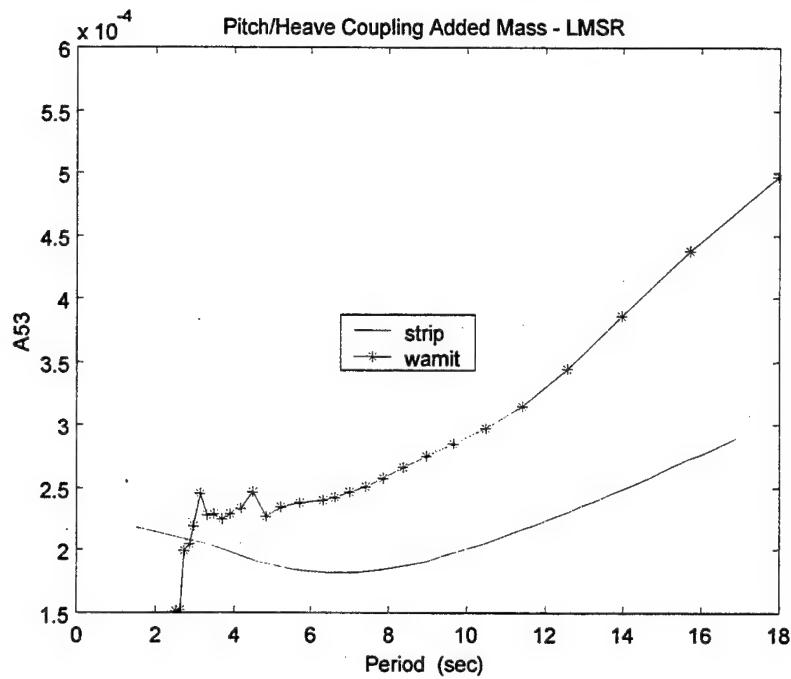


Figure 7. Plot of Strip Theory and Wamit Program Comparisons for Pitch/Heave Added Mass for the LMSR.

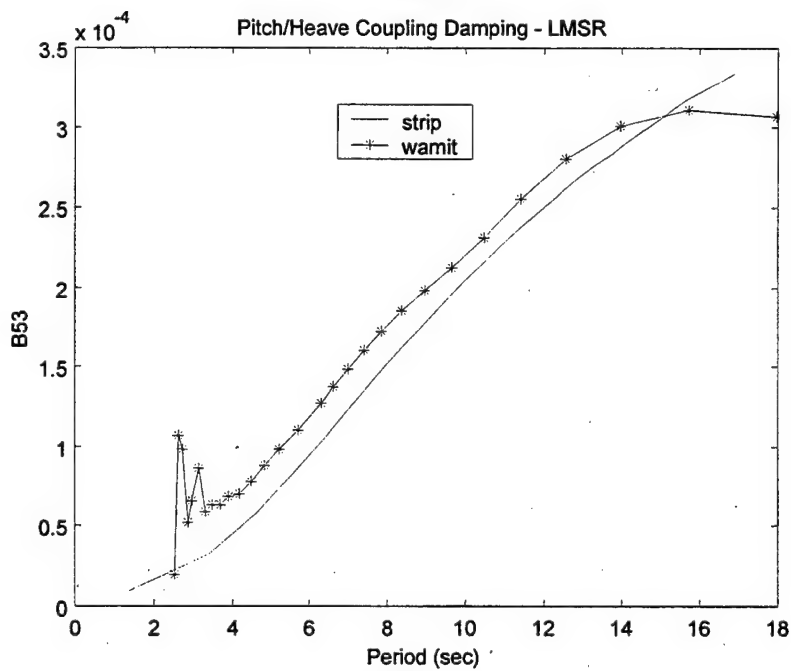


Figure 8. Plot of Strip Theory and Wamit Program Comparisons for Pitch/Heave Damping for the LMSR.

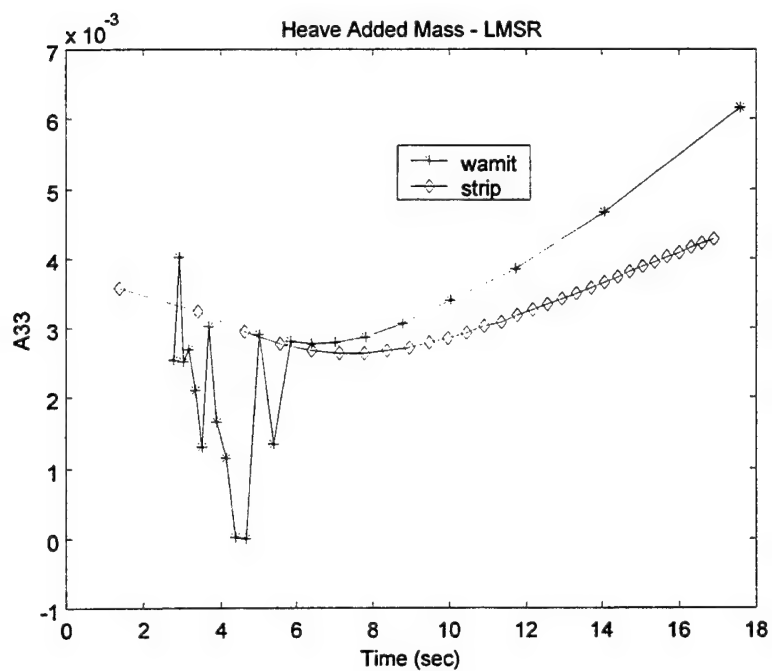


Figure 9. Plot of Strip Theory and Wamit Program Comparisons for Heave Added Mass for the Old LMSR Data.

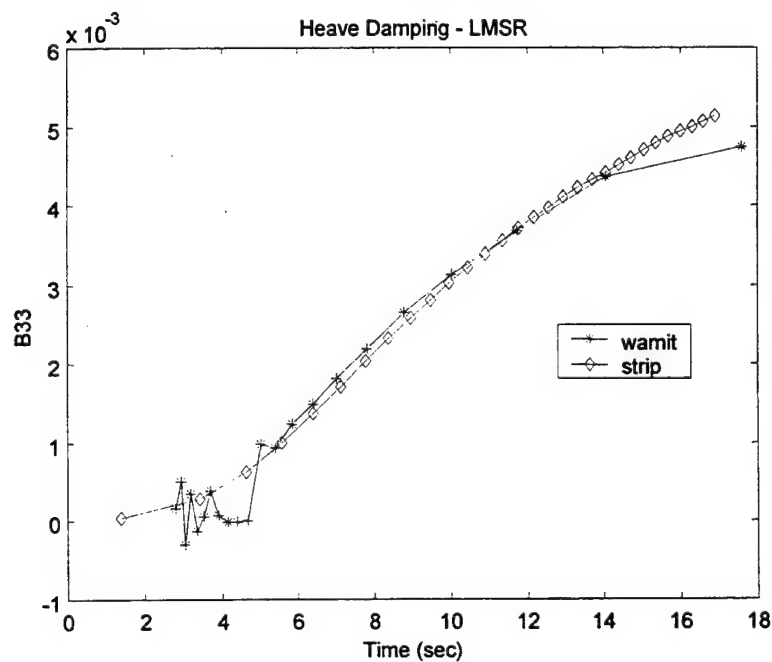


Figure 10. Plot of Strip Theory and Wamit Program Comparisons for Heave Damping for the Old LMSR Data.

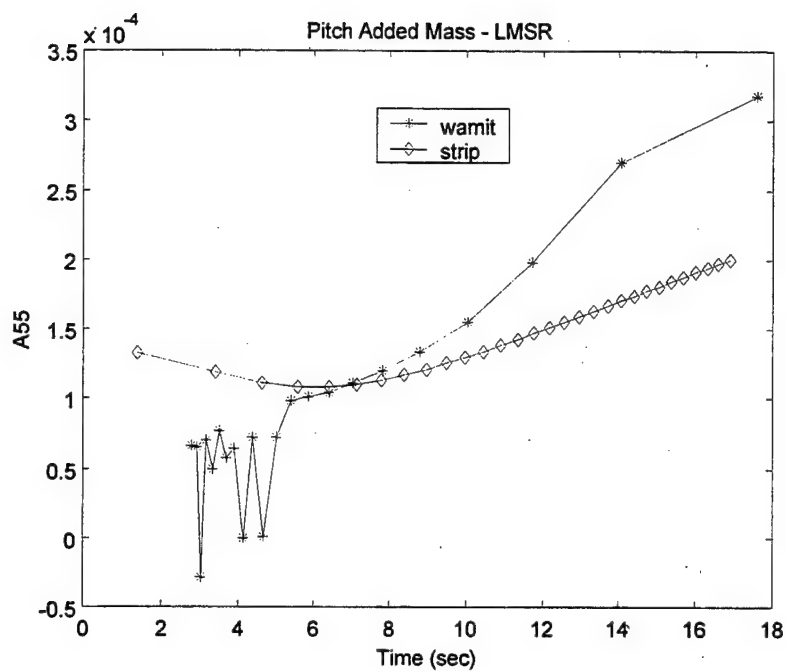


Figure 11. Plot of Strip Theory and Wamit Program Comparisons for Pitch Added Mass for the Old LMSR Data.

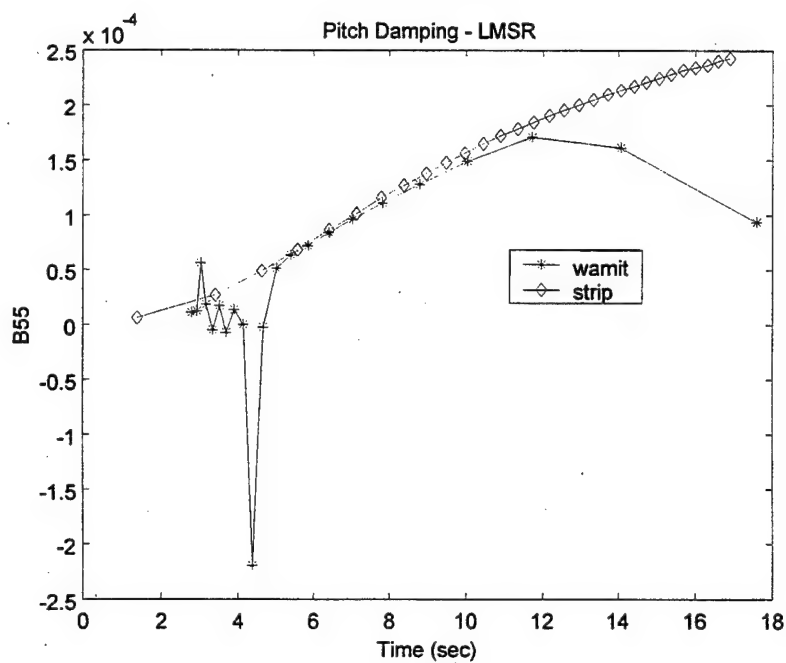


Figure 12. Plot of Strip Theory and Wamit Program Comparisons for Pitch Damping for the Old LMSR Data.

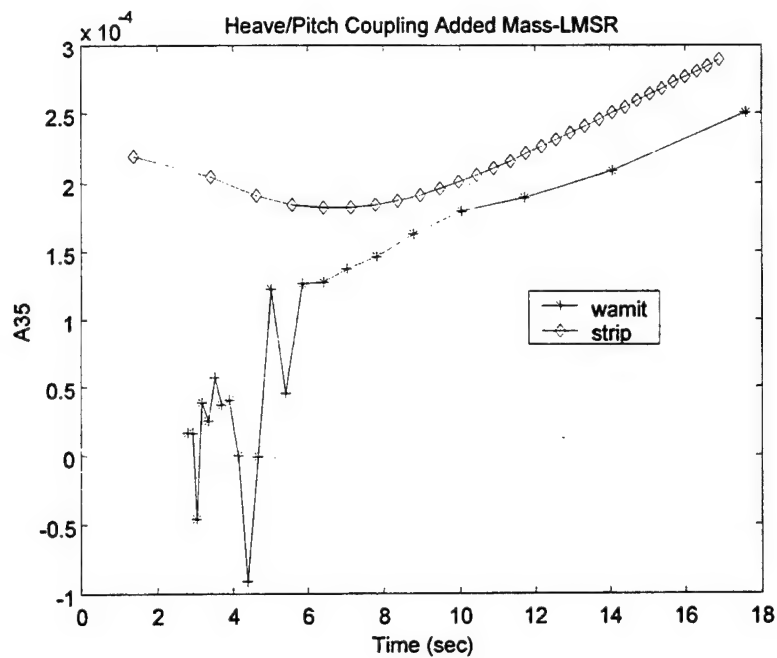


Figure 13. Plot of Strip Theory and Wamit Program Comparisons for Heave/Pitch Added Mass for the Old LMSR Data.

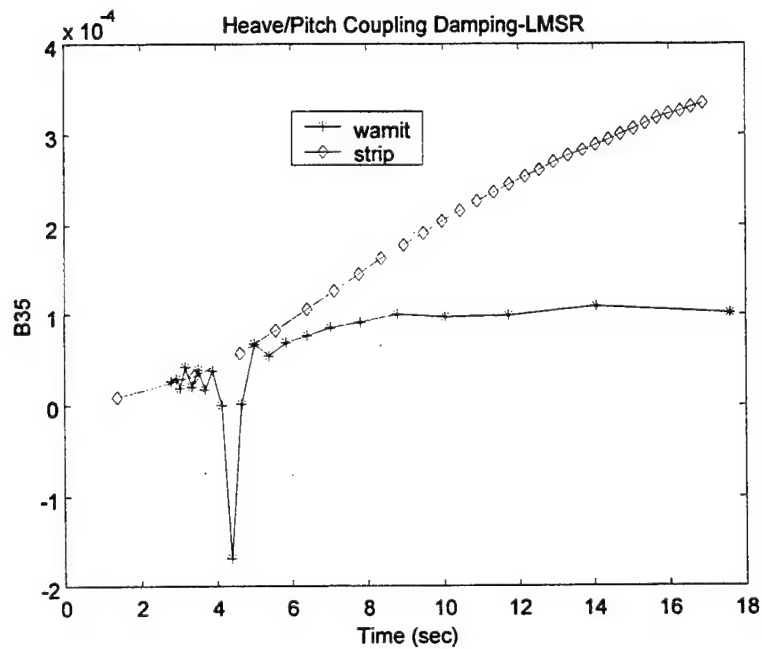


Figure 14. Plot of Strip Theory and Wamit Program Comparisons for Heave/Pitch Damping for the Old LMSR Data.

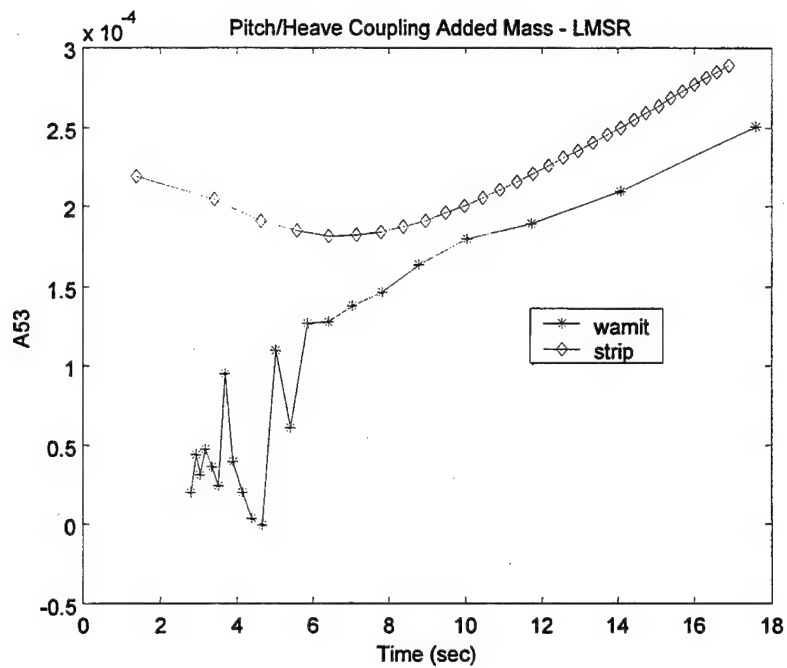


Figure 15. Plot of Strip Theory and Wamit Program Comparisons for Pitch/Heave Added Mass for the Old LMSR

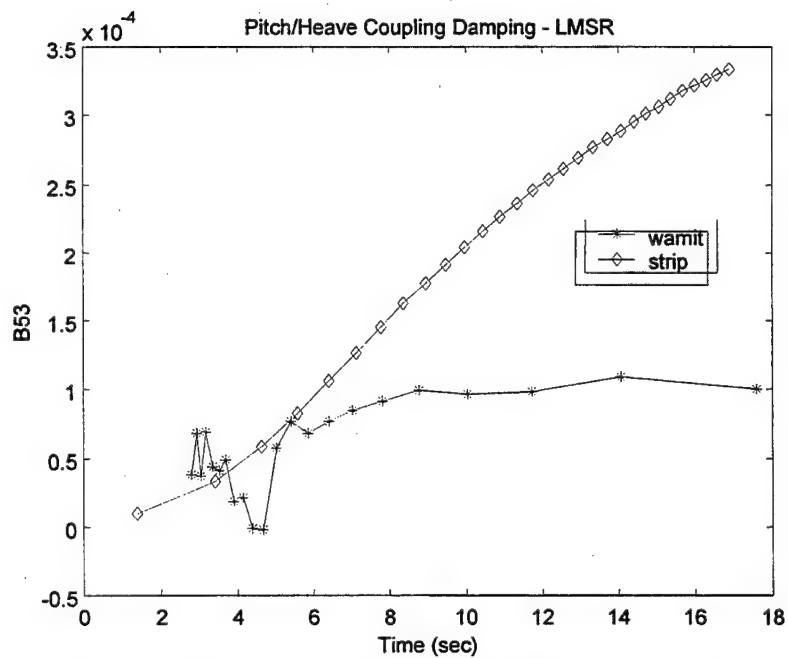


Figure 16. Plot of Strip Theory and Wamit Program Comparisons for Heave/Pitch Damping for the Old LMSR Data.

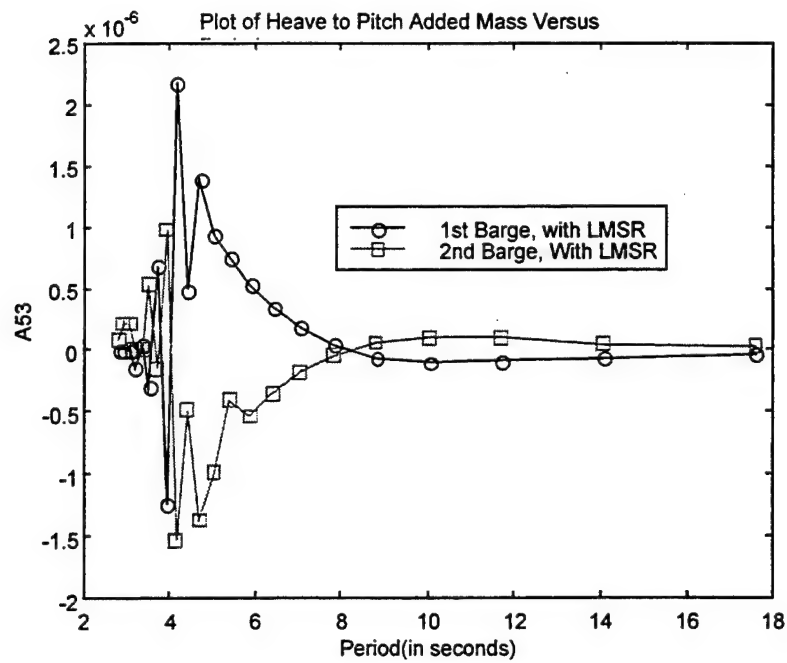


Figure 17. Plot of Multiple Barge Comparison for Heave to Pitch Added Mass.

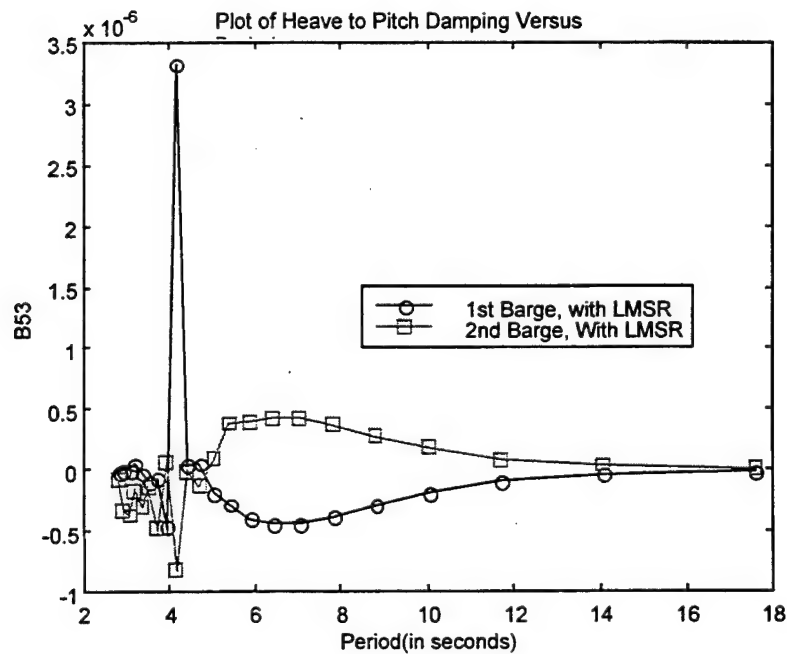


Figure 18. Plot of Multiple Barge Comparison for Heave to Pitch Damping.

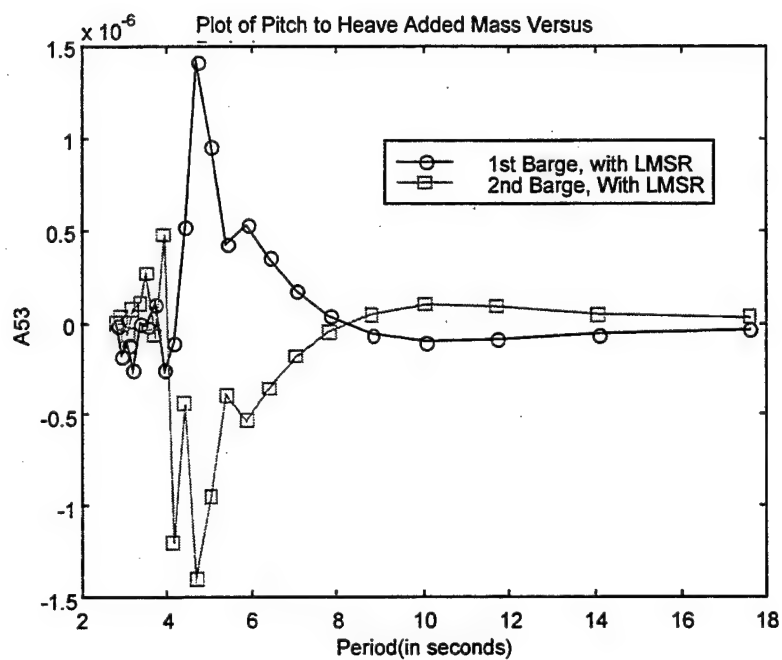


Figure 19. Plot of Multiple Barge Comparison for Pitch to Heave Added Mass.

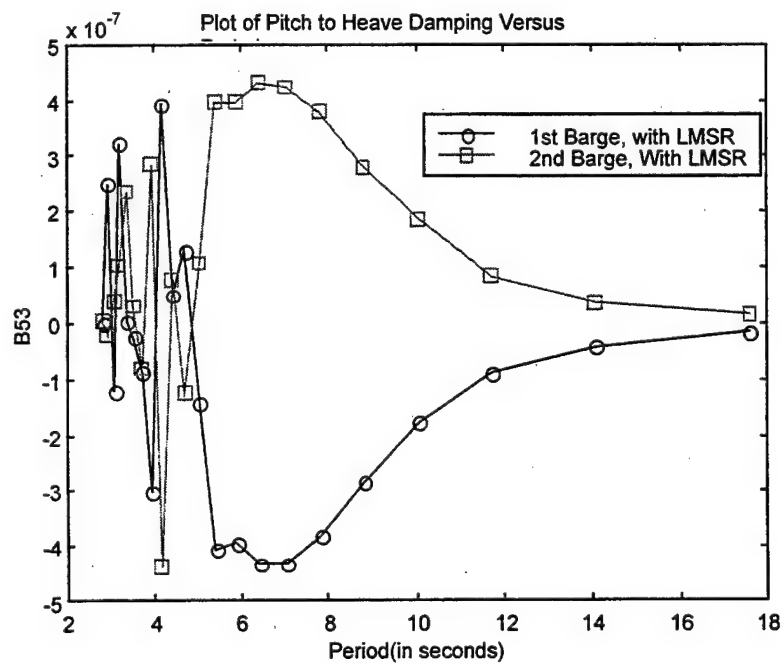


Figure 20. Plot of Multiple Barge Comparison for Pitch to Heave Damping.

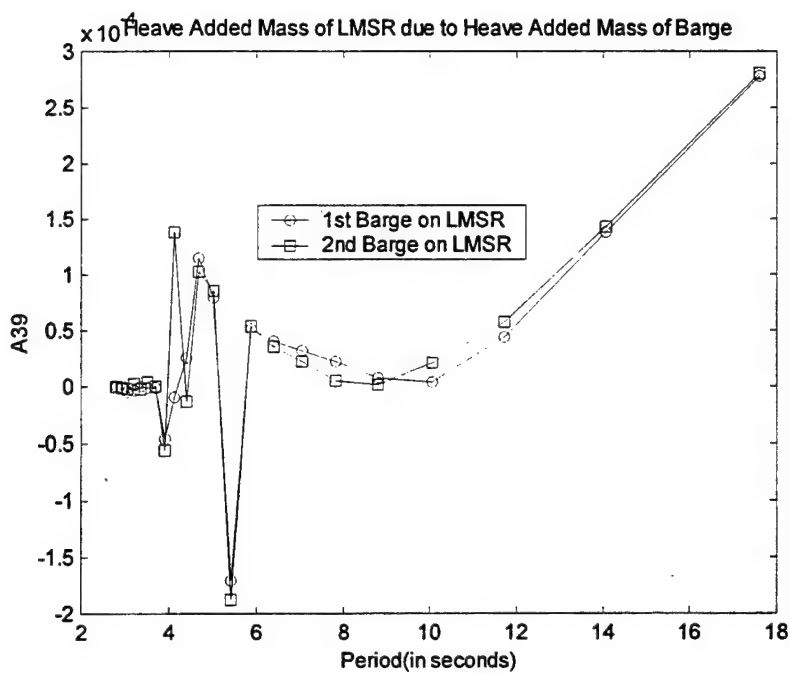


Figure 21. Plot of Multiple Barge Comparison for Heave Added Mass of LMSR due to Heave Added Mass of Barge.

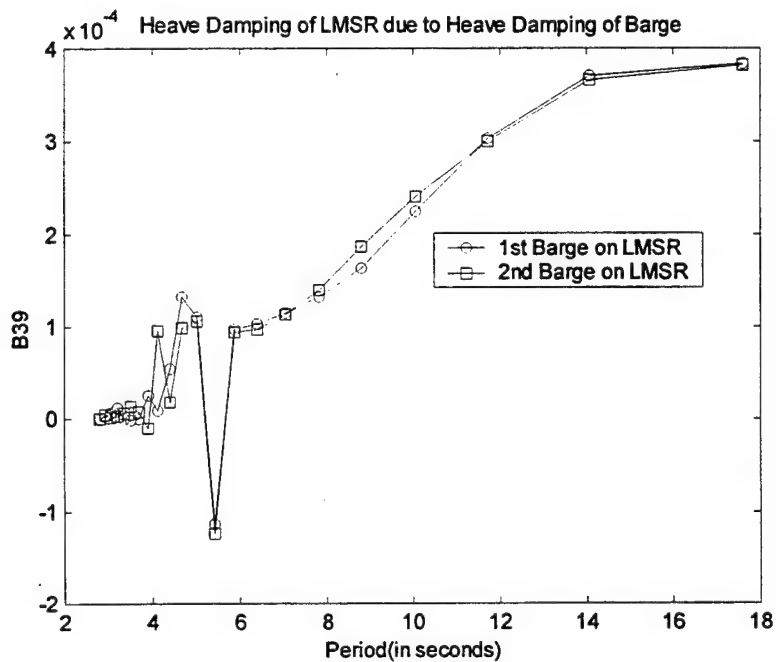


Figure 22. Plot of Multiple Barge Comparison for Heave Damping of LMSR due to Heave Damping of Barge.

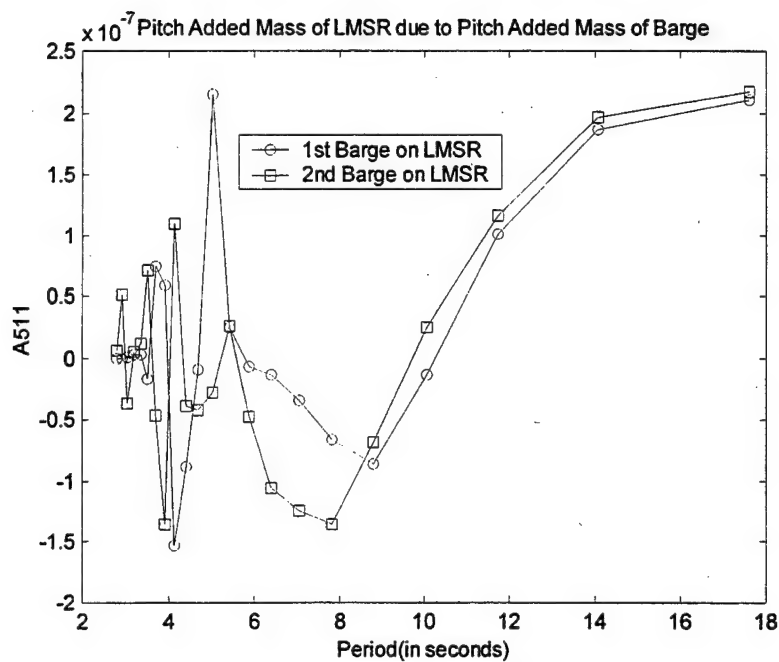


Figure 23. Plot of Multiple Barge Comparison for Pitch Added Mass of LMSR due to Pitch Added Mass of Barge.

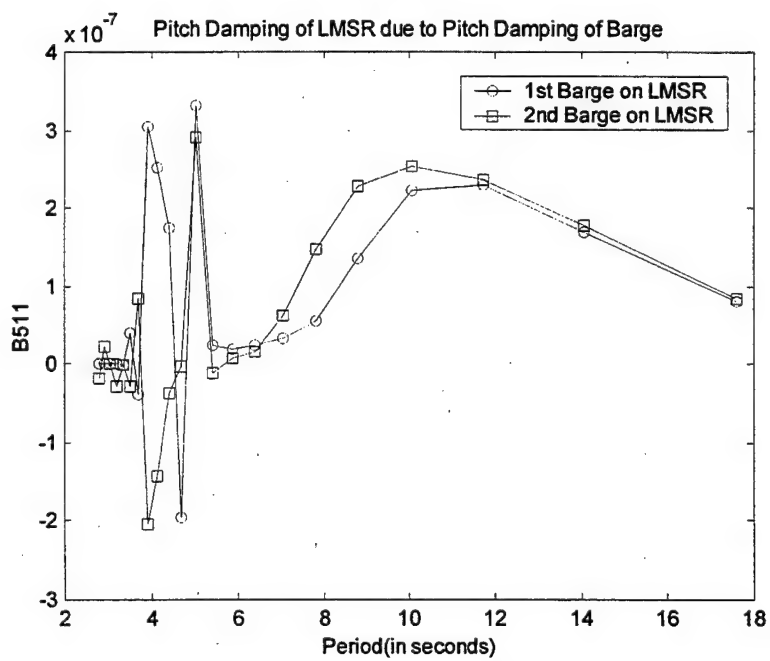


Figure 24. Plot of Multiple Barge Comparison for Pitch Damping of LMSR due to Pitch Damping of Barge.

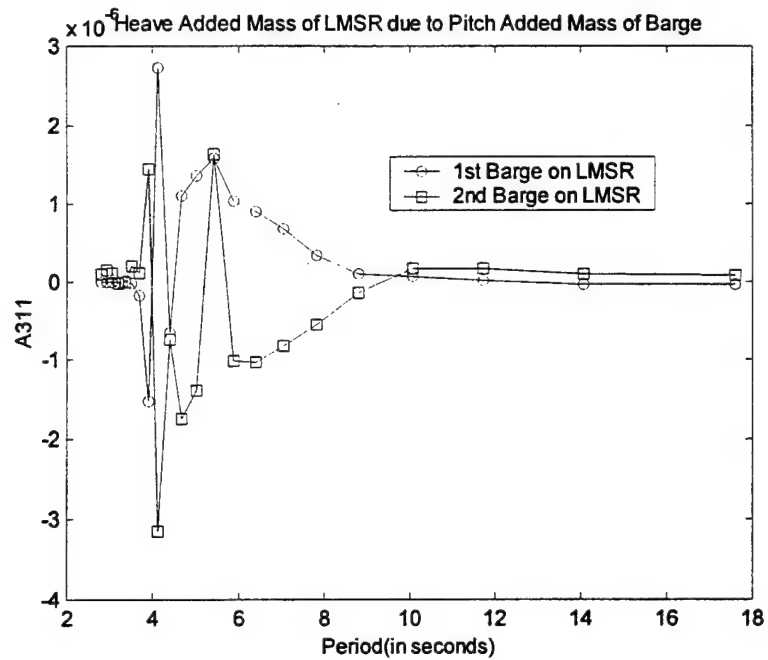


Figure 25. Plot of Multiple Barge Comparison for Heave Added Mass of LMSR due to Pitch Added Mass of Barge.

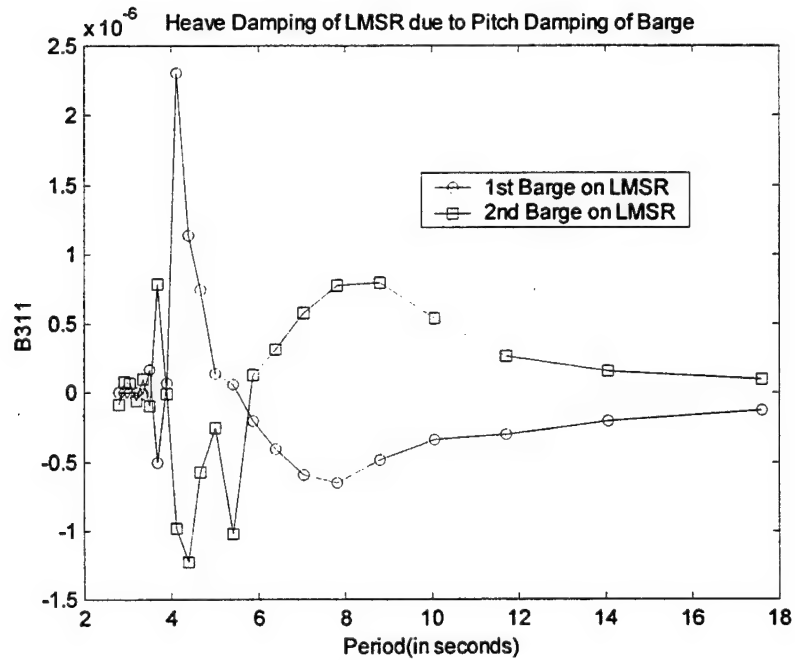


Figure 26. Plot of Multiple Barge Comparison for Heave Damping of LMSR due to Pitch Damping of Barge.

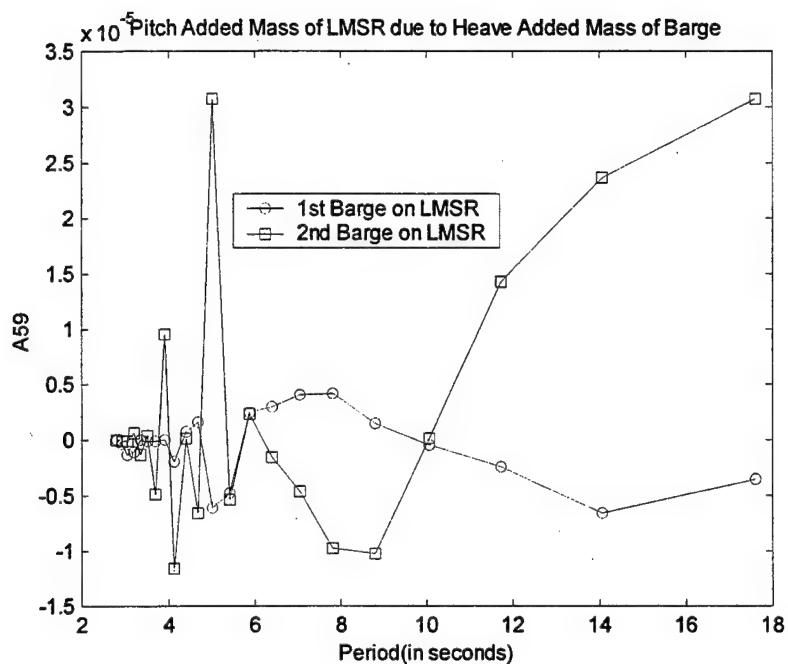


Figure 27. Plot of Multiple Barge Comparison for Pitch Added Mass of LMSR due to Heave Added Mass of Barge.

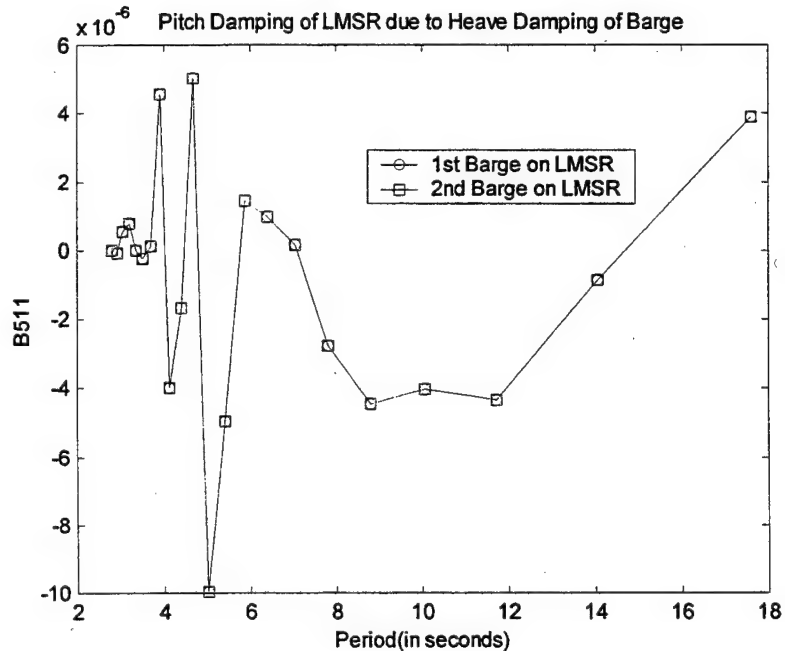


Figure 28. Plot of Multiple Barge Comparison for Pitch Damping of LMSR due to Heave Damping of Barge.

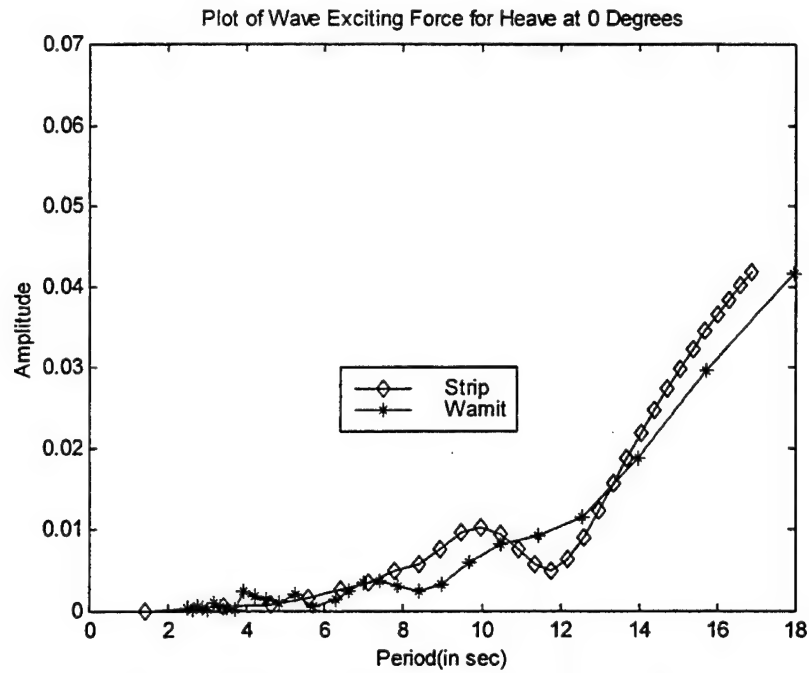


Figure 29. Plot of Strip Theory and Wamit Program Comparisons for Heave Exciting Force at an Incident Wave Angle of 0 Degrees for the LMSR.

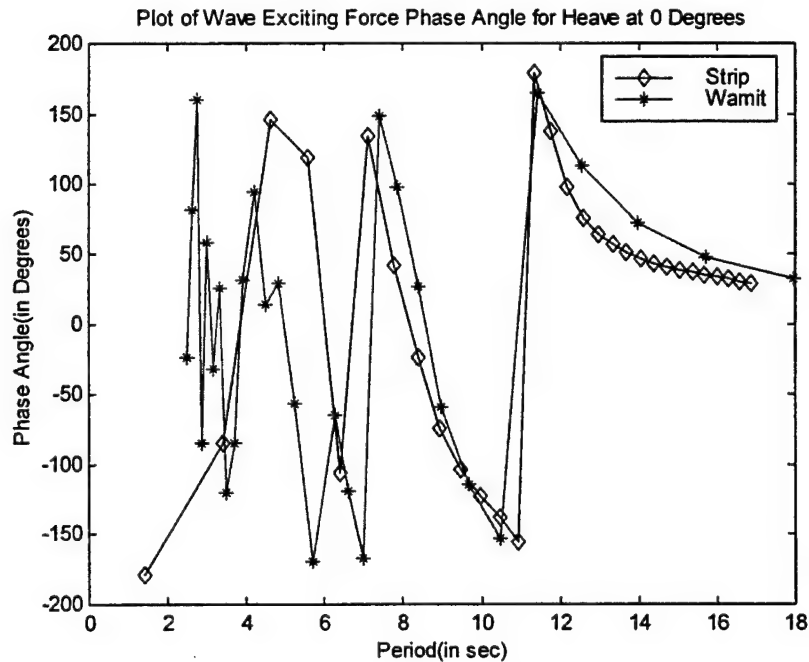


Figure 30. Plot of Strip Theory and Wamit Program Comparisons for Heave Exciting Force Phase Angle at an Incident Wave Angle of 0 Degrees for the LMSR.

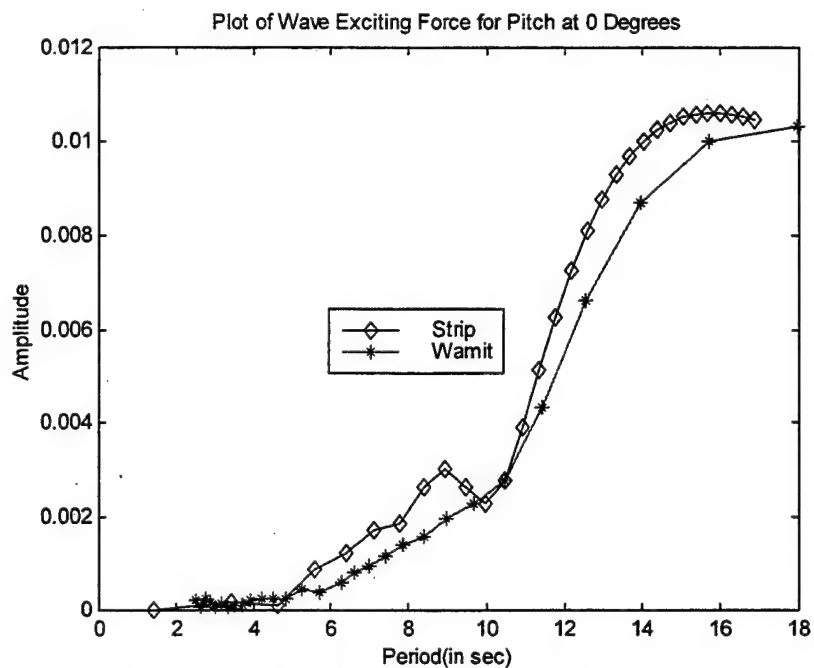


Figure 31. Plot of Strip Theory and Wamit Program Comparisons for Pitch Exciting Force at an Incident Wave Angle of 0 Degrees for the LMSR

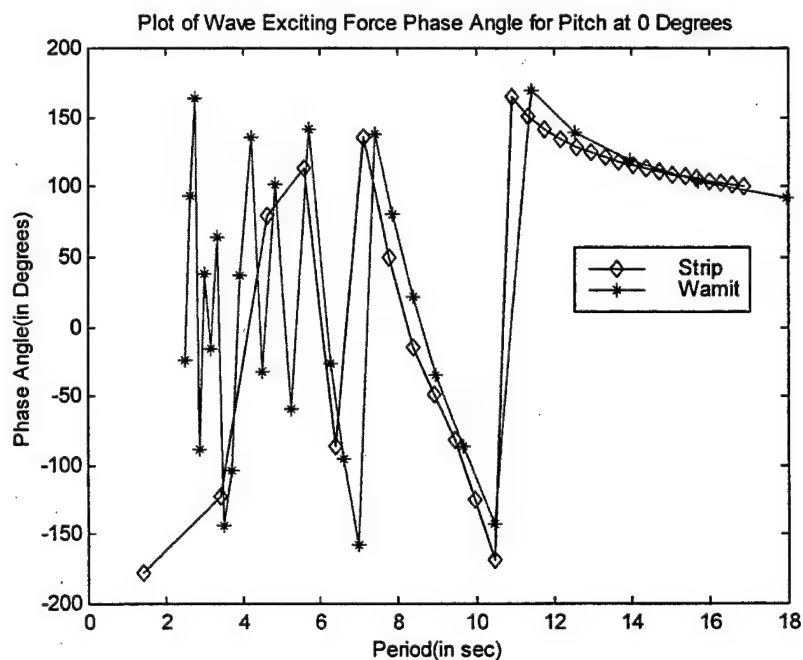


Figure 32. Plot of Strip Theory and Wamit Program Comparisons for Pitch Exciting Force Phase Angle at an Incident Wave Angle of 0 Degrees for the LMSR.

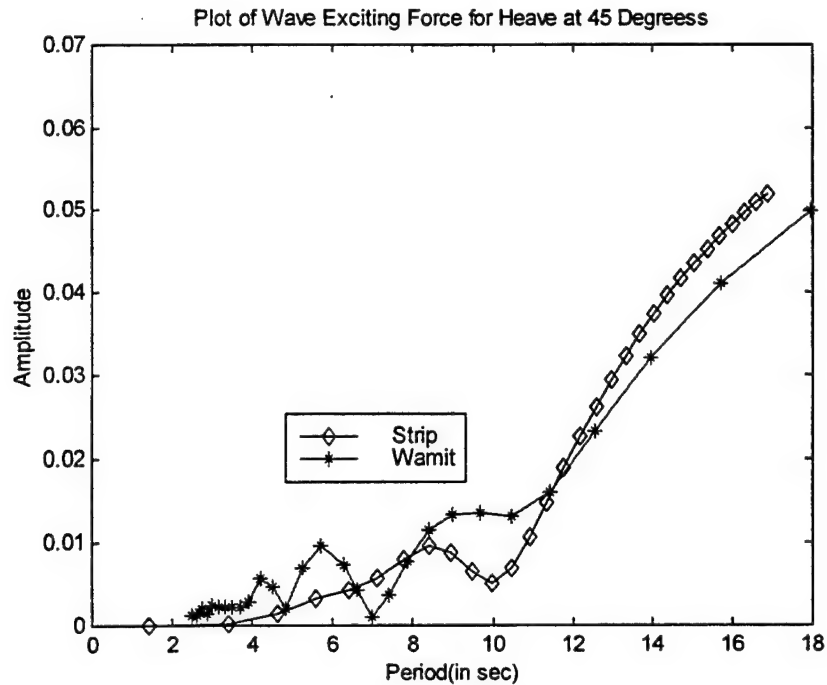


Figure 33. Plot of Strip Theory and Wamit Program Comparisons for Heave Exciting Force at an Incident Wave Angle of 45 Degrees for the LMSR

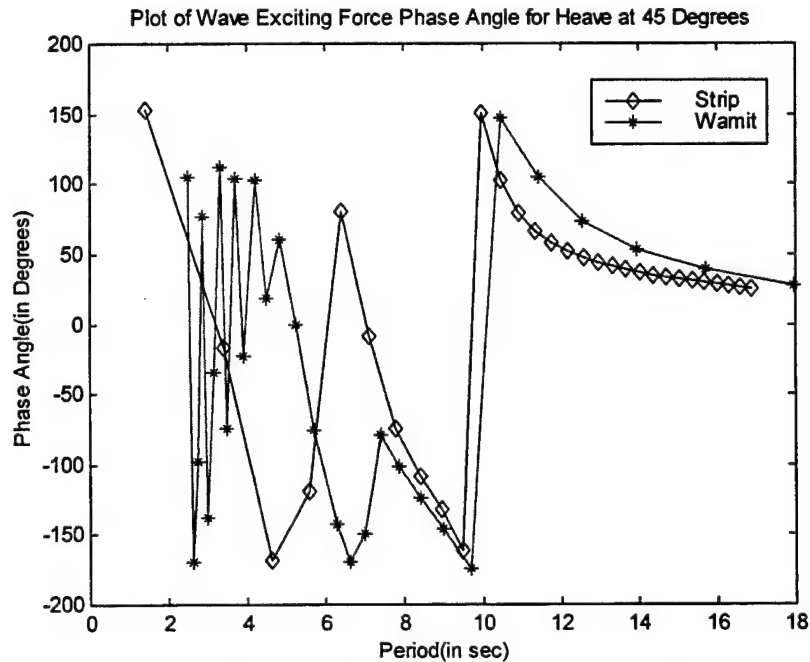


Figure 34. Plot of Strip Theory and Wamit Program Comparisons for Heave Exciting Force Phase Angle at an Incident Wave Angle of 45 Degrees for the LMSR.

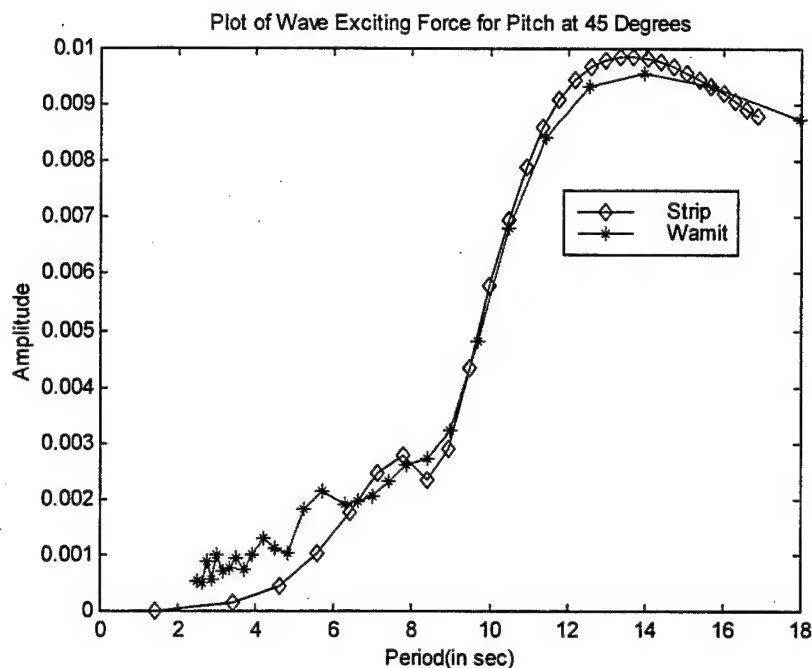


Figure 35. Plot of Strip Theory and Wamit Program Comparisons for Pitch Exciting Force at an Incident Wave Angle of 45 Degrees for the LMSR

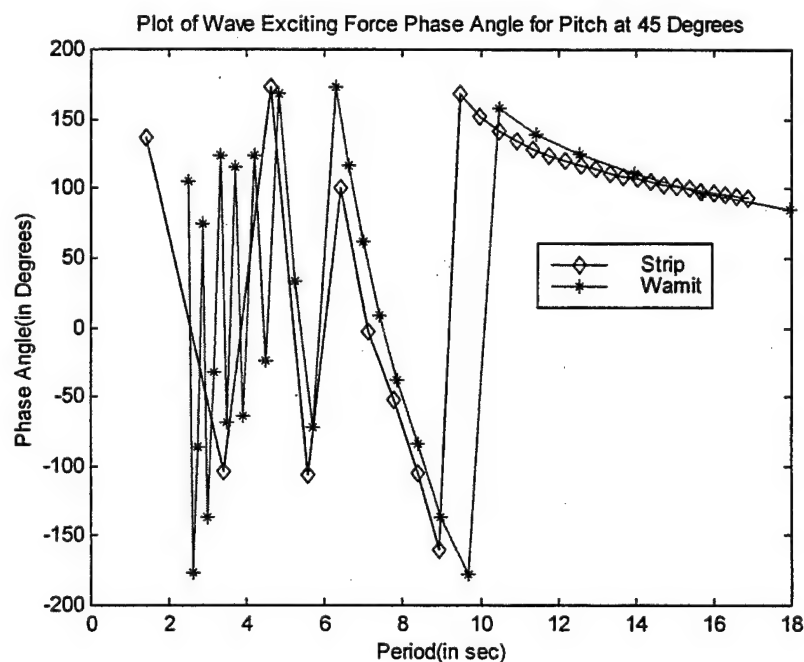


Figure 36. Plot of Strip Theory and Wamit Program Comparisons for Pitch Exciting Force Phase Angle at an Incident Wave Angle of 45 Degrees for the LMSR.

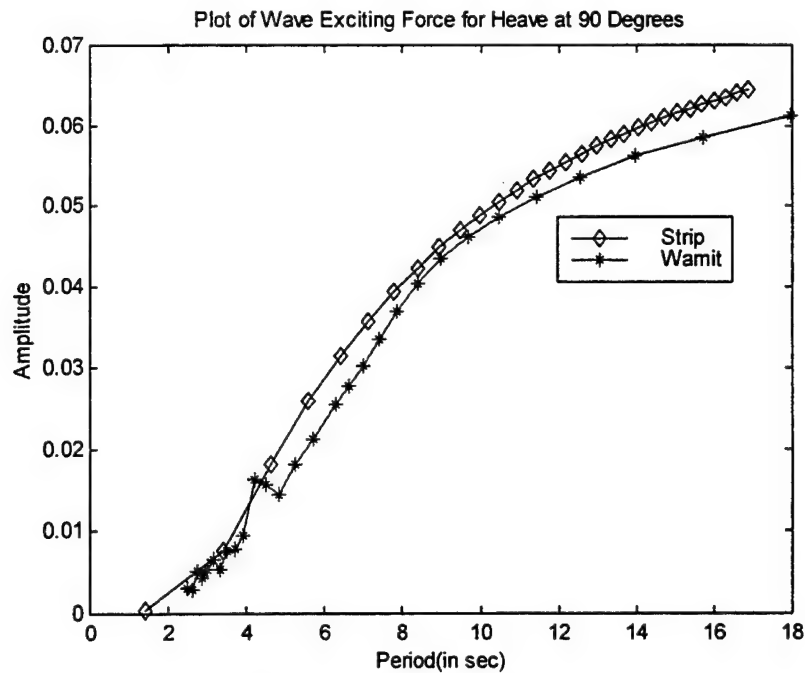


Figure 37. Plot of Strip Theory and Wamit Program Comparisons for Heave Exciting Force at an Incident Wave Angle of 90 Degrees for the LMSR.

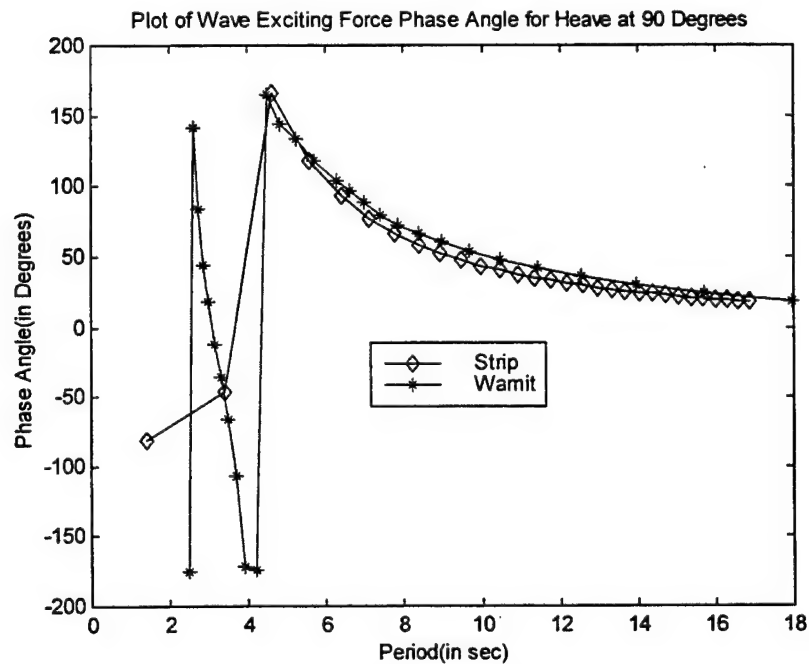


Figure 38. Plot of Strip Theory and Wamit Program Comparisons for Heave Exciting Force Phase Angle at an Incident Wave Angle of 90 Degrees for the LMSR.

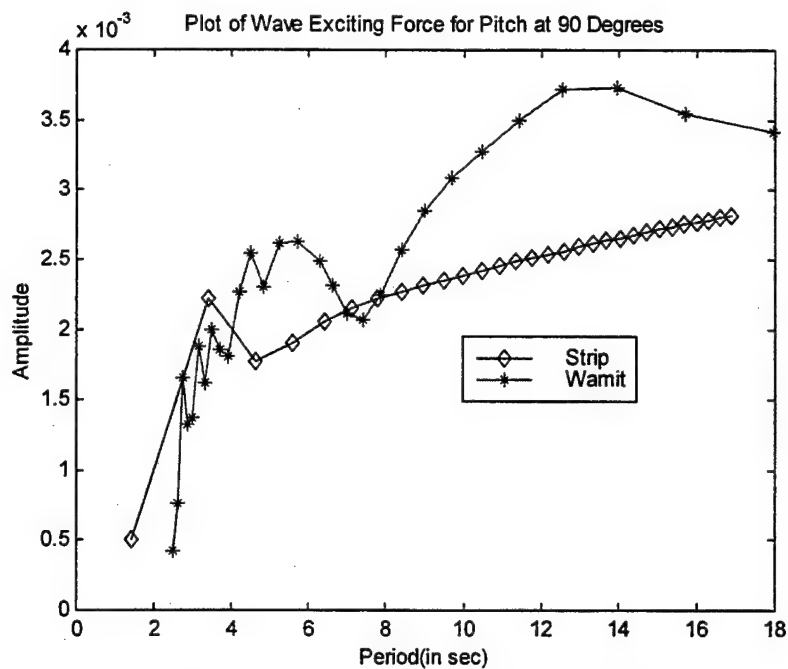


Figure 39. Plot of Strip Theory and Wamit Program Comparisons for Pitch Exciting Force at an Incident Wave Angle of 90 Degrees for the LMSR.

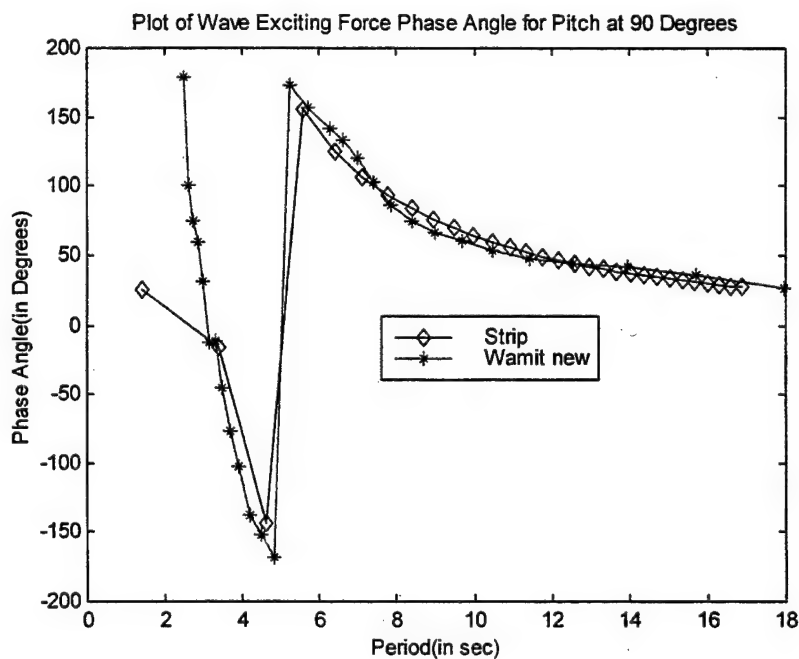


Figure 40. Plot of Strip Theory and Wamit Program Comparisons for Pitch Exciting Force Phase Angle at an Incident Wave Angle of 90 Degrees for the LMSR.

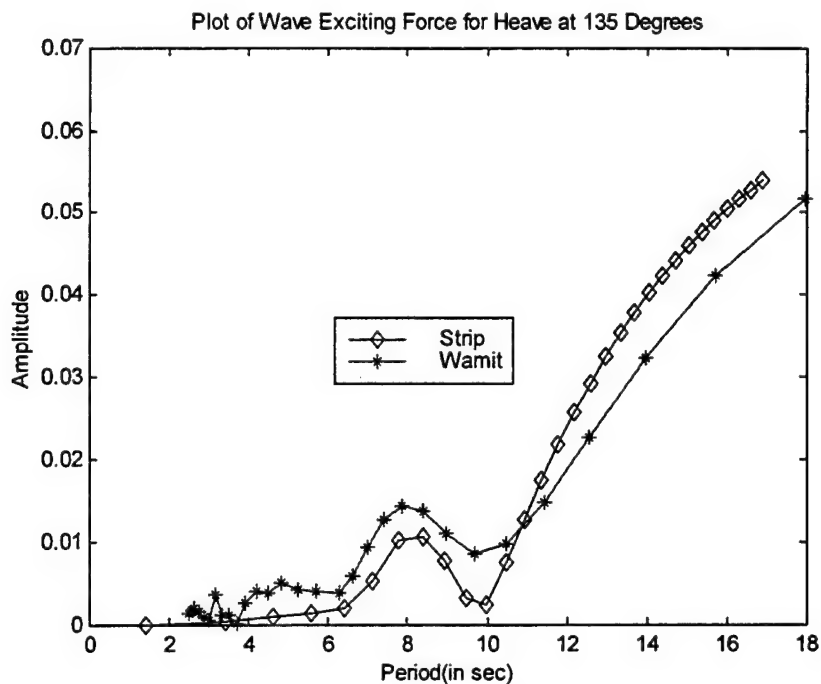


Figure 41. Plot of Strip Theory and Wamit Program Comparisons for Heave Exciting Force at an Incident Wave Angle of 135 Degrees for the LMSR.

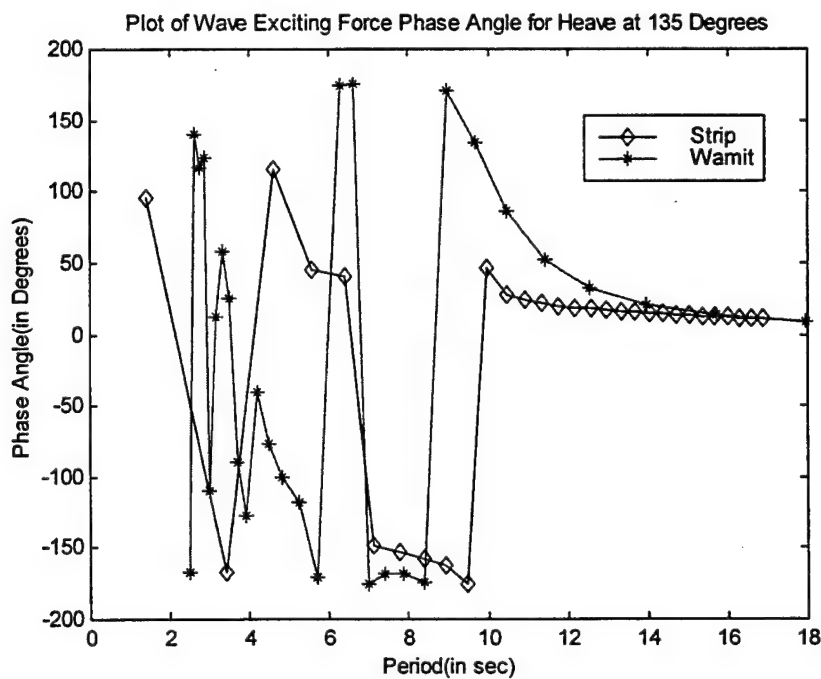


Figure 42. Plot of Strip Theory and Wamit Program Comparisons for Heave Exciting Force Phase Angle at an Incident Wave Angle of 135 Degrees for the LMSR.

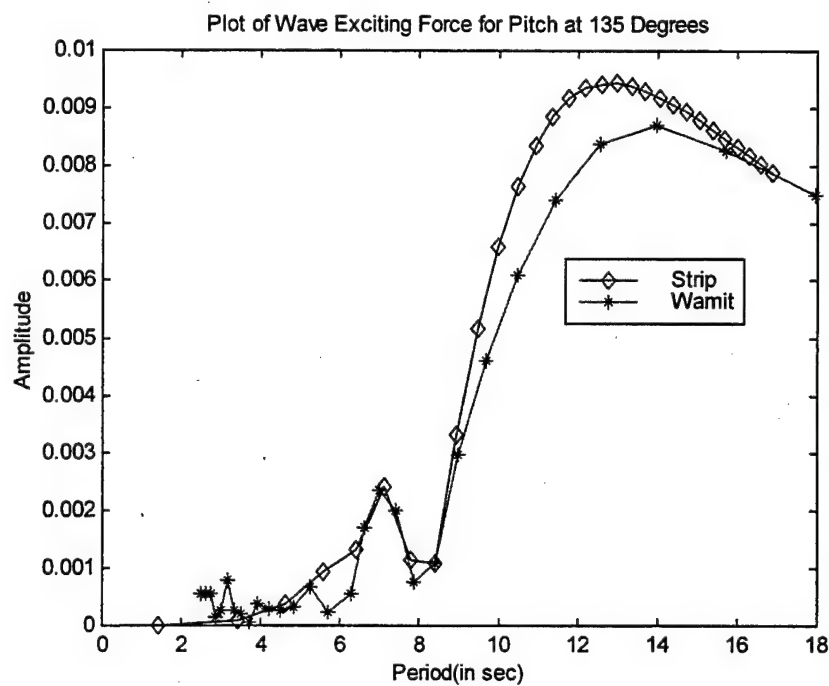


Figure 43. Plot of Strip Theory and Wamit Program Comparisons for Pitch Exciting Force at an Incident Wave Angle of 135 Degrees for the LMSR.

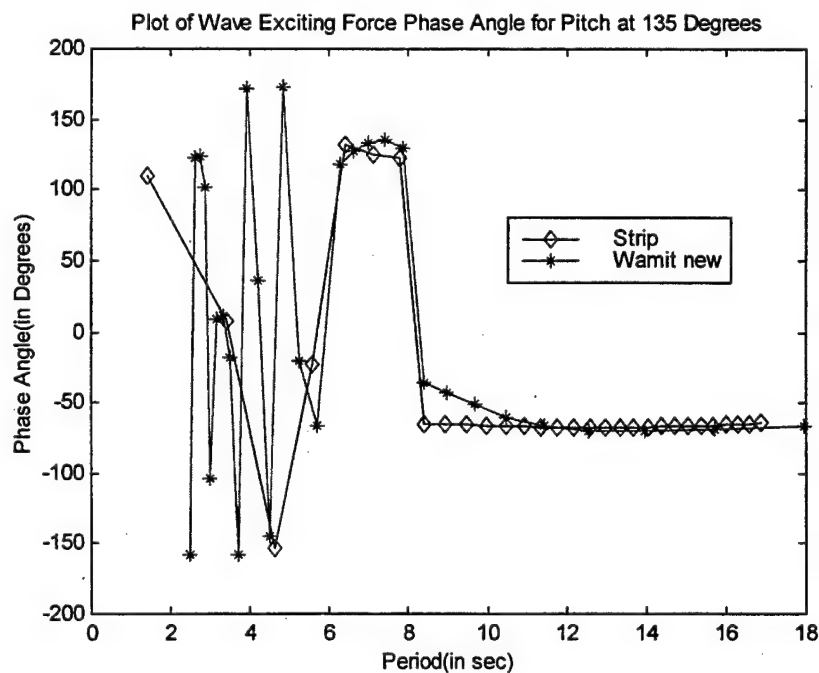


Figure 44. Plot of Strip Theory and Wamit Program Comparisons for Pitch Exciting Force Phase Angle at an Incident Wave Angle of 135 Degrees for the LMSR.

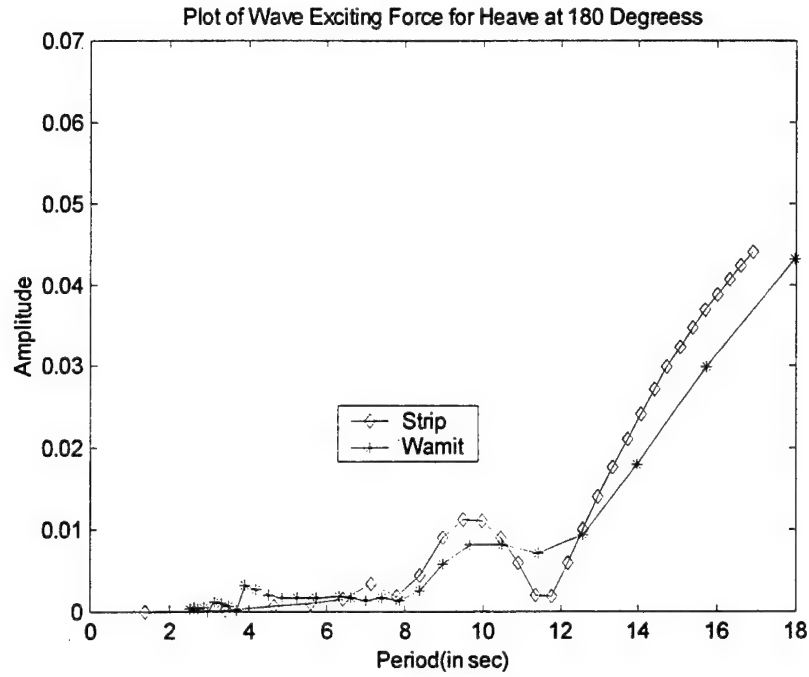


Figure 45. Plot of Strip Theory and Wamit Program Comparisons for Heave Exciting Force at an Incident Wave Angle of 180 Degrees for the LMSR.

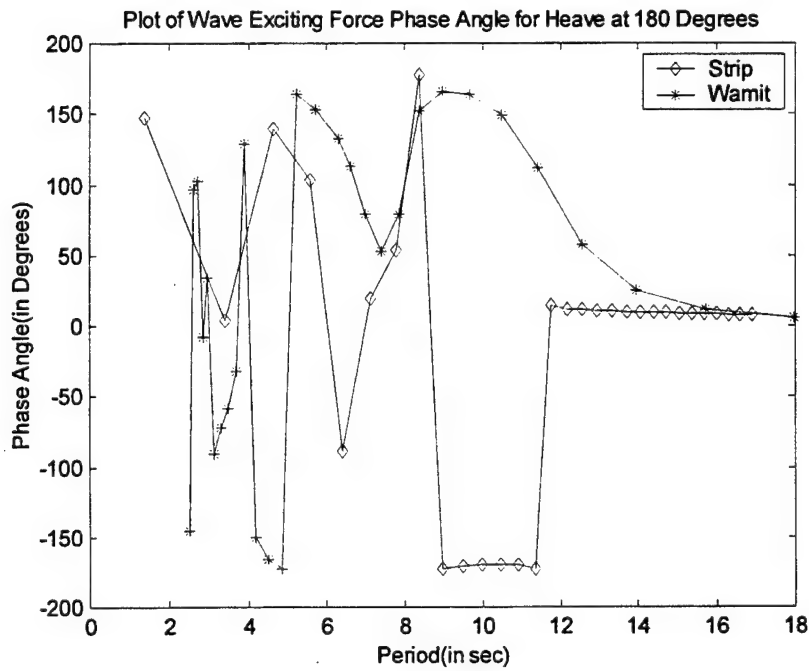


Figure 46. Plot of Strip Theory and Wamit Program Comparisons for Heave Exciting Force Phase Angle at an Incident Wave Angle of 180 Degrees for the LMSR.

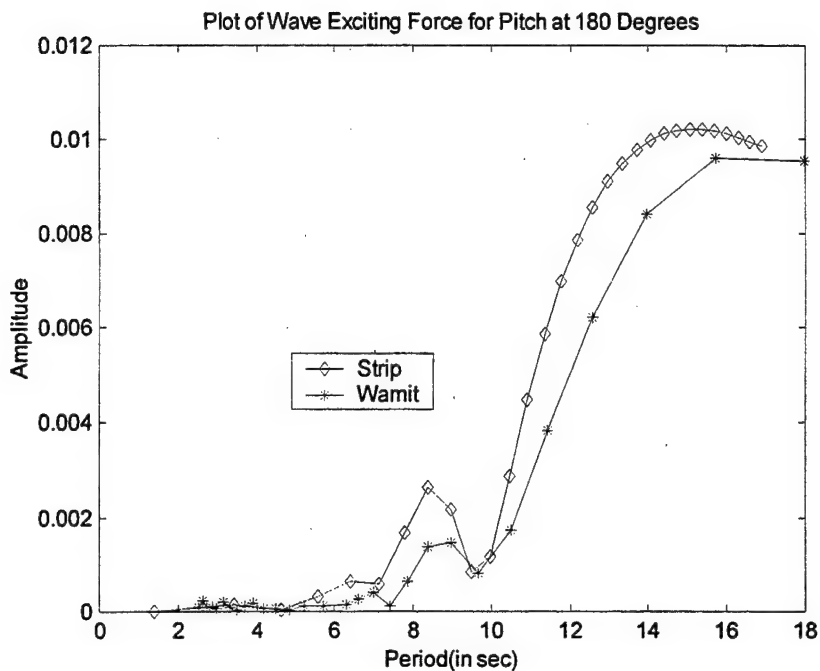


Figure 47. Plot of Strip Theory and Wamit Program Comparisons for Pitch Exciting Force at an Incident Wave Angle of 180 Degrees for the LMSR.

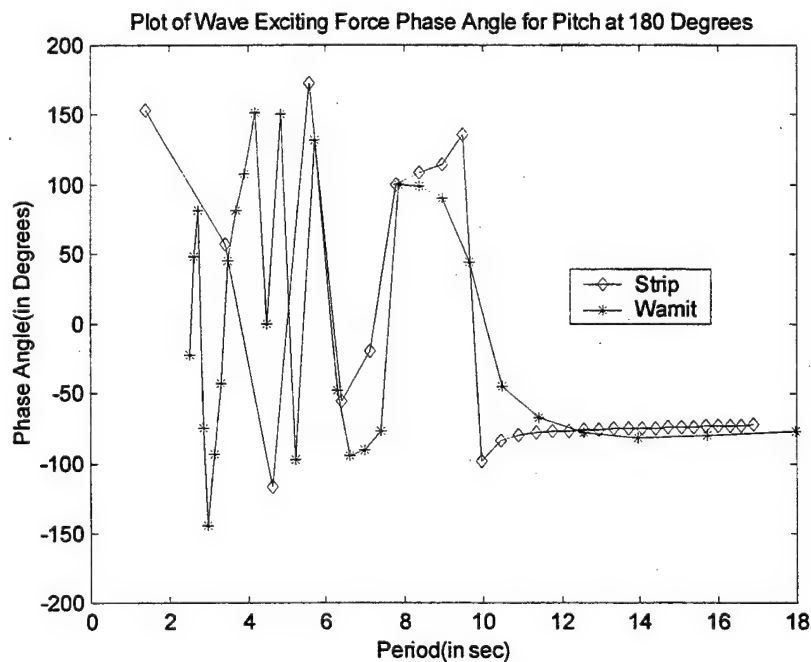


Figure 48. Plot of Strip Theory and Wamit Program Comparisons for Pitch Exciting Force Phase Angle at an Incident Wave Angle of 180 Degrees for the LMSR.

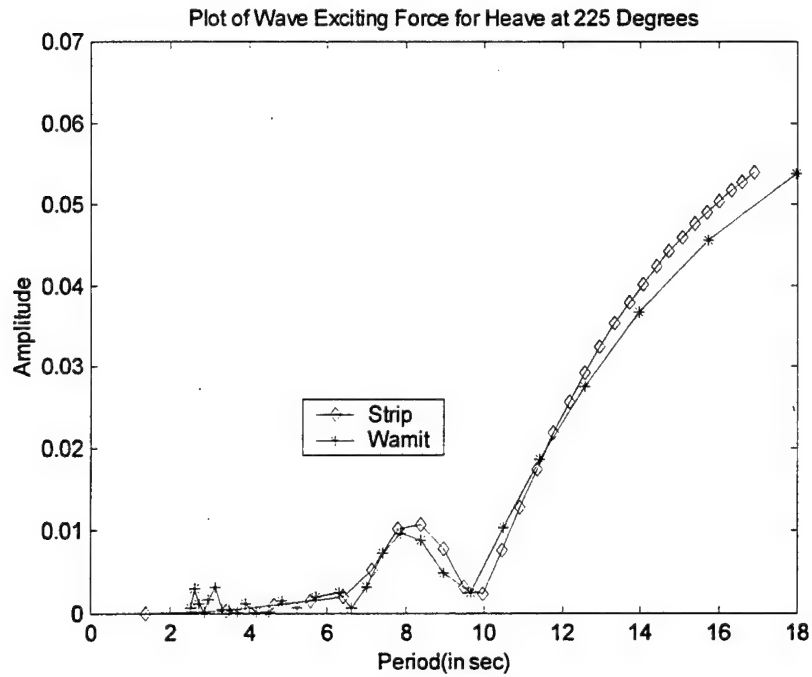


Figure 49. Plot of Strip Theory and Wamit Program Comparisons for Heave Exciting Force at an Incident Wave Angle of 225 Degrees for the LMSR.

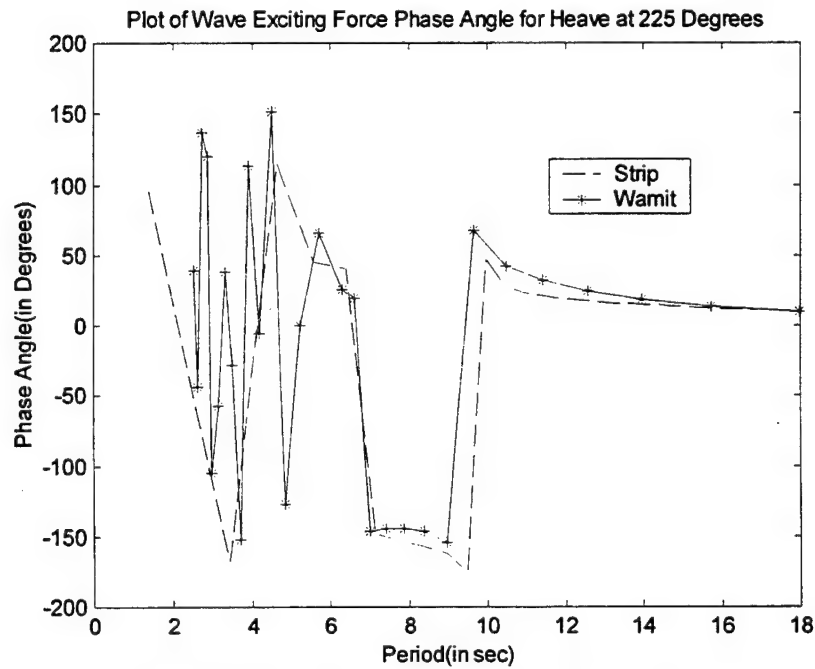


Figure 50. Plot of Strip Theory and Wamit Program Comparisons for Heave Exciting Force Phase Angle at an Incident Wave Angle of 225 Degrees for the LMSR.

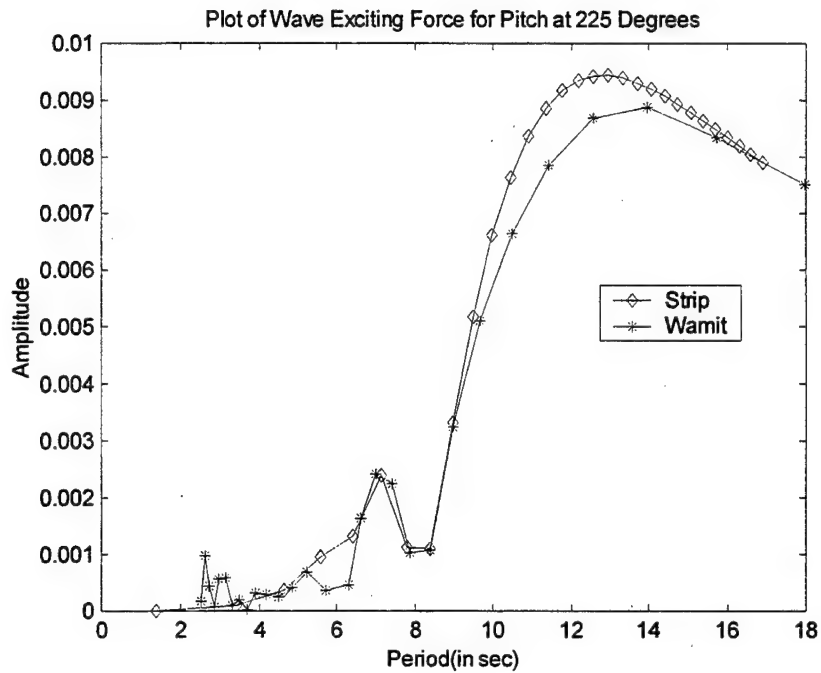


Figure 51. Plot of Strip Theory and Wamit Program Comparisons for Pitch Exciting Force at an Incident Wave Angle of 225 Degrees for the LMSR.

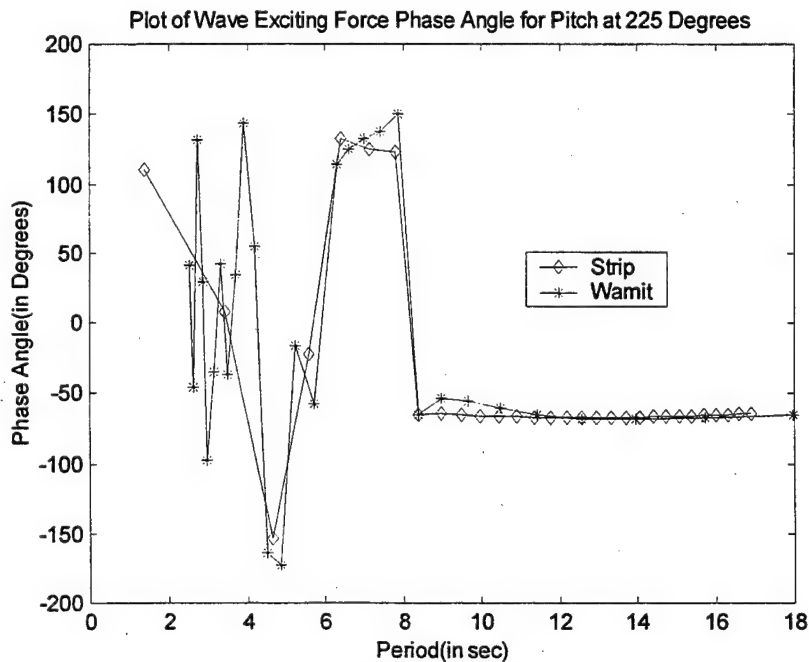


Figure 52. Plot of Strip Theory and Wamit Program Comparisons for Pitch Exciting Force Phase Angle at an Incident Wave Angle of 225 Degrees for the LMSR.

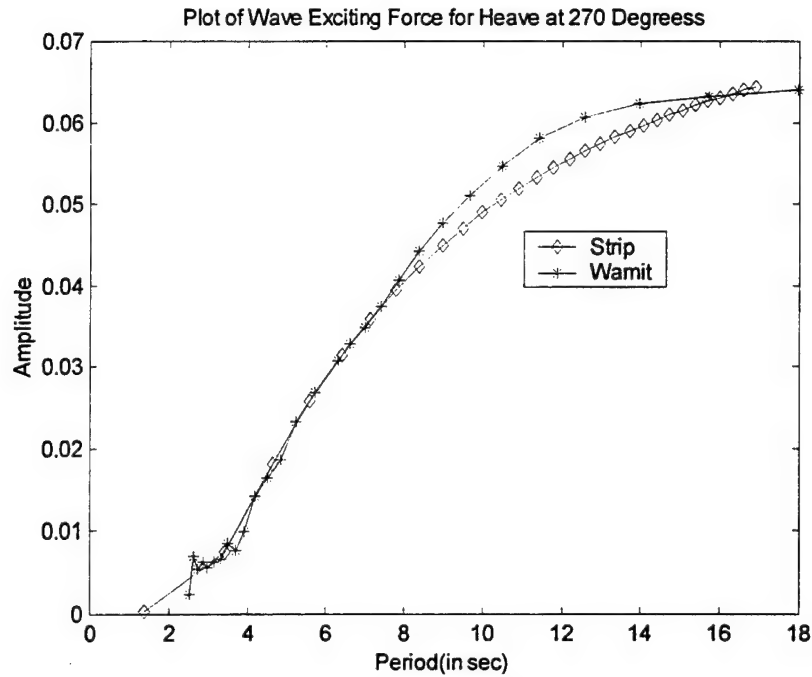


Figure 53. Plot of Strip Theory and Wamit Program Comparisons for Heave Exciting Force at an Incident Wave Angle of 270 Degrees for the LMSR.

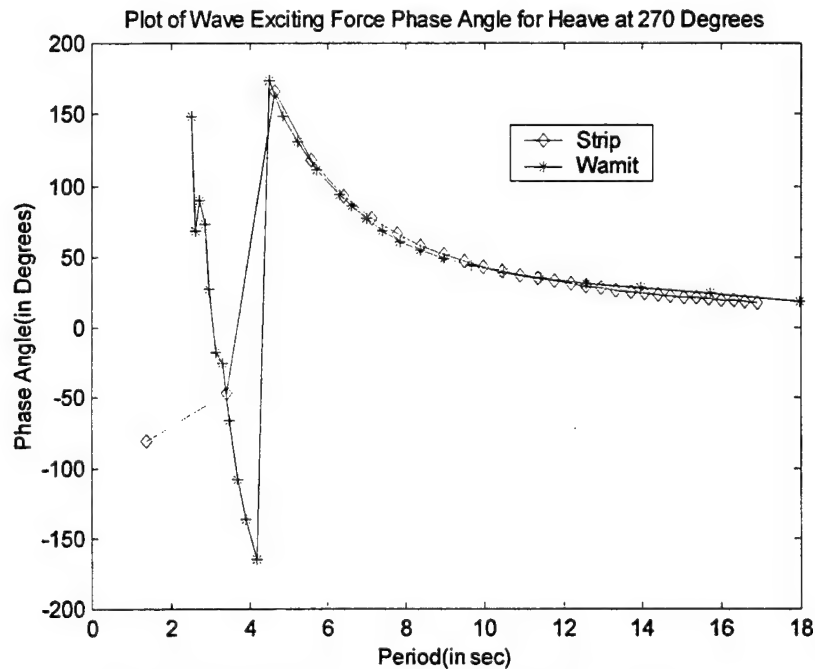


Figure 54. Plot of Strip Theory and Wamit Program Comparisons for Heave Exciting Force Phase Angle at an Incident Wave Angle of 270 Degrees for the LMSR.

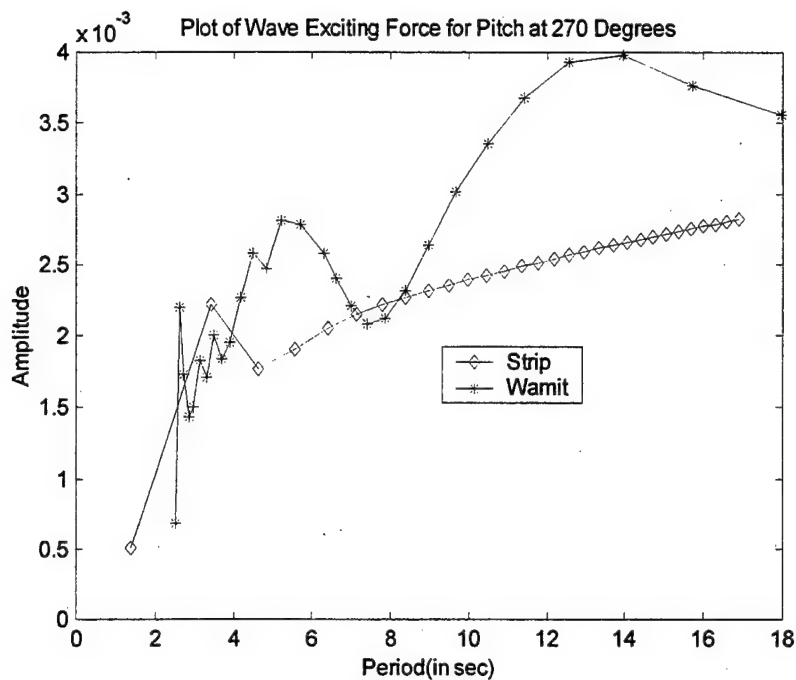


Figure 55. Plot of Strip Theory and Wamit Program Comparisons for Pitch Exciting Force Phase Angle at an Incident Wave Angle of 270 Degrees for the LMSR.

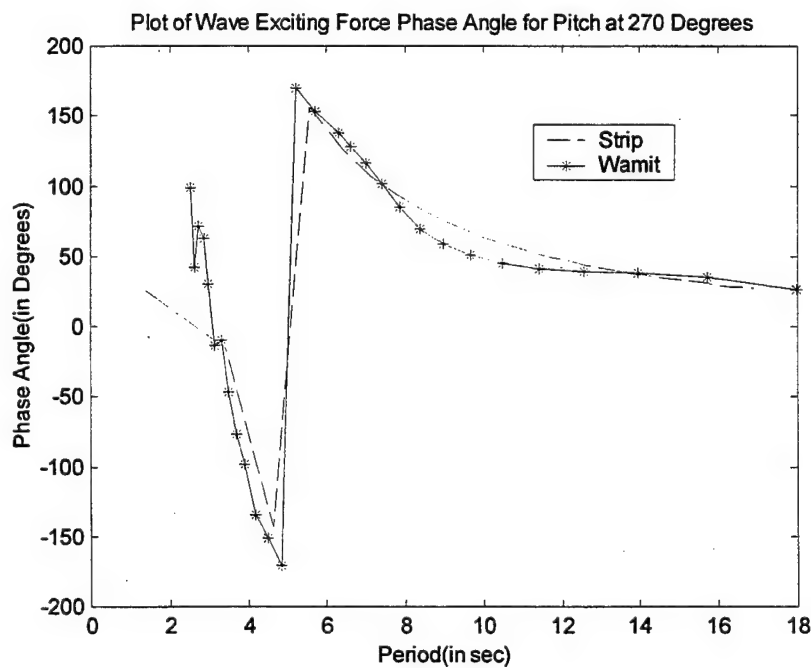


Figure 56. Plot of Strip Theory and Wamit Program Comparisons for Pitch Exciting Force Phase Angle at an Incident Wave Angle of 270 Degrees for the LMSR.

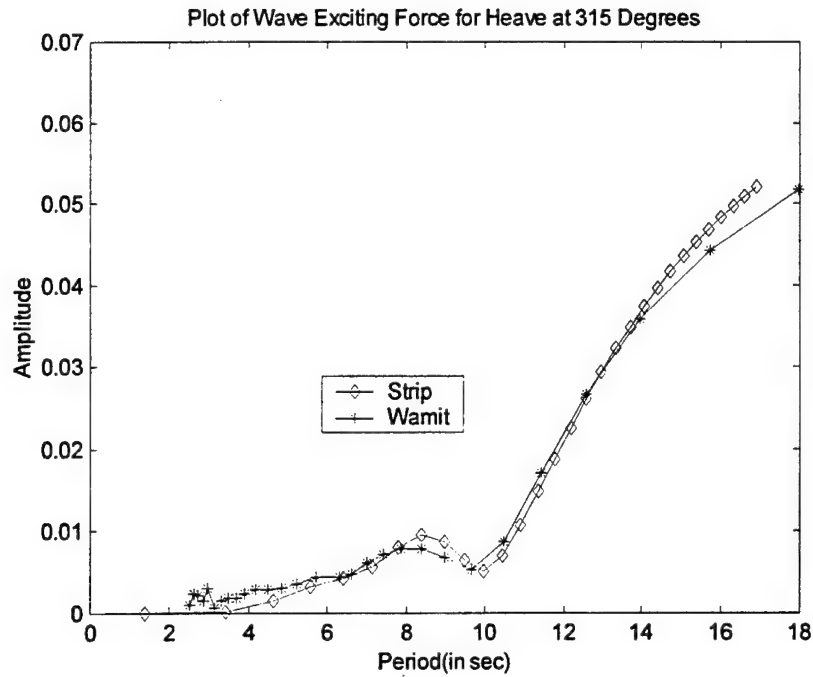


Figure 57. Plot of Strip Theory and Wamit Program Comparisons for Heave Exciting Force at an Incident Wave Angle of 315 Degrees for the LMSR

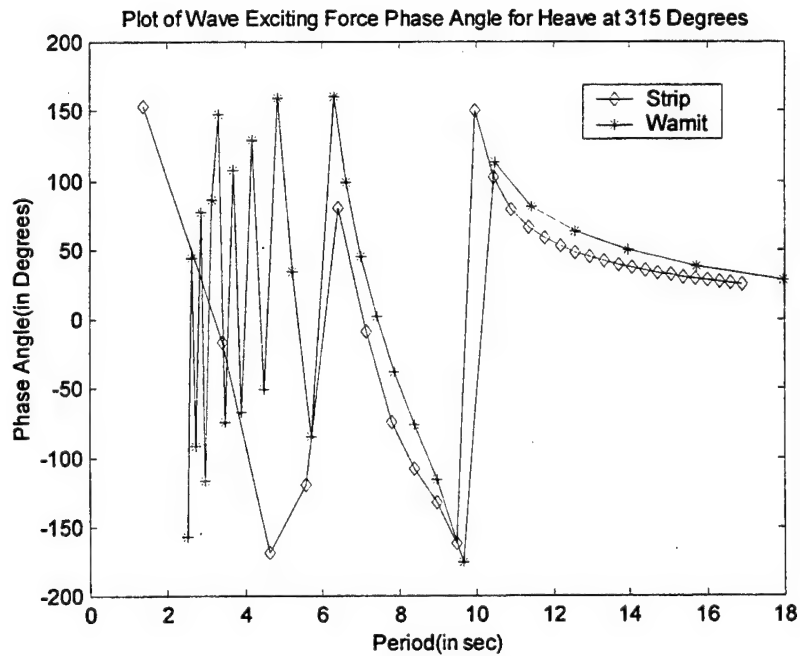


Figure 58. Plot of Strip Theory and Wamit Program Comparisons for Heave Exciting Force Phase Angle at an Incident Wave Angle of 315 Degrees for the LMSR.

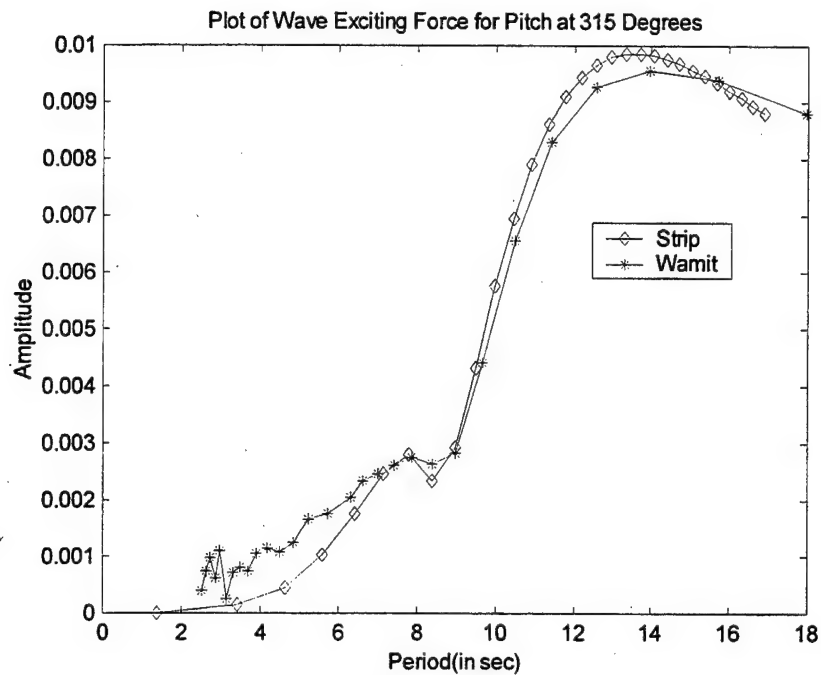


Figure 59. Plot of Strip Theory and Wamit Program Comparisons for Pitch Exciting Force at an Incident Wave Angle of 315 Degrees for the LMSR

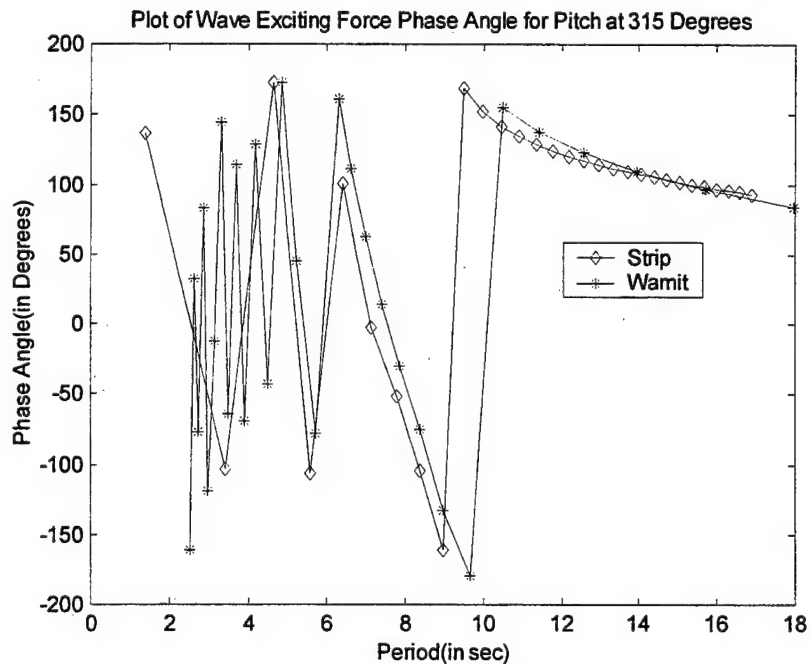


Figure 60. Plot of Strip Theory and Wamit Program Comparisons for Pitch Exciting Force Phase Angle at an Incident Wave Angle of 315 Degrees for the LMSR.

B. ROLL-ON, ROLL-OFF DISCHARGE FACILITY (BARGE) ANALYSIS

1. Introduction

The hydrodynamic characteristics of the Roll-On, Roll-Off Discharge Facility (RRDF) are presented in Figures 61 through 106. These figures present a very detailed analysis of the barge and describe the effects of the large medium speed roll-on roll-off vessel (LMSR) on the barge.

2. Data Analysis

Figure 61 illustrates the added mass in heave for a barge unit by itself and also the leading (first) and trailing (second) barges located on the starboard side of the ship. The results displayed in all the figures are in nondimensional form as described in Table 1. It should be noted that the characteristic length which is utilized to nondimensionalize the values for the barges are that of the ship and not of the barge. The reasoning for this is to ensure all numbers are nondimensionalized using the same method, which allows for a more accurate comparison of results.

The results displayed are those for the three-dimensional (3-D) solver only, which modeled the RRDF as a square platform with shallow draft. The actual dimensions for the RRDF are given in Table 3. Due to the lack of a precise draft, the results generated by the use of the strip theory solver were determined to be erroneous, exhibiting large divergences from the 3-D solver for many different values. Therefore, data was compared against a stationary barge labeled "1 Barge" in the figures. This generated the basis for establishing the relative significance of hydrodynamic proximity effects. The results of Figures 61 through 72 quantify the proximity effects on the heave and pitch

added mass and damping. These figures demonstrate the difference from the baseline data of the single barge to the barges adjacent to the LMSR is up to 30 percent. The irregular oscillatory behavior of the plots at lower periods is attributed to artificially generated high frequency interactions due to panel discretization effects.

Results from the wave exciting forces are shown in Figures 73 through 106. These figures display the non-dimensional heaving force and pitching moment amplitudes and phase angles, for the headings ranging from zero to 360 degrees at intervals of 45 degrees. Headings of zero degrees indicate waves coming directly from the bow of the RRDF, 90 degrees from the starboard beam, 180 degrees from the stern, and 270 degrees from the port beam. The results clearly indicated the significance, often two or more times higher, of the proximity affect on overall exciting forces. The very large effect of proximity forces was most clearly noted in the following figures:

a. Proximity Induced Exciting Force

Significant effect on pitch for beam seas as evidenced in Figure 83. Here the pitch force is essentially zero for the single barge case which is expected due to hull geometry. Therefore, any non-zero forces acting on the barges are entirely due to the presence of the LMSR. Similar results are found when the wave angle is from 270 degrees in Figure 99.

b. Sheltering/Magnification Effect

It should be noted that both the heave and pitch exciting forces are significantly larger when the waves are from 90 degrees compared to when the waves are from 270 degrees. The reason for this disparity is due to the incident waves being reflected off the

starboard side of the LMSR and then impacting upon the RRDF's which again create a magnification effect in the 90 degree case. By contrast, when the wave direction is from 270 degrees the incident waves are scattered by the port side of the ship that produces a sheltering effect on the RRDF's from wave action.

3. Figures

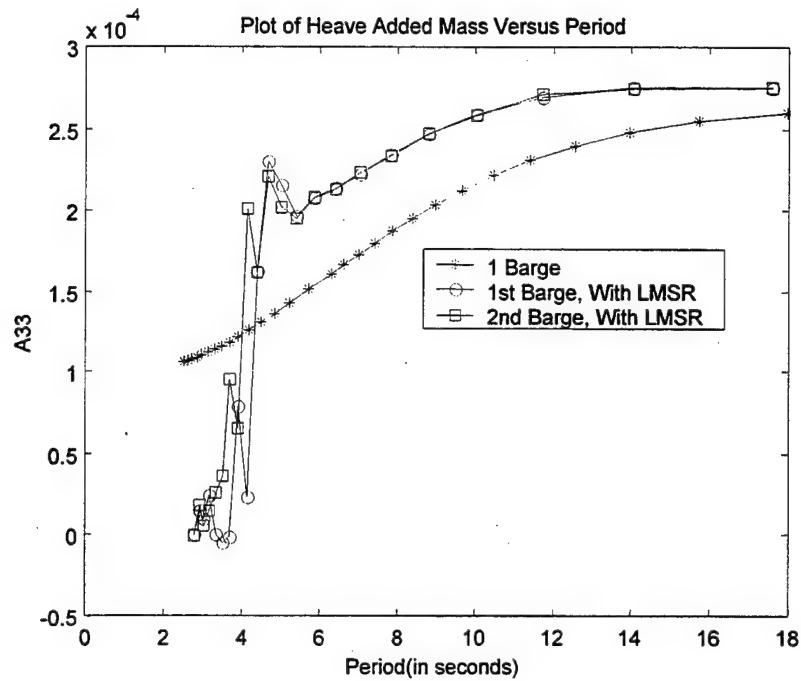


Figure 61. Plot of Single Barge and Multiple Barge Comparisons for Heave Added Mass.

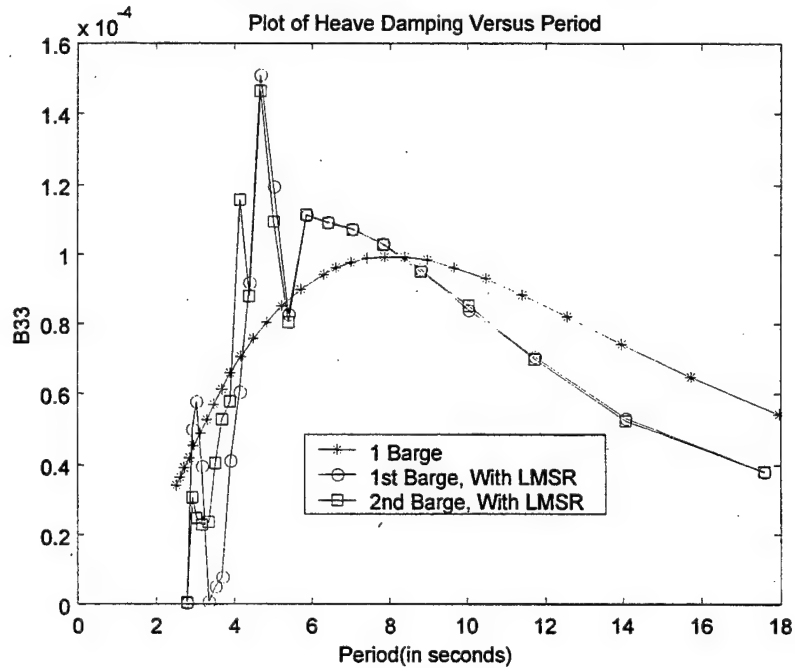


Figure 62. Plot of One Barge and Multiple Barge Comparisons for Heave Damping.

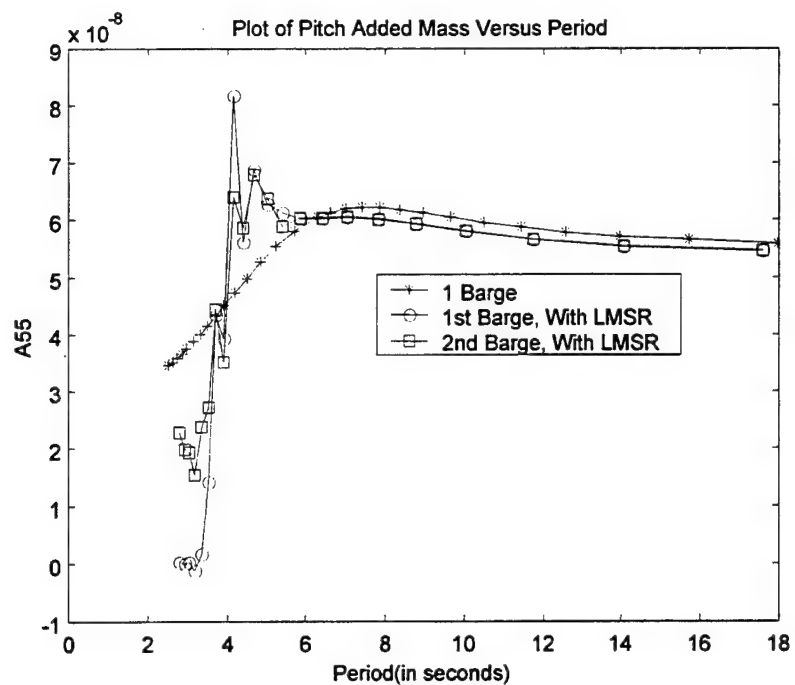


Figure 63. Plot of One Barge and Multiple Barge Comparisons for Pitch Added Mass.

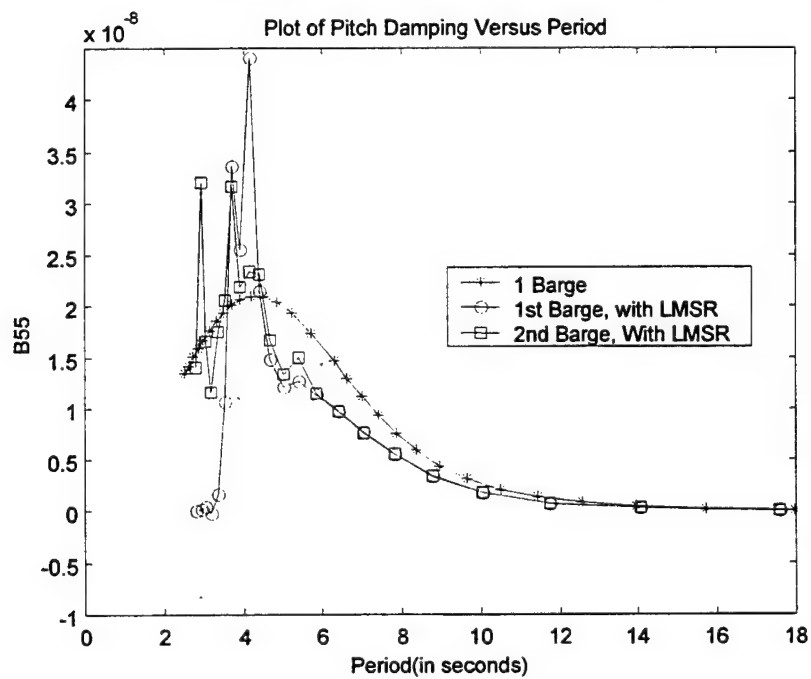


Figure 64. Plot of One Barge and Multiple Barge Comparisons for Pitch Damping.

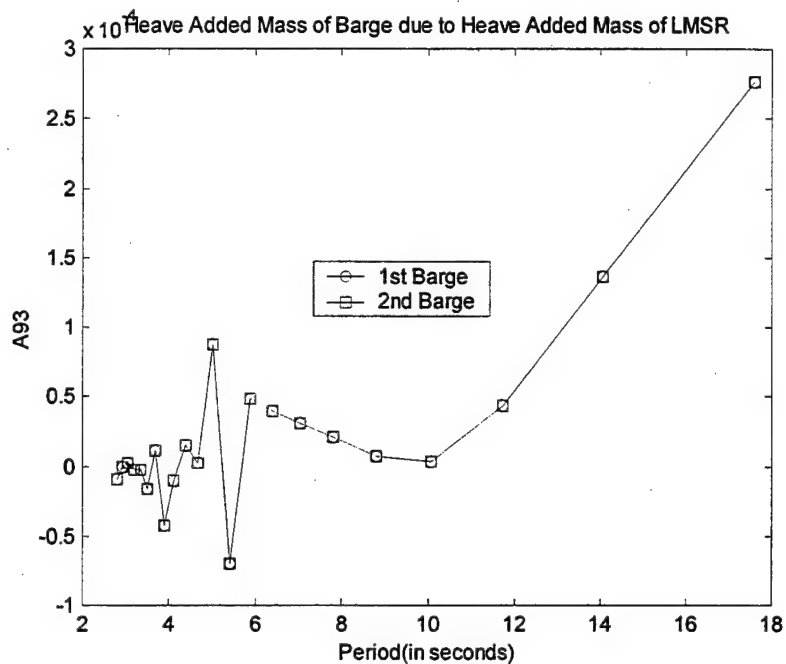


Figure 65. Plot of Multiple Barge Comparisons for Heave Added Mass of Barge Due to Heave Added Mass of LMSR.

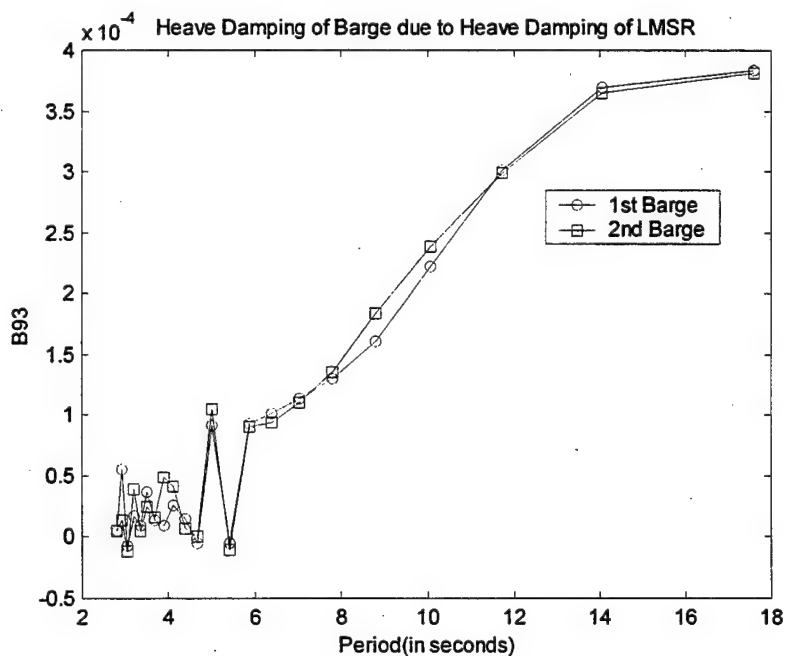


Figure 66. Plot of Multiple Barge Comparisons for Heave Damping of Barge Due to Heave Damping of LMSR.

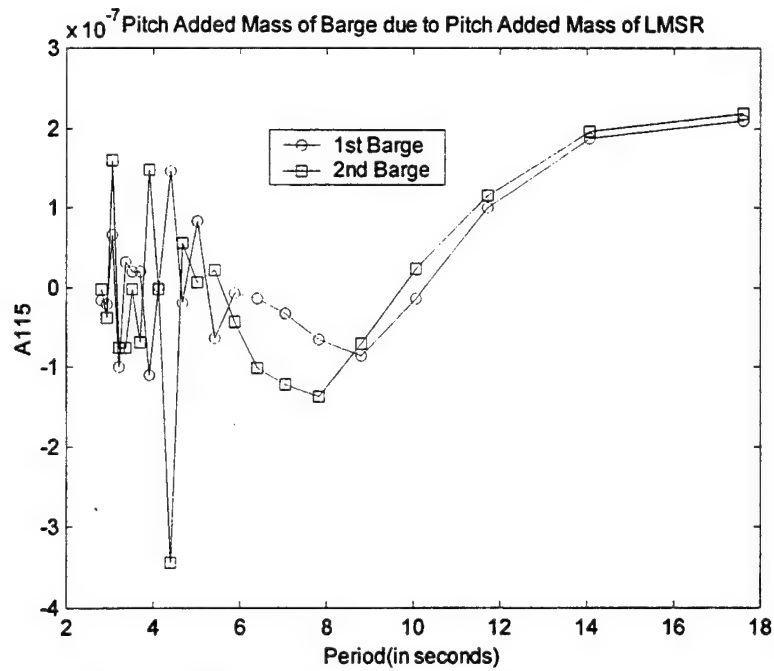


Figure 67. Plot of Multiple Barge Comparisons for Pitch Added Mass of Barge Due to Pitch Added Mass of LMSR.

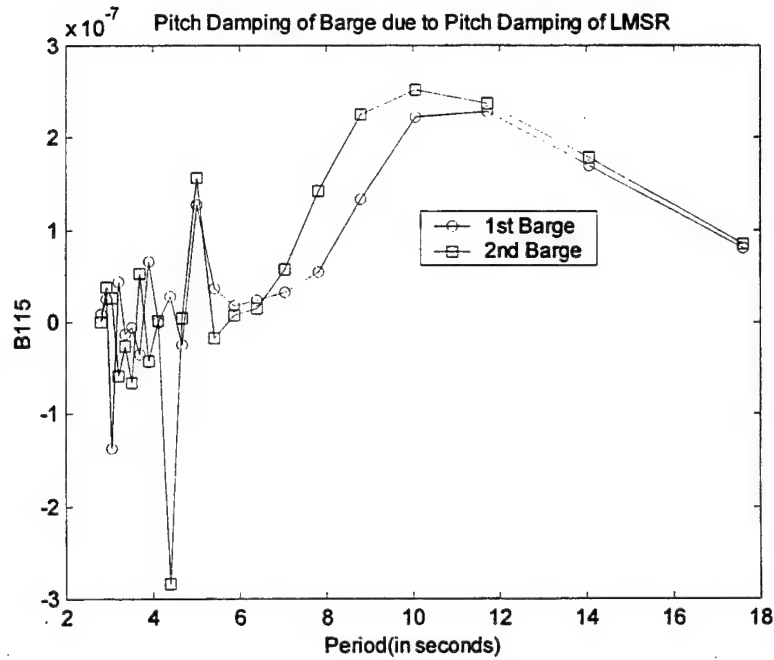


Figure 68. Plot of Multiple Barge Comparisons for Pitch Damping of Barge Due to Pitch Damping of LMSR.

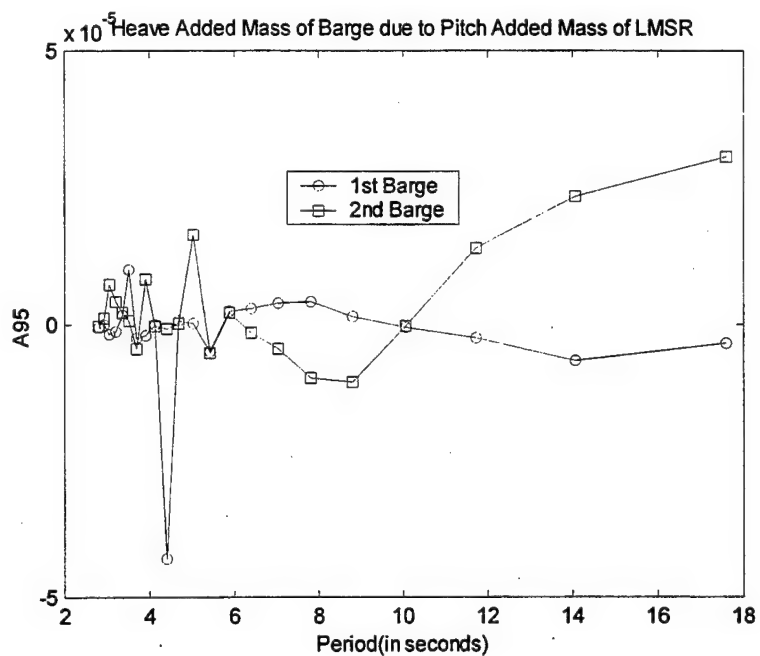


Figure 69. Plot of Multiple Barge Comparisons for Heave Added Mass of Barge Due to Pitch Added Mass of LMSR.

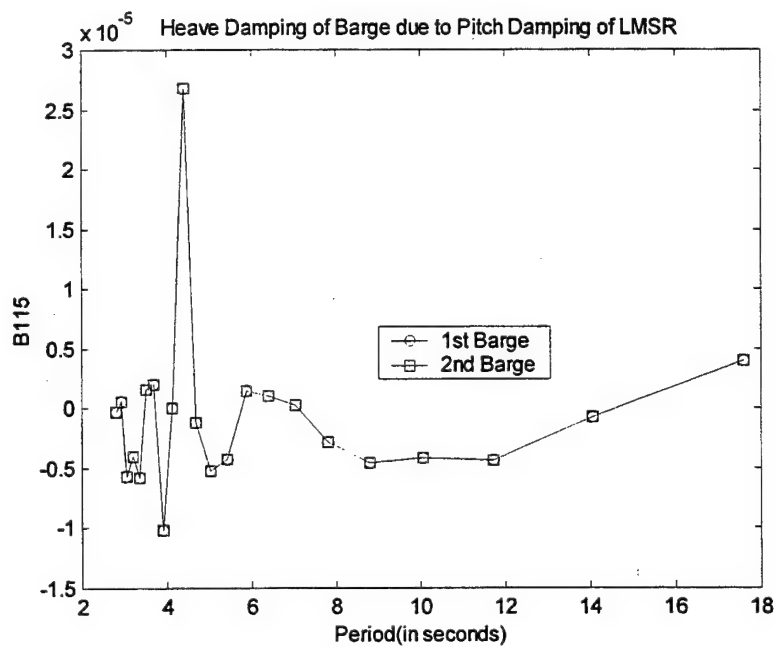


Figure 70. Plot of Multiple Barge Comparisons for Heave Damping of Barge Due to Pitch Damping of LMSR.

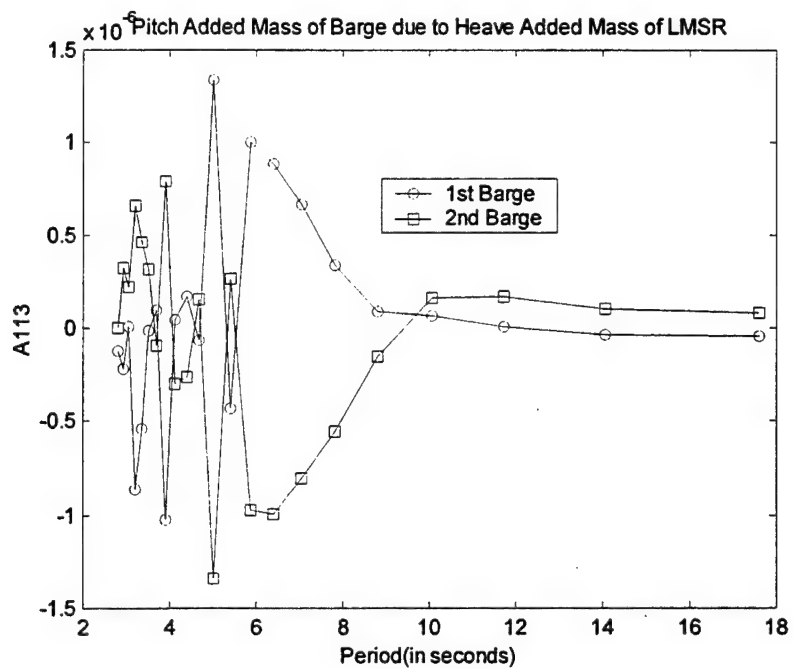


Figure 71. Plot of Multiple Barge Comparisons for Pitch Added Mass of Barge Due to Heave Added Mass of LMSR.

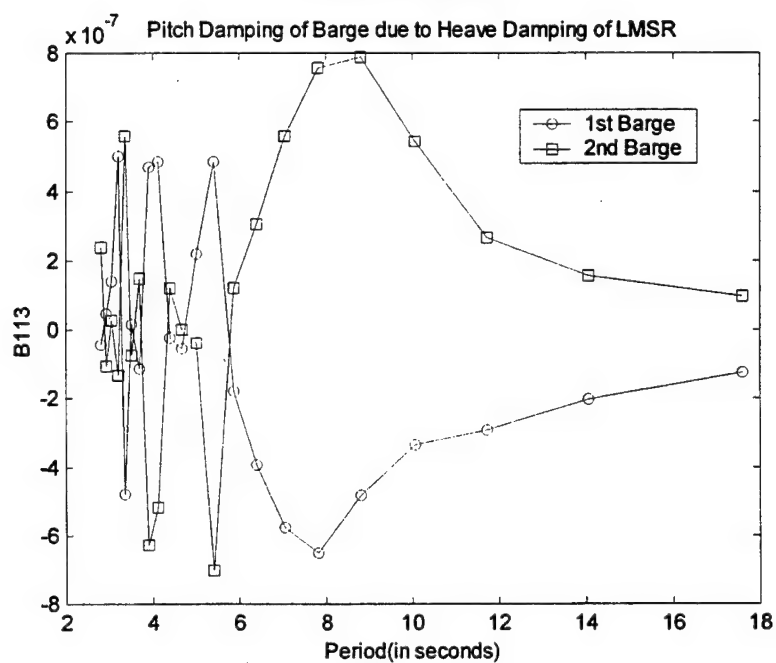


Figure 72. Plot of Multiple Barge Comparisons for Pitch Damping of Barge Due to Heave Damping of LMSR.

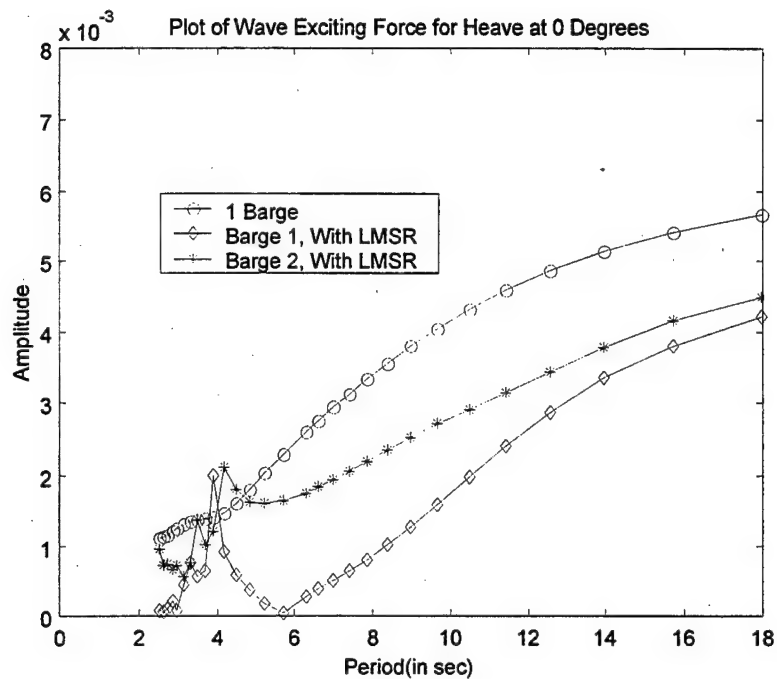


Figure 73. Plot of One Barge and Multiple Barge Comparisons for Heave Exciting Force at an Incident Wave Angle of 0 Degrees.

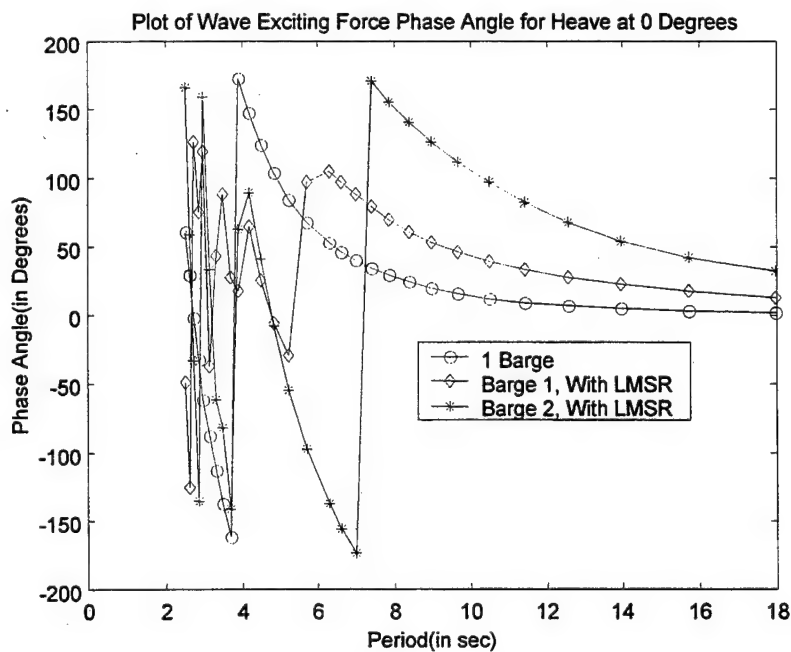


Figure 74. Plot of One Barge and Multiple Barge Comparisons for Heave Exciting Force Phase Angle at an Incident Wave Angle of 0 Degrees.

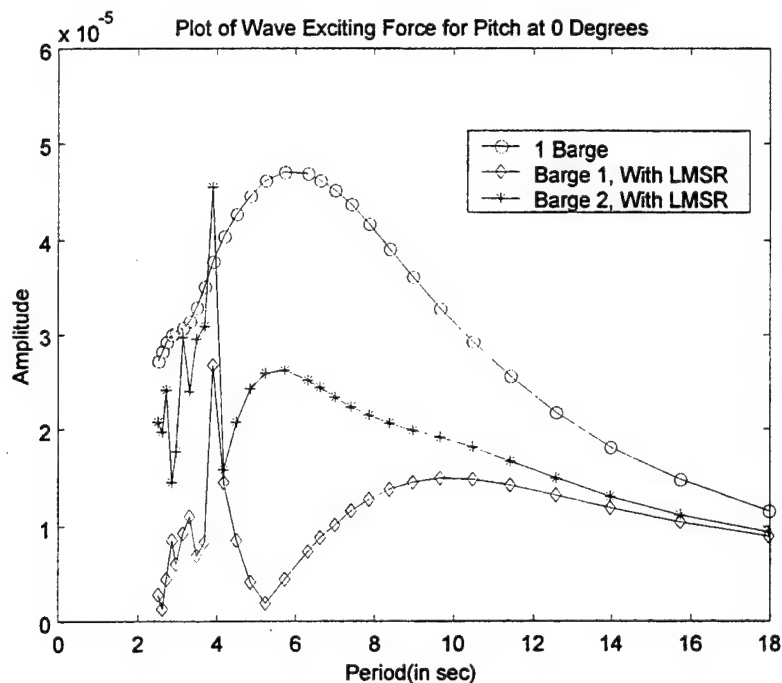


Figure 75. Plot of One Barge and Multiple Barge Comparisons for Pitch Exciting Force at an Incident Wave Angle of 0 Degrees.

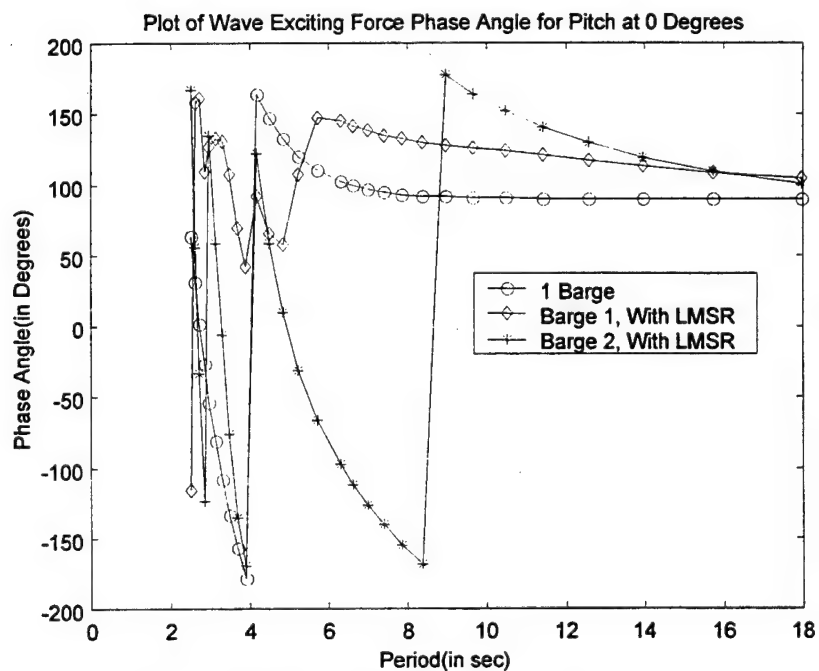


Figure 76. Plot of One Barge and Multiple Barge Comparisons for Pitch Exciting Force Phase Angle at an Incident Wave Angle of 0 Degrees.

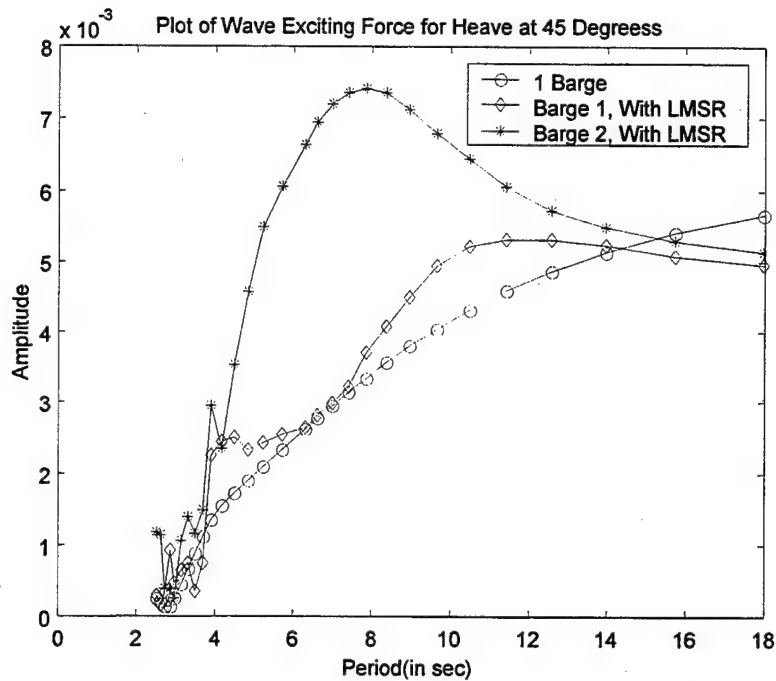


Figure 77. Plot of One Barge and Multiple Barge Comparisons for Heave Exciting Force at an Incident Wave Angle of 45 Degrees.

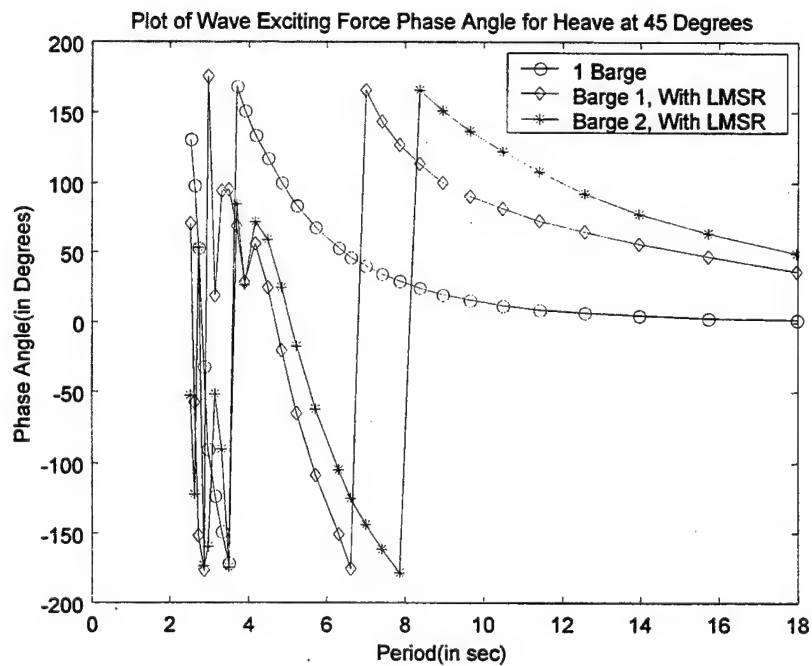


Figure 78. Plot of One Barge and Multiple Barge Comparisons for Heave Exciting Force Phase Angle at an Incident Wave Angle of 45 Degrees.

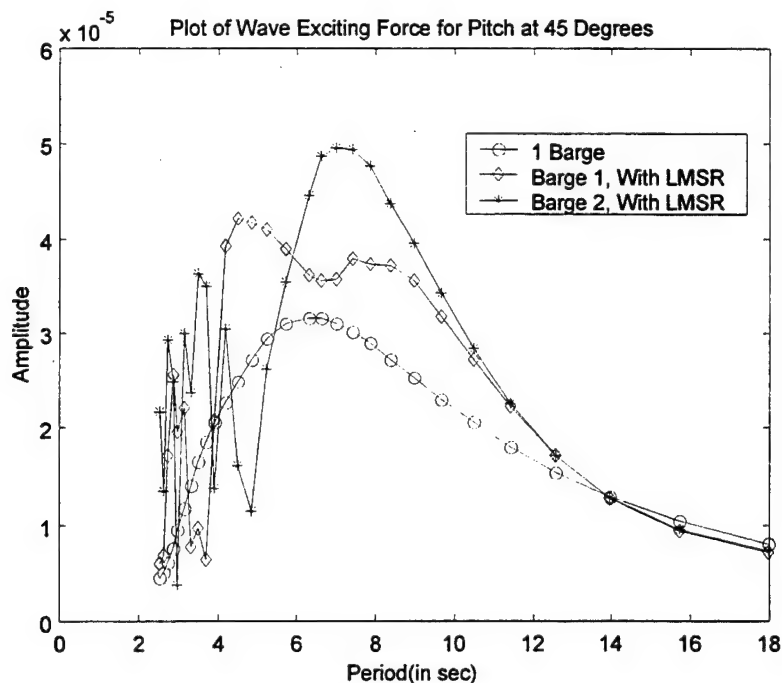


Figure 79. Plot of One Barge and Multiple Barge Comparisons for Pitch Exciting Force at an Incident Wave Angle of 45 Degrees.

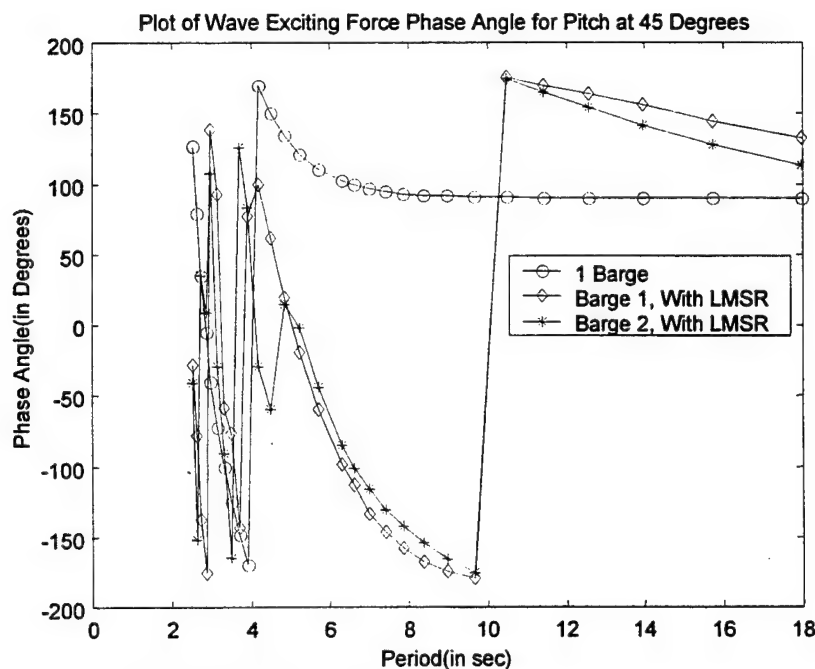


Figure 80. Plot of One Barge and Multiple Barge Comparisons for Pitch Exciting Force Phase Angle at an Incident Wave Angle of 45 Degrees.

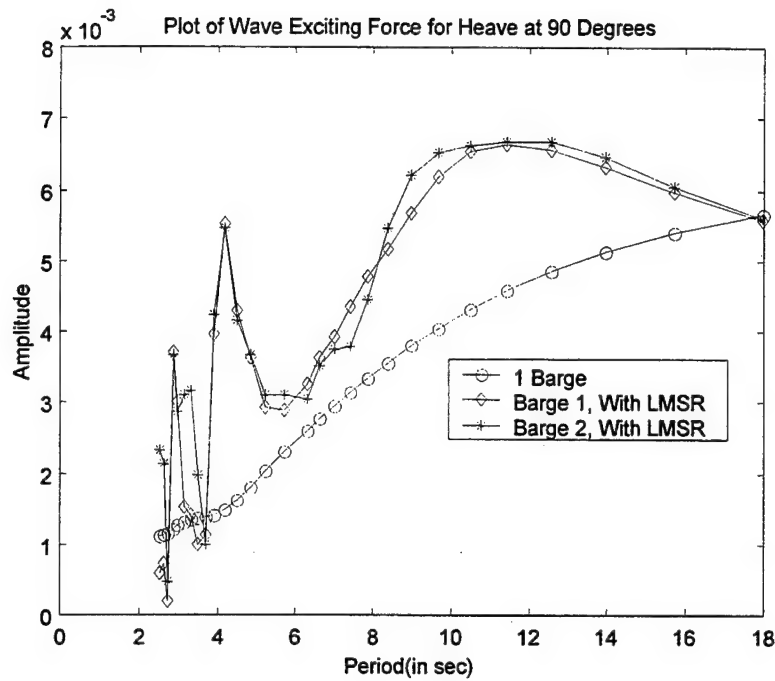


Figure 81. Plot of One Barge and Multiple Barge Comparisons for Heave Exciting Force at an Incident Wave Angle of 90 Degrees.

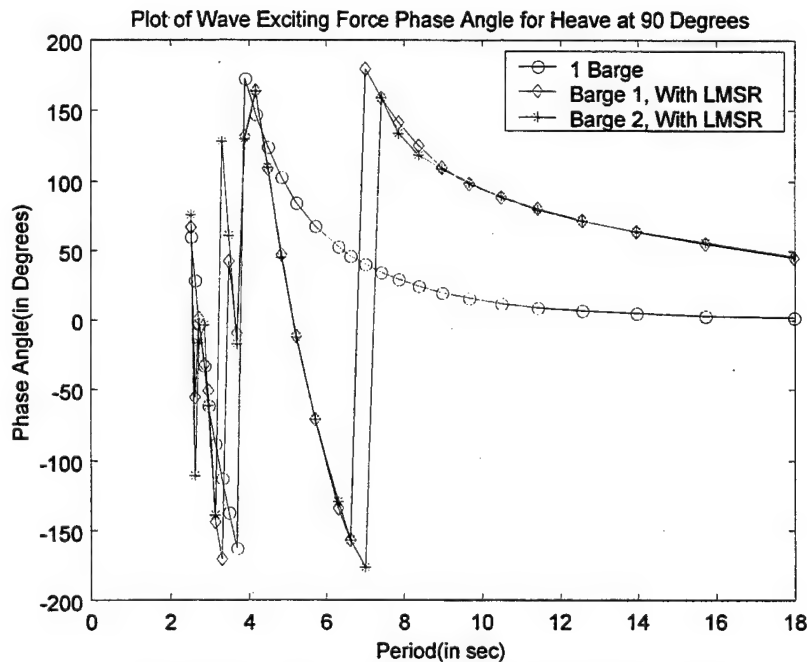


Figure 82. Plot of One Barge and Multiple Barge Comparisons for Heave Exciting Force Phase Angle at an Incident Wave Angle of 90 Degrees.

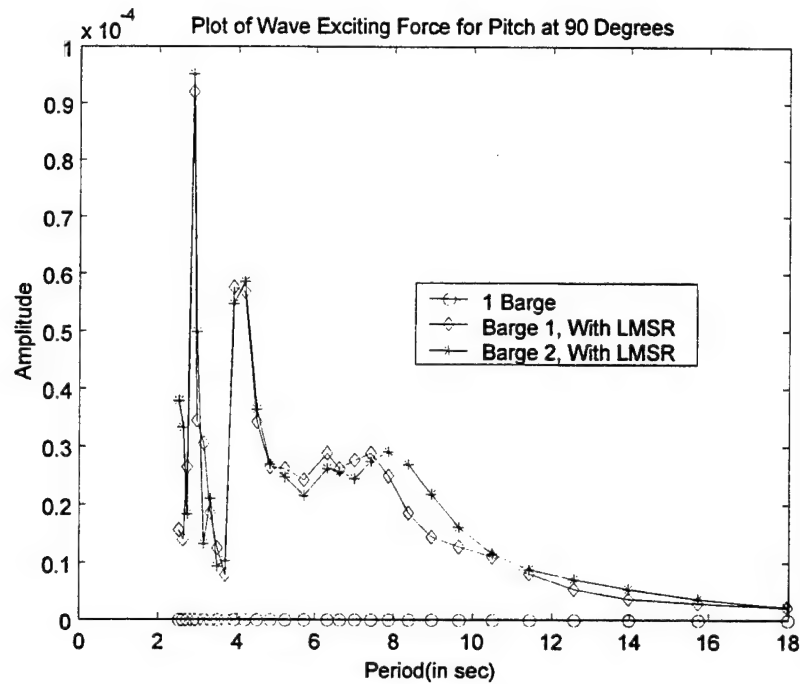


Figure 83. Plot of One Barge and Multiple Barge Comparisons for Pitch Exciting Force at an Incident Wave Angle of 90 Degrees.

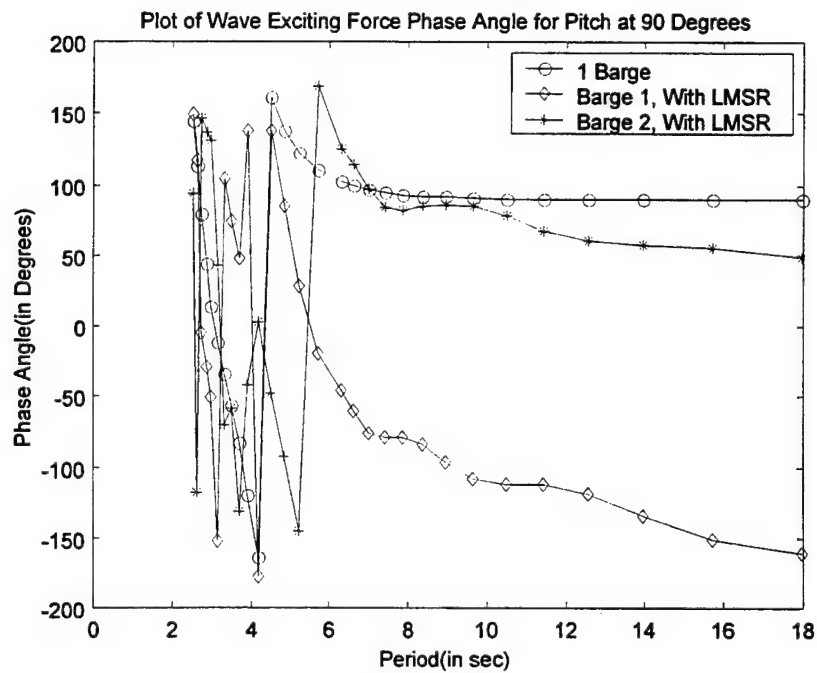


Figure 84. Plot of One Barge and Multiple Barge Comparisons for Pitch Exciting Force Phase Angle at an Incident Wave Angle of 90 Degrees.

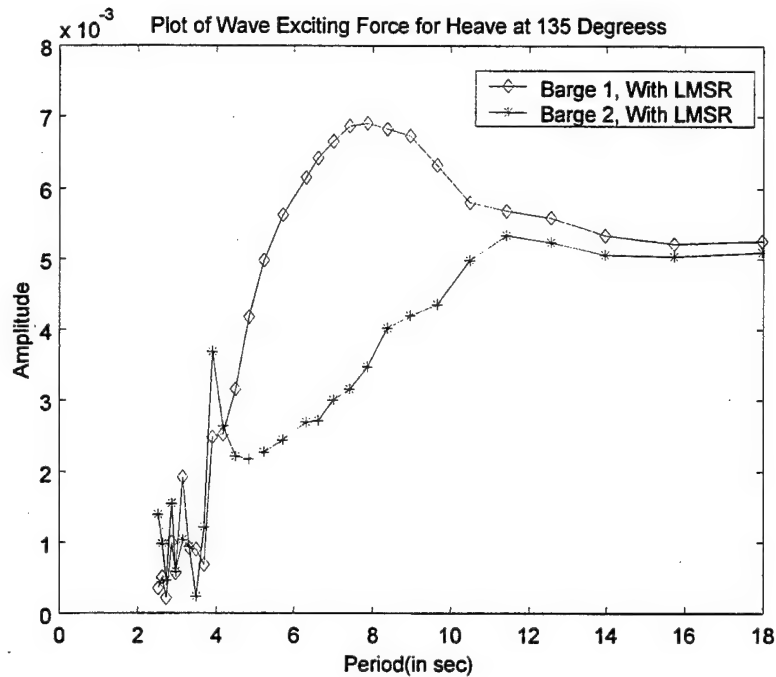


Figure 85. Plot of Multiple Barge Comparisons for Heave Exciting Force at an Incident Wave Angle of 135 Degrees.

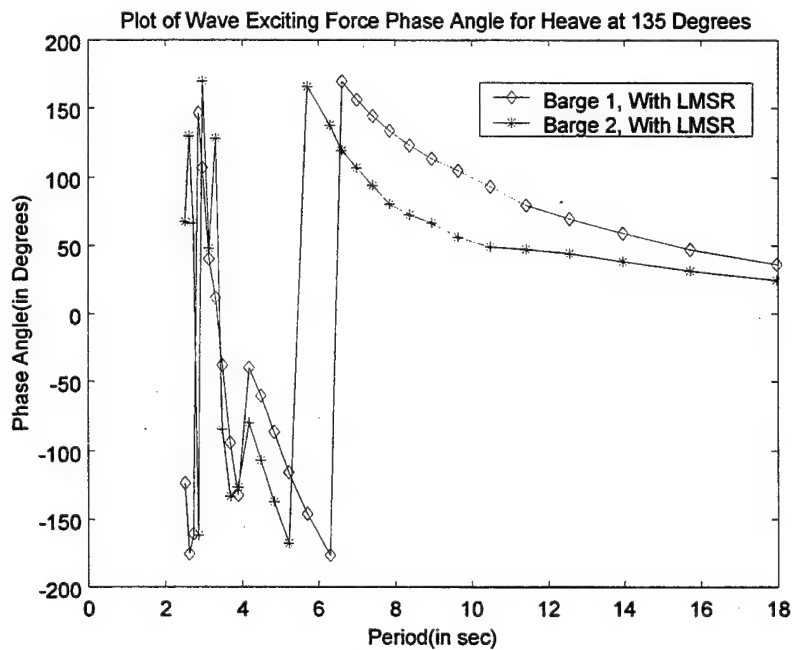


Figure 86. Plot of Multiple Barge Comparisons for Heave Exciting Force Phase Angle at an Incident Wave Angle of 135 Degrees.

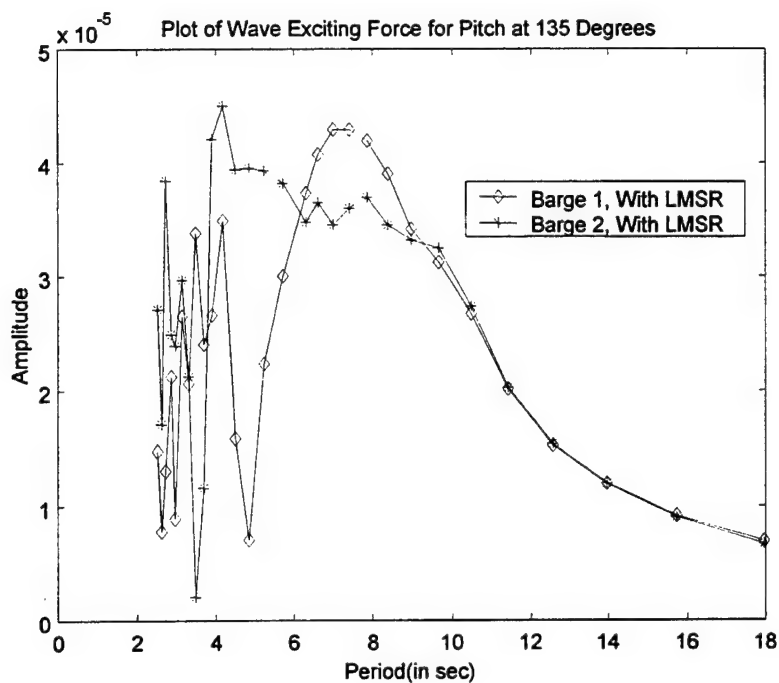


Figure 87. Plot of Multiple Barge Comparisons for Pitch Exciting Force at an Incident Wave Angle of 135 Degrees.

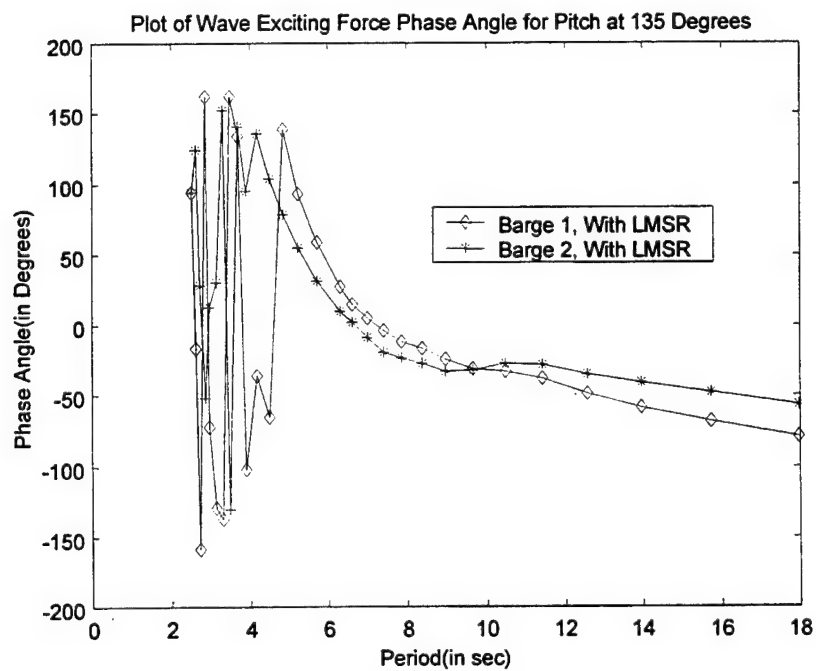


Figure 88. Plot of Multiple Barge Comparisons for Pitch Exciting Force Phase Angle at an Incident Wave Angle of 135 Degrees.

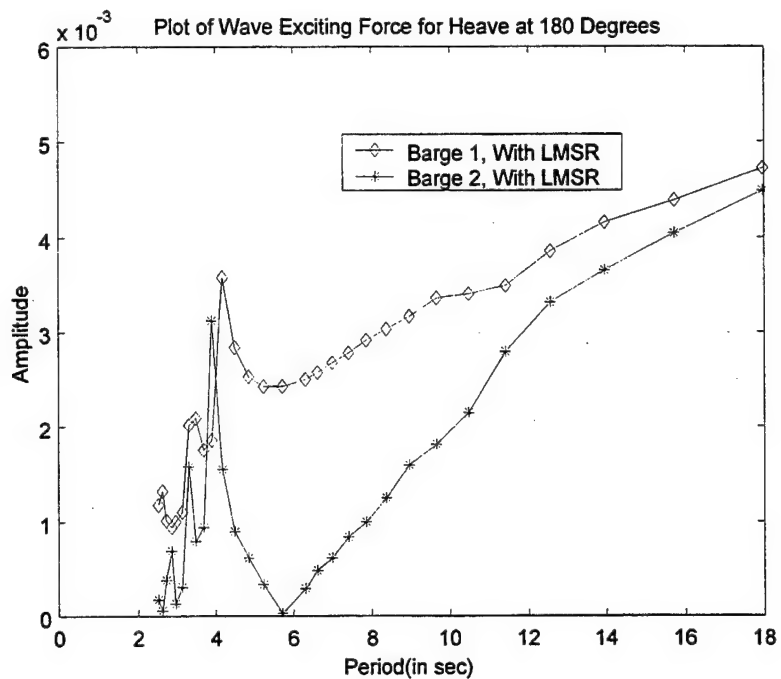


Figure 89. Plot of Multiple Barge Comparisons for Heave Exciting Force at an Incident Wave Angle of 180 Degrees.

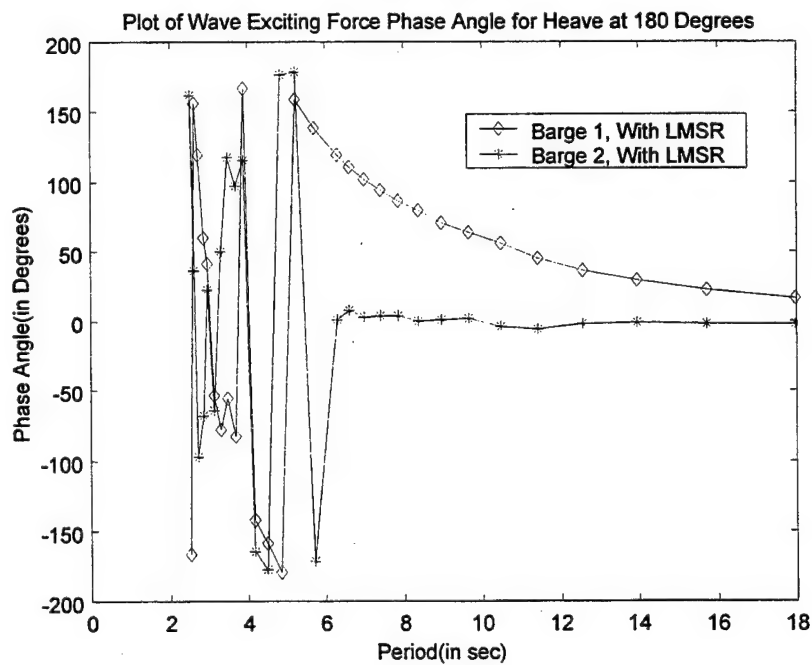


Figure 90. Plot of Multiple Barge Comparisons for Heave Exciting Force Phase Angle at an Incident Wave Angle of 180 Degrees.

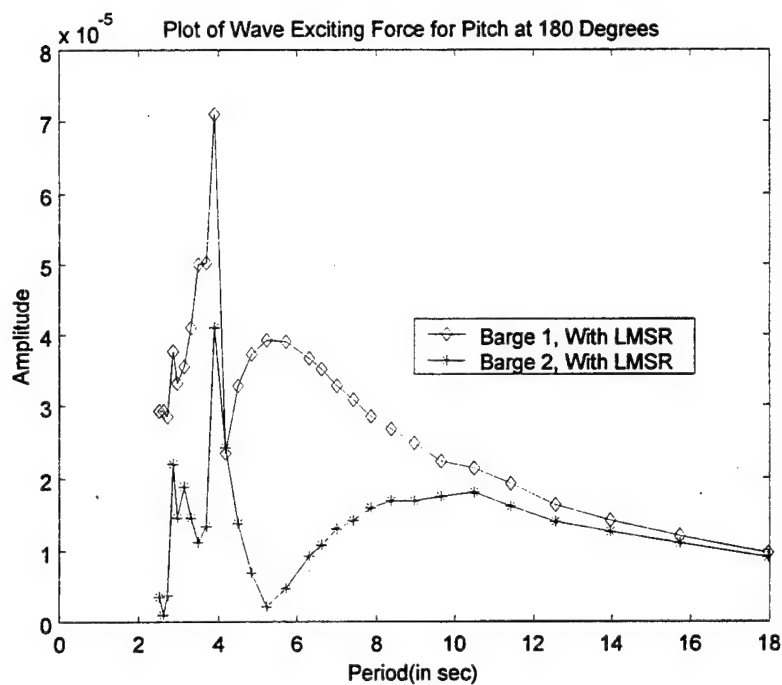


Figure 91. Plot of Multiple Barge Comparisons for Pitch Exciting Force at an Incident Wave Angle of 180 Degrees.

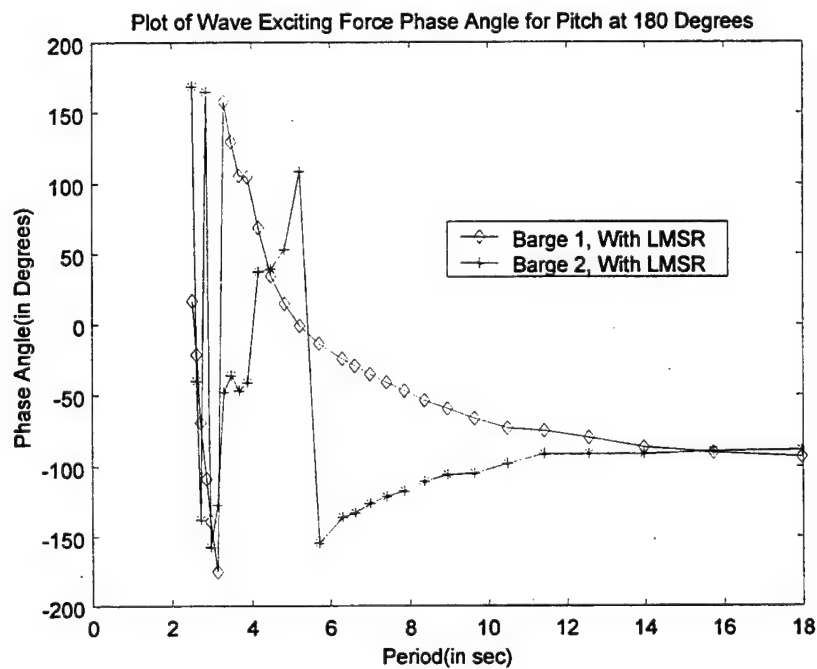


Figure 92. Plot of Multiple Barge Comparisons for Pitch Exciting Force Phase Angle at an Incident Wave Angle of 180 Degrees.

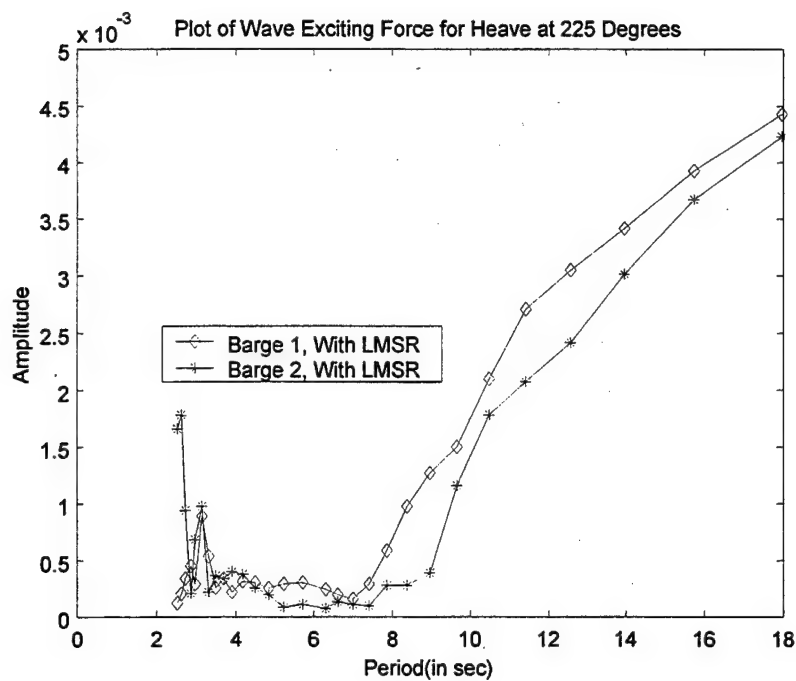


Figure 93. Plot of Multiple Barge Comparisons for Heave Exciting Force at an Incident Wave Angle of 225Degrees.

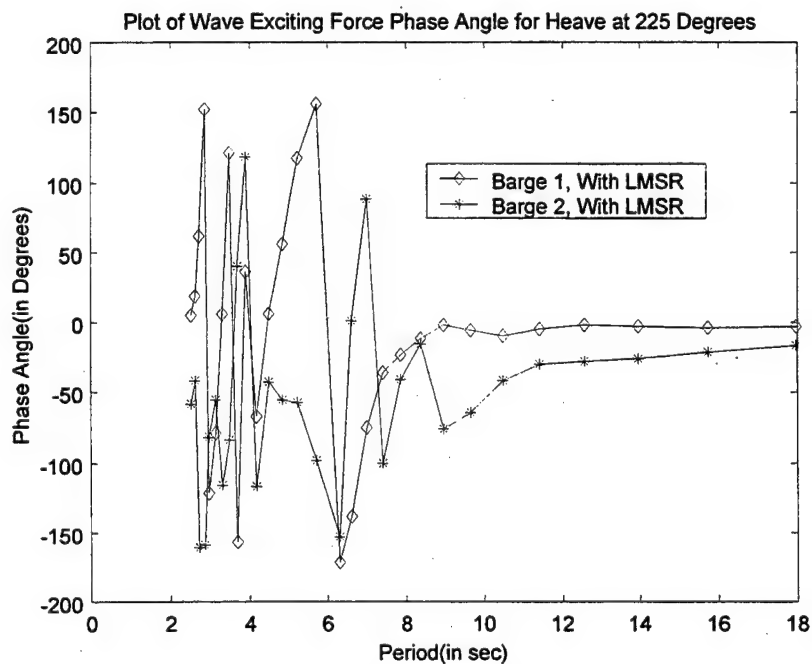


Figure 94. Plot of Multiple Barge Comparisons for Heave Exciting Force Phase Angle at an Incident Wave Angle of 225 Degrees.

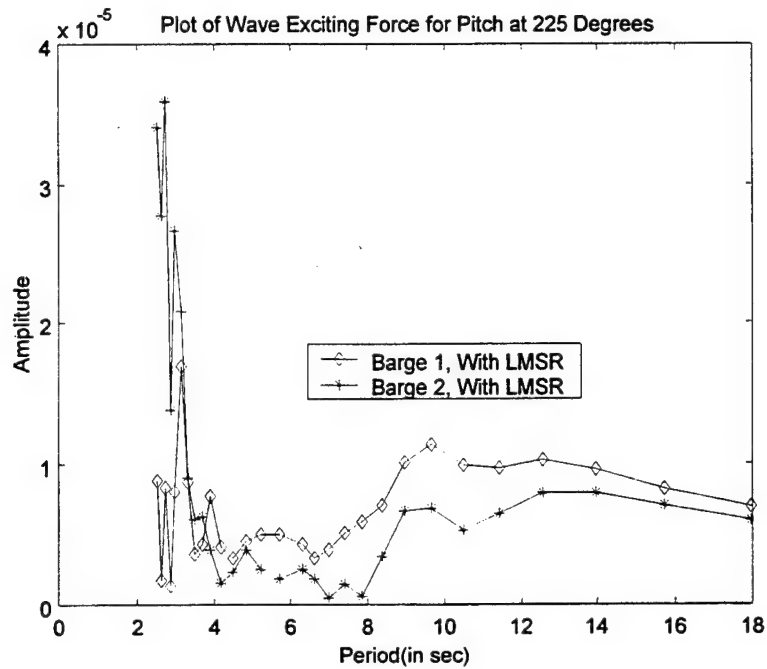


Figure 95. Plot of Multiple Barge Comparisons for Pitch Exciting Force at an Incident Wave Angle of 225 Degrees.

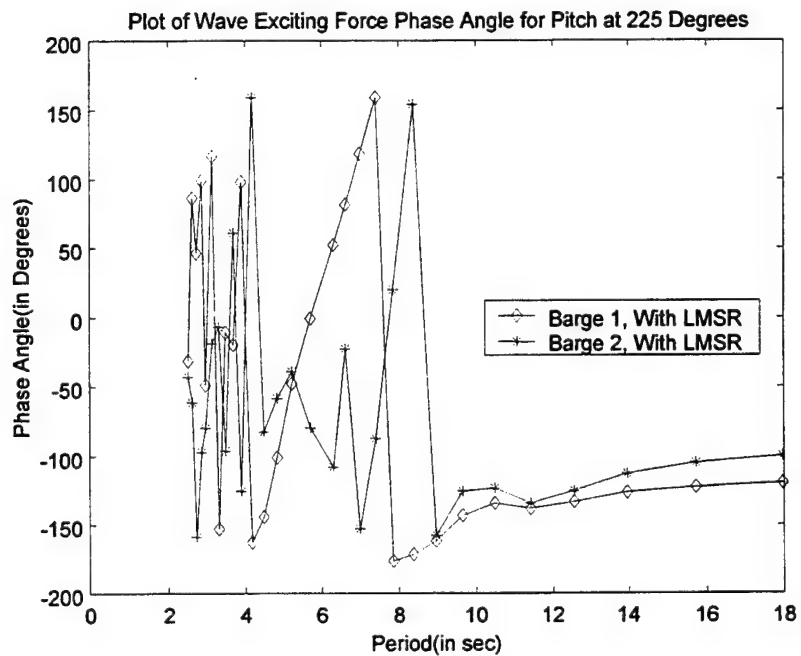


Figure 96. Plot of Multiple Barge Comparisons for Pitch Exciting Force Phase Angle at an Incident Wave Angle of 225 Degrees.

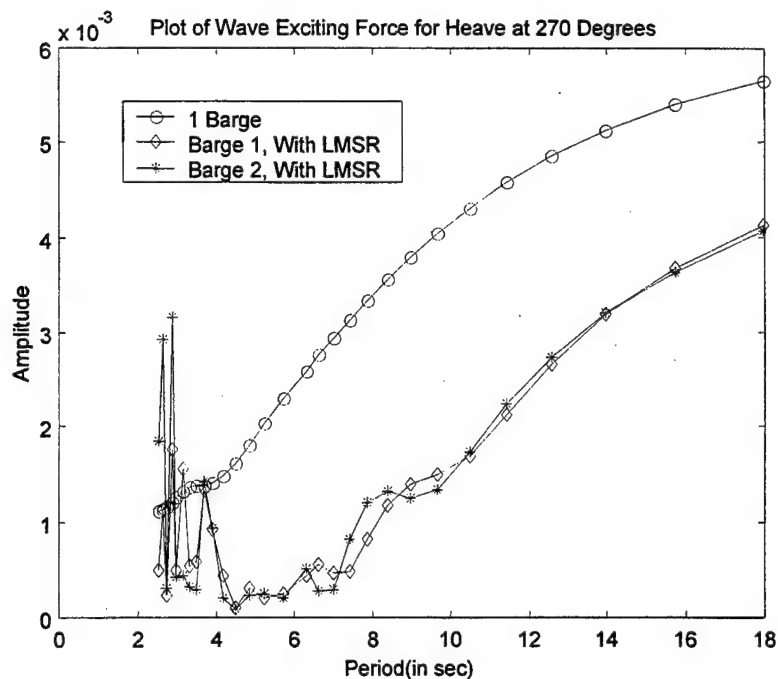


Figure 97. Plot of One Barge and Multiple Barge Comparisons for Heave Exciting Force at an Incident Wave Angle of 270 Degrees.

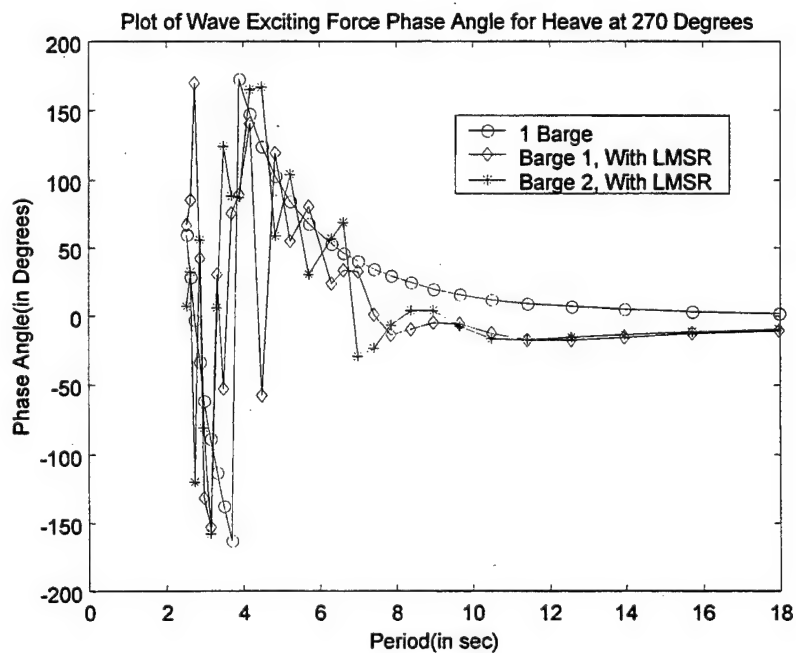


Figure 98. Plot of One Barge and Multiple Barge Comparisons for Heave Exciting Force Phase Angle at an Incident Wave Angle of 270 Degrees.

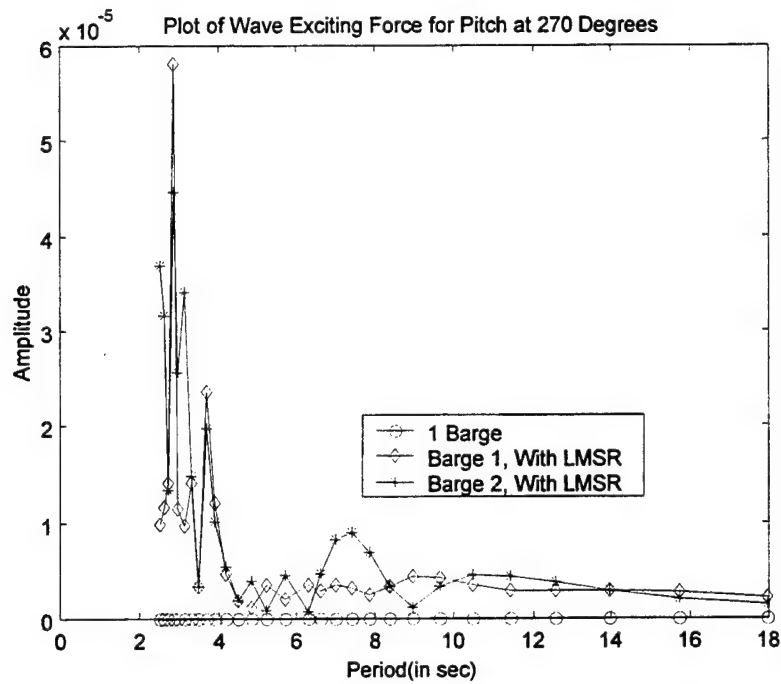


Figure 99. Plot of One Barge and Multiple Barge Comparisons for Pitch Exciting Force at an Incident Wave Angle of 270 Degrees.

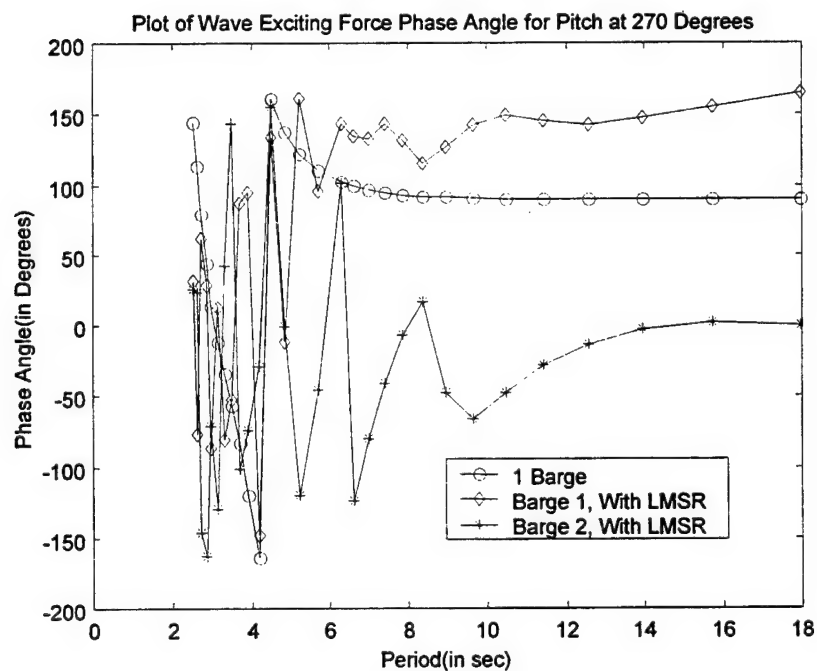


Figure 100. Plot of One Barge and Multiple Barge Comparisons for Pitch Exciting Force Phase Angle at an Incident Wave Angle of 270 Degrees.

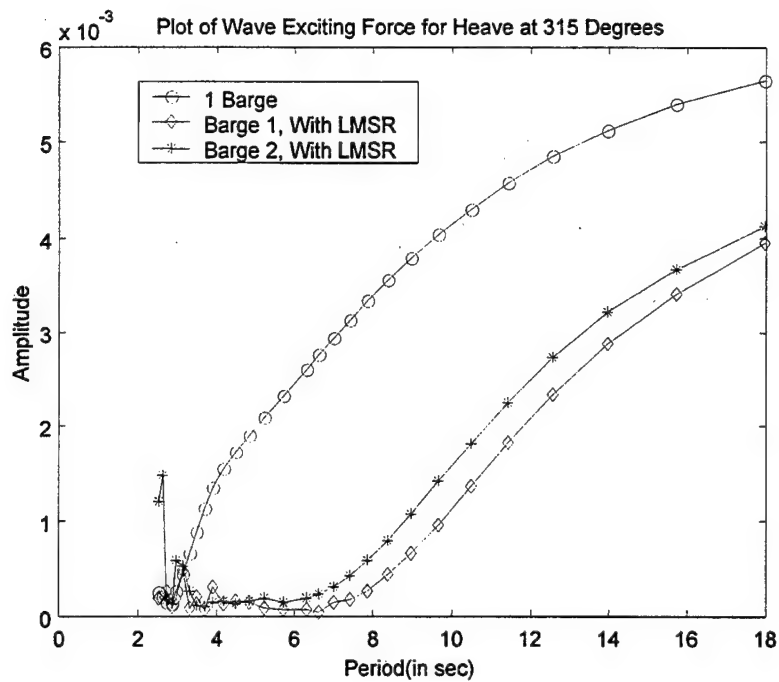


Figure 101. Plot of One Barge and Multiple Barge Comparisons for Heave Exciting Force at an Incident Wave Angle of 315 Degrees.

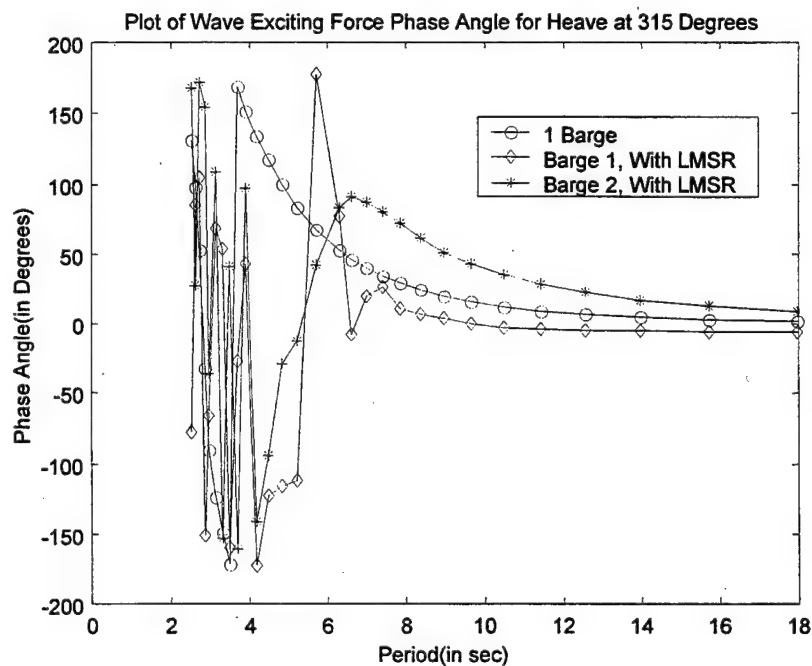


Figure 102. Plot of One Barge and Multiple Barge Comparisons for Heave Exciting Force Phase Angle at an Incident Wave Angle of 315 Degrees.

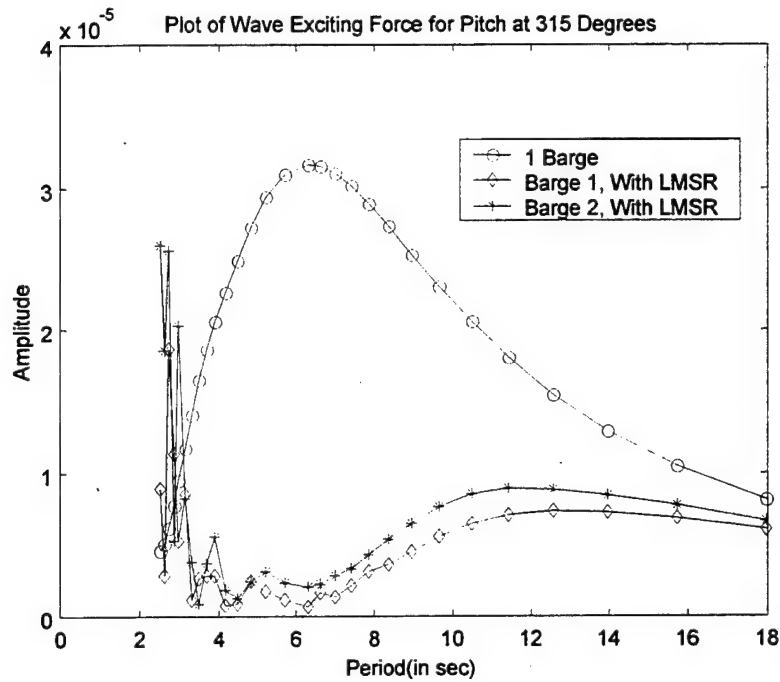


Figure 103. Plot of One Barge and Multiple Barge Comparisons for Pitch Exciting Force at an Incident Wave Angle of 315 Degrees.

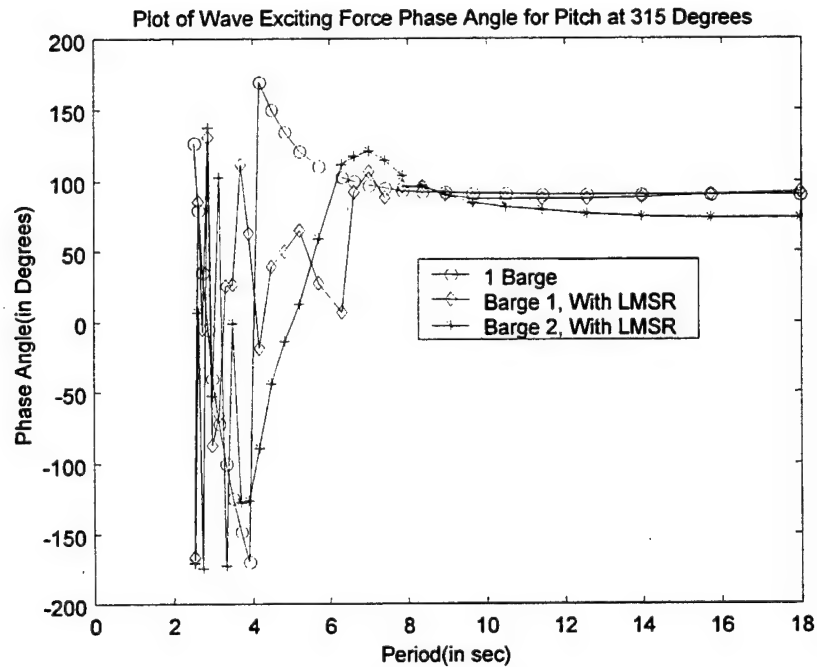


Figure 104. Plot of One Barge and Multiple Barge Comparisons for Pitch Exciting Force Phase Angle at an Incident Wave Angle of 315 Degrees.

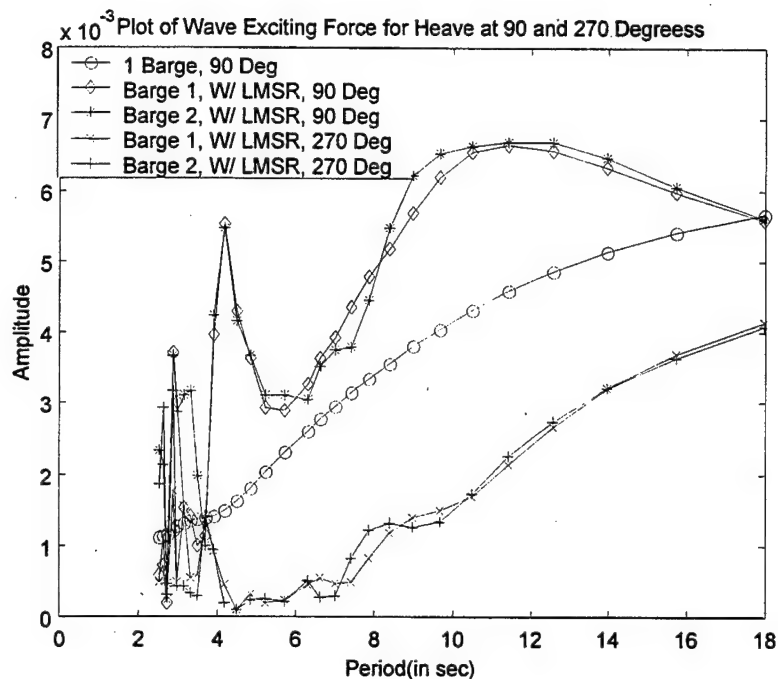


Figure 105. Plot of One Barge and Multiple Barge Comparisons for Heave Exciting Force at an Incident Wave Angle of 90 Degrees and 270 Degrees.

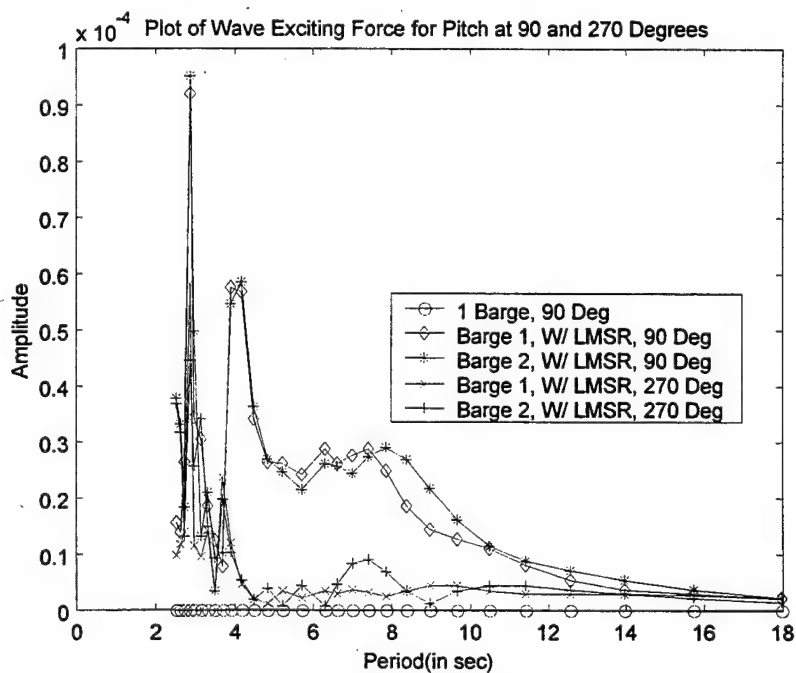


Figure 106. Plot of One Barge and Multiple Barge Comparisons for Pitch Exciting Force at an Incident Wave Angle of 90 Degrees and 270 Degrees.

C. RAMP ANALYSIS

1. Introduction

The forces on the ramp exerted from the hydrodynamic motions of the LMSR and barge are presented in Figures 107 through 131a. These figures show the overall forces on the pinned locations that connect the ramp to the LMSR and the barge. To derive these forces, the data utilized was that obtained from WAMIT as this data produced excellent results when compared with actual wave tank model tests. The ramp is assumed to be a rigid body for analysis and stiffness of the spring connections is assumed to be proportional to the hydrostatic heave stiffness of the LMSR or barge, depending on which pinned connection is being analyzed. Table 4 shows the dimensions of the ramp.

Description	Dimensions
Ramp Length (in Feet, Pivot to Pivot)	165
Ramp Width (in Feet, Overall)	20
Ramp Weight	96.94 Long Tons

Table 4. Ramp Dimensions

2. Data Analysis

Figures 107 through 122 show a plot of the ramp force magnitudes for the three-pinned connections. It is clear that the pinned connection that receives the largest peak magnitude force is the third king pin which connects the ramp to the barge. The connection that receives the largest force throughout the entire range is the first pinned connection. The third connection receives up to 5 times the magnitude of force as compared to the pinned connections attaching the ramp to the LMSR at the peak frequency. The first king pin has a force about 1.5 times greater than the third connection

throughout the entire range. The forces on the barge's king pin are largest when the waves are from 90 and 270 degrees.

When looking at the individual king pin for the LMSR and the barge, comparisons were made between the actual force at the pinned connection and the hydrodynamic heave force acting on the vessel. This data is displayed in Figures 123, 125, and 127 where the actual force which each king pin experiences is higher than the hydrodynamic heave force on the vessel at higher wave frequencies. The force that the ramp connections experience drops off at longer periods.

Figures 107 through 122 and 129 through 131a show the changes in overall excitation force on the pinned connection if different spring stiffnesses are assumed to exist. As can be seen in Figures 129, 130, and 131, the larger the value of the spring constant, the greater the magnitude of force which each king pin observes. This implies that a lower stiffness value for the spring connection is one method of minimizing excitation forces on the pinned connections.

3. Figures

Plot of Ramp³ Force Magnitudes at Various Angles for 1st Pinned Connection, K=0.01C33

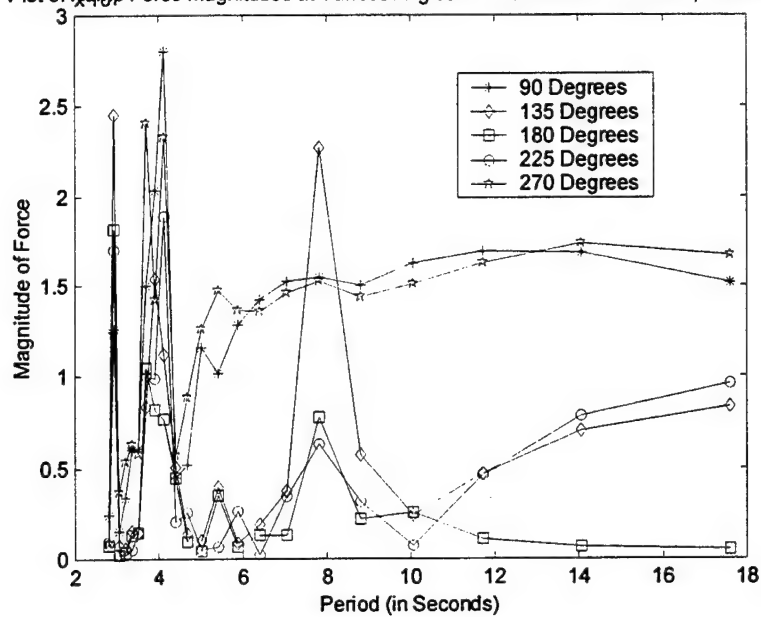


Figure 107. Plot of Ramp Exciting Force on the First Pinned Connections at Various Wave Angles with a Spring Constant of 0.01.

Plot of Ramp Force Magnitudes at Various Angles for 1st Pinned Connection

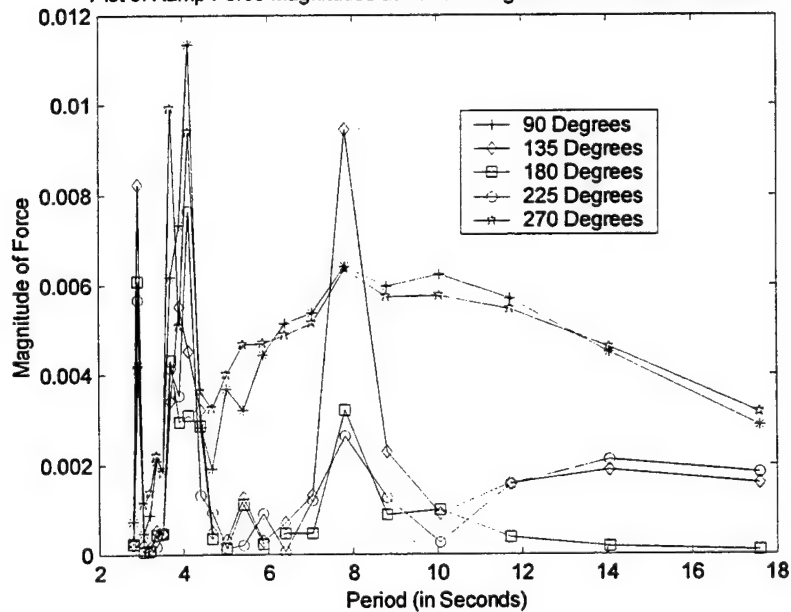


Figure 108. Plot of Ramp Exciting Force on the 1st Pinned Connection at Various Wave Angles with a Spring Constant of 0.1.

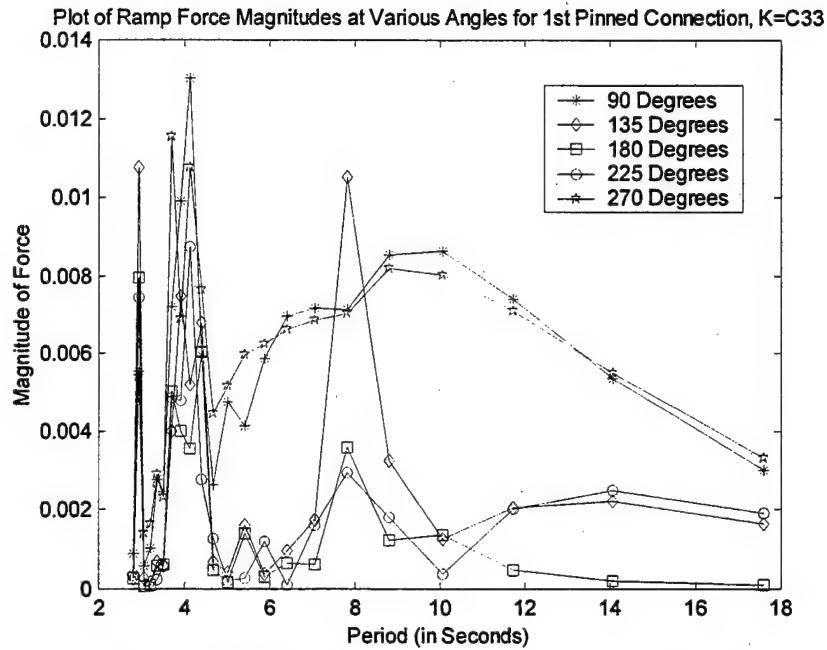


Figure 109. Plot of Ramp Exciting Force on the First Pinned Connections at Various Wave Angles with a Spring Constant of 1.

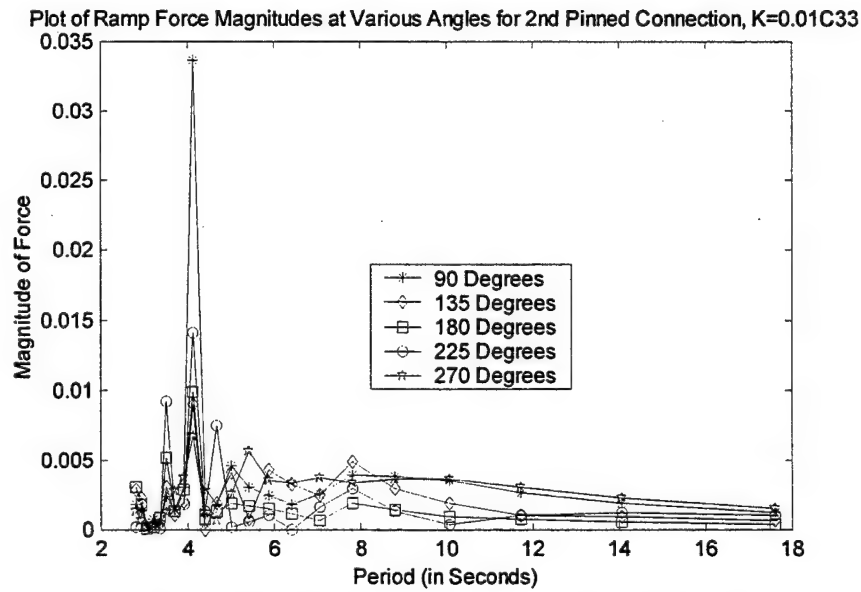


Figure 110. Plot of Ramp Exciting Force on the Second Pinned Connections at Various Wave Angles with a Spring Constant of 0.01.

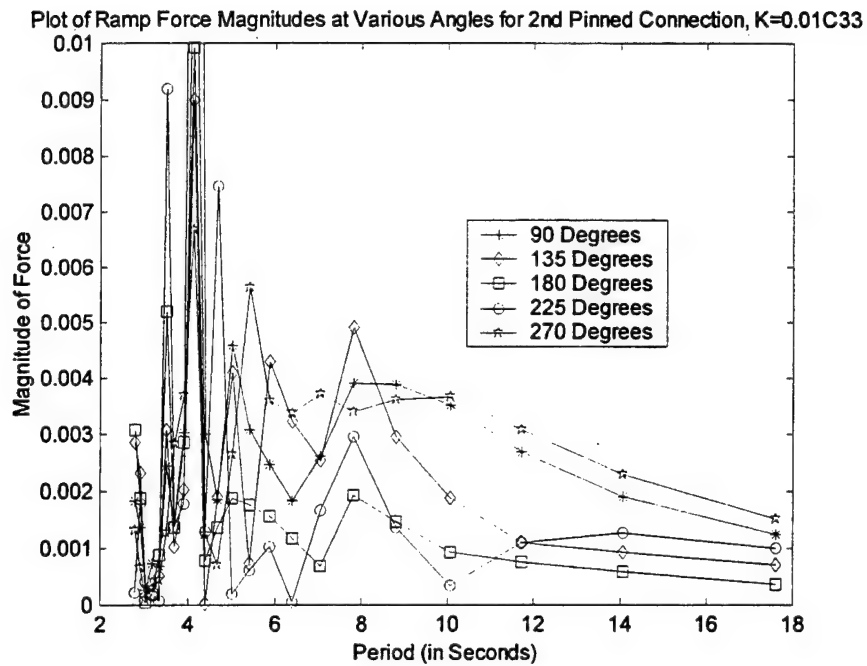


Figure 110a. Plot of Ramp Exciting Force on the Second Pinned Connections at Various Wave Angles with a Spring Constant of 0.01.

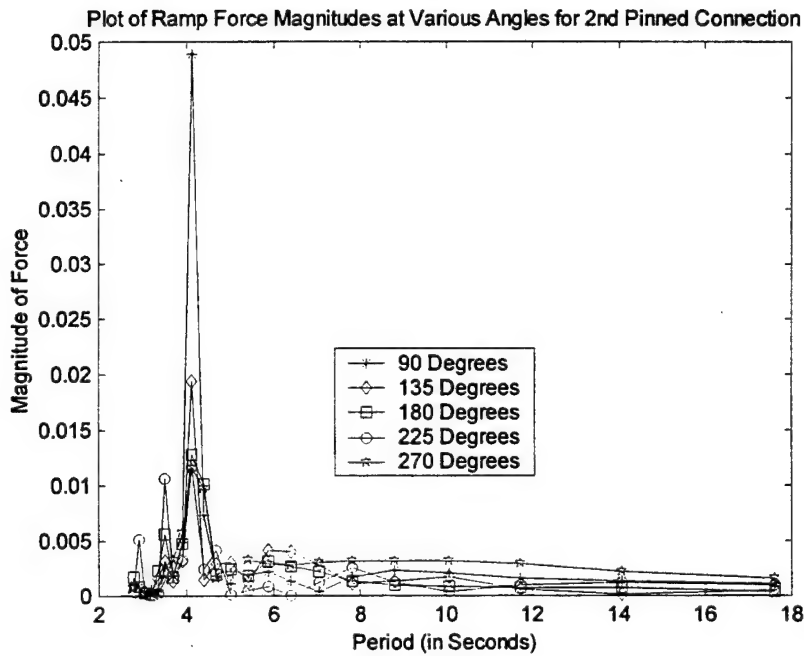


Figure 111. Plot of Ramp Exciting Force on the 2nd Pinned Connection at Various Wave Angles with a Spring Constant of 0.1.

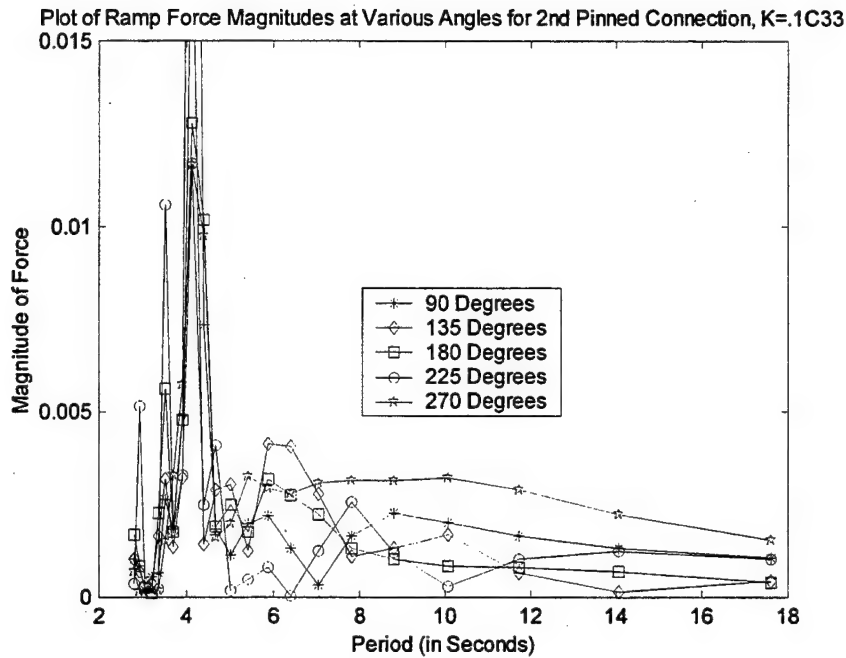


Figure 111a. Plot of Ramp Exciting Force on the 2nd Pinned Connection at Various Wave Angles with a Spring Constant of 0.1.

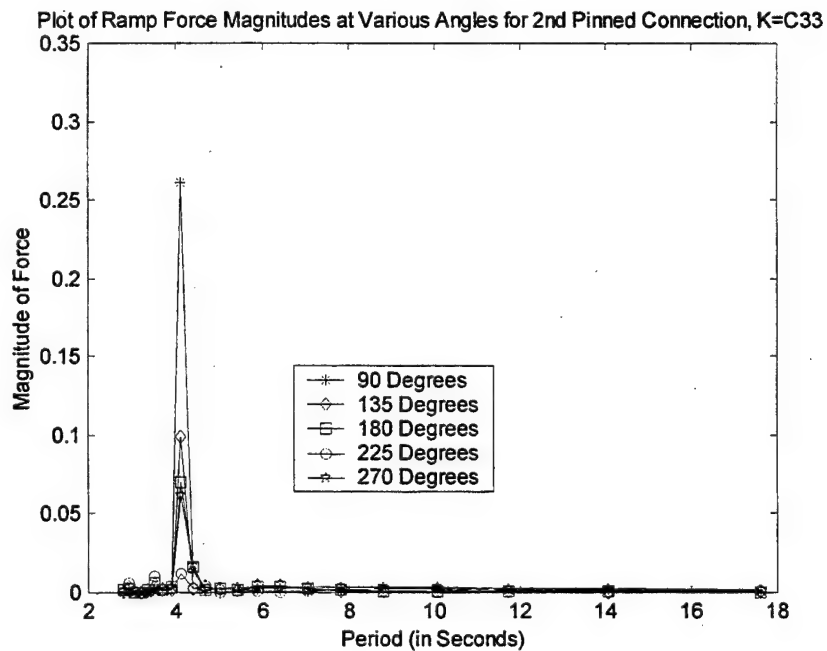


Figure 112. Plot of Ramp Exciting Force on the Second Pinned Connection at Various Wave Angles with a Spring Constant of 1.

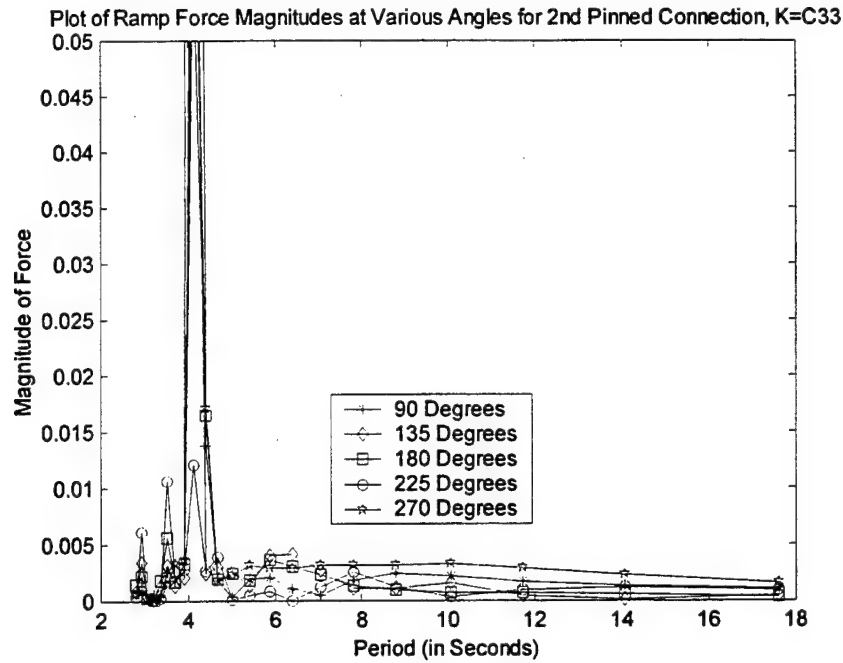


Figure 112a. Plot of Ramp Exciting Force on the Second Pinned Connection at Various Wave Angles with a Spring Constant of 1.

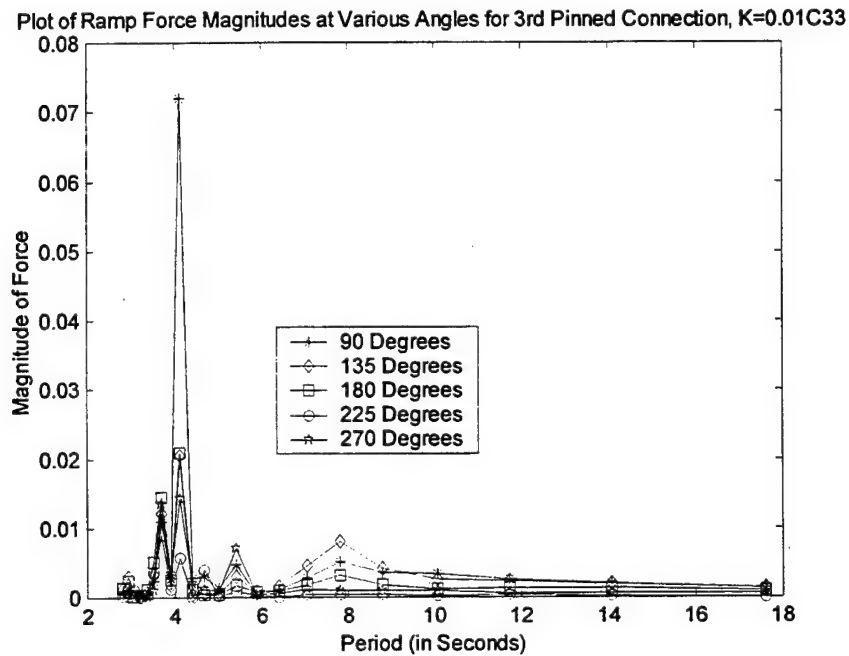


Figure 113. Plot of Ramp Exciting Force on the Third Pinned Connection at Various Wave Angles with a Spring Constant of 0.01.

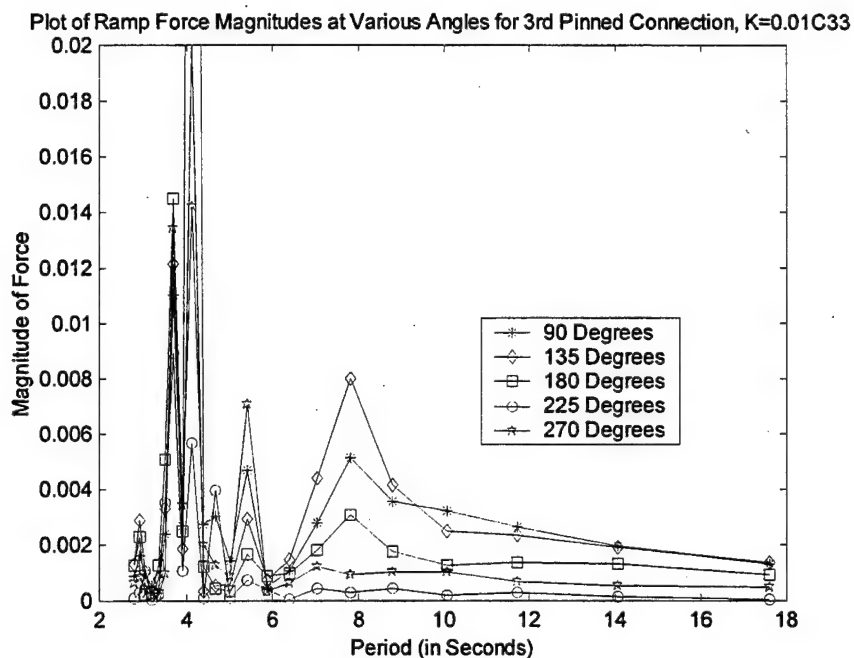


Figure 113a. Plot of Ramp Exciting Force on the Third Pinned Connection at Various Wave Angles with a Spring Constant of 0.01.

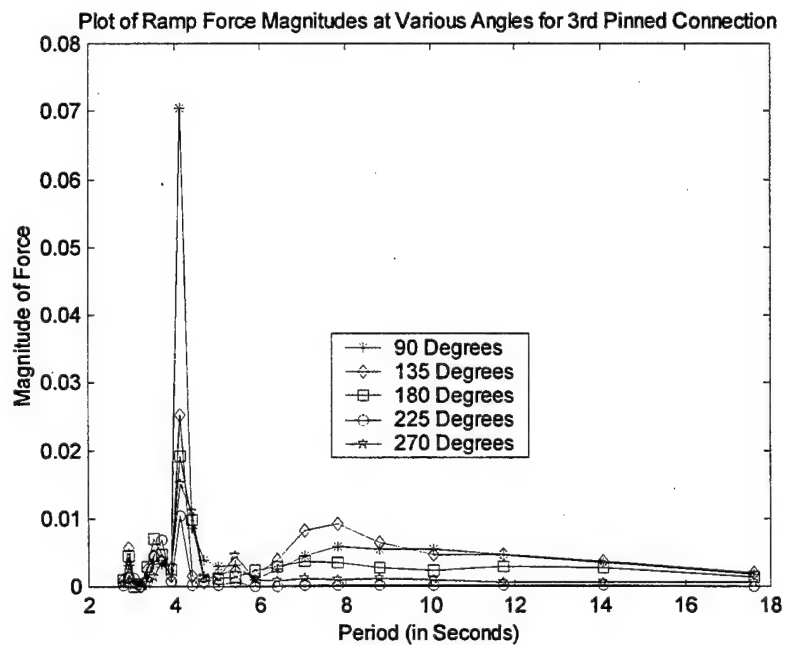


Figure 114. Plot of Ramp Exciting Force on the 3rd Pinned Connection at Various Wave Angles with a Spring Constant of 0.1.

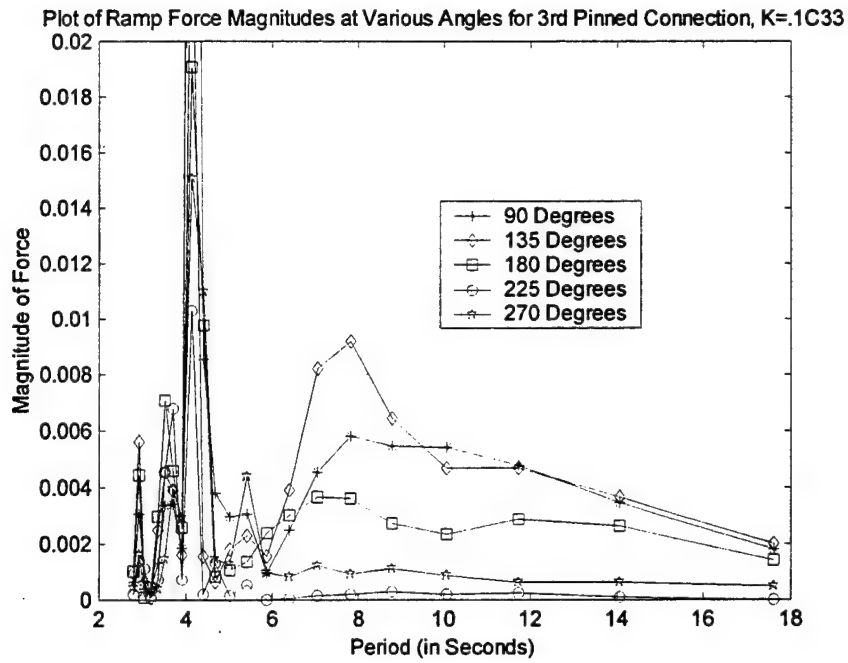


Figure 114a. Plot of Ramp Exciting Force on the 3rd Pinned Connection at Various Wave Angles with a Spring Constant of 0.1.

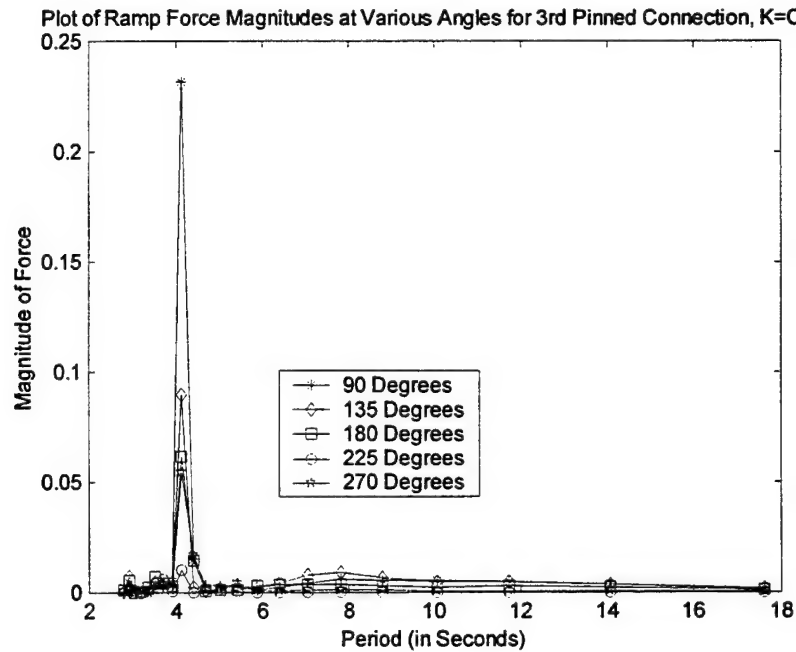


Figure 115. Plot of Ramp Exciting Force on the Third Pinned Connections at Various Wave Angles with a Spring Constant of 1.

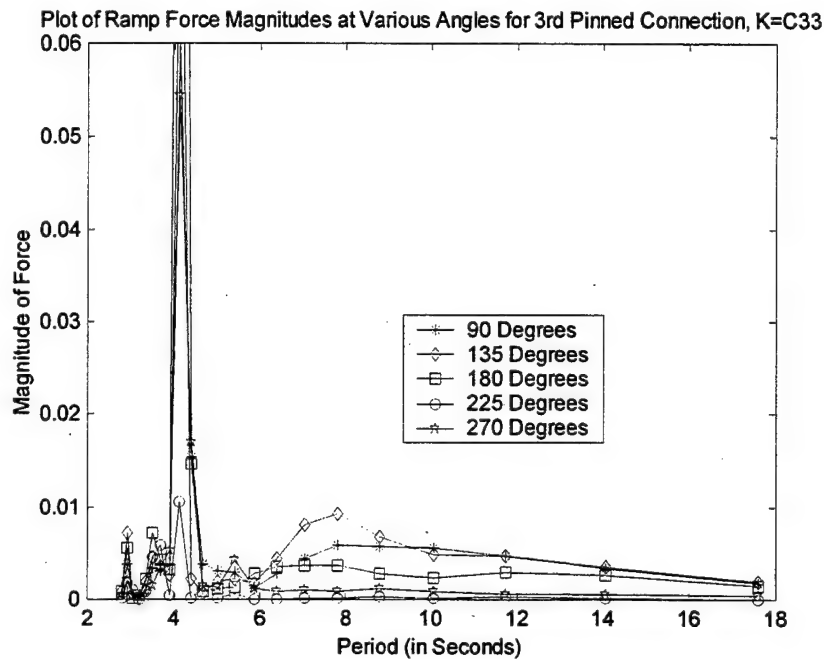


Figure 115a. Plot of Ramp Exciting Force on the Third Pinned Connections at Various Wave Angles with a Spring Constant of 1.

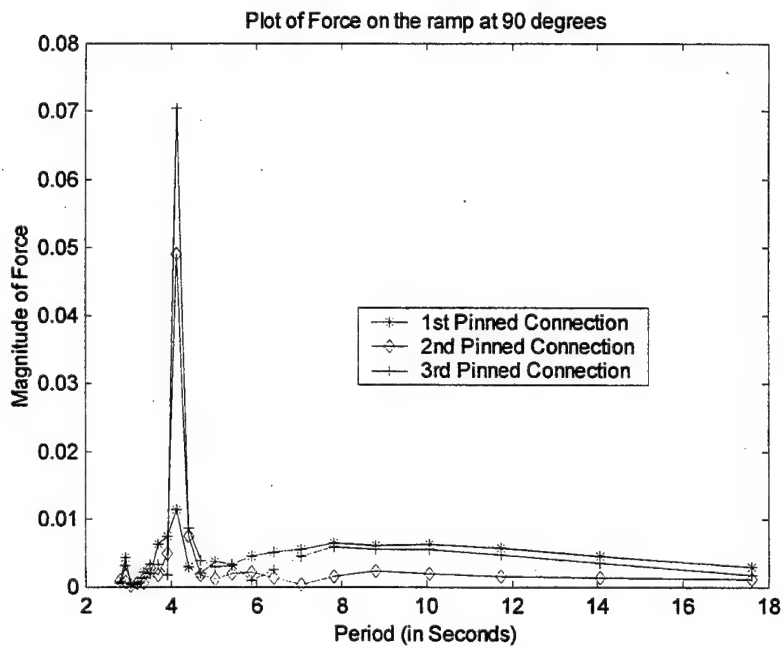


Figure 116. Plot of Ramp Exciting Force on all Three Pinned Connections at a Wave Angle of 90 Degrees with a Spring Constant of 0.1.

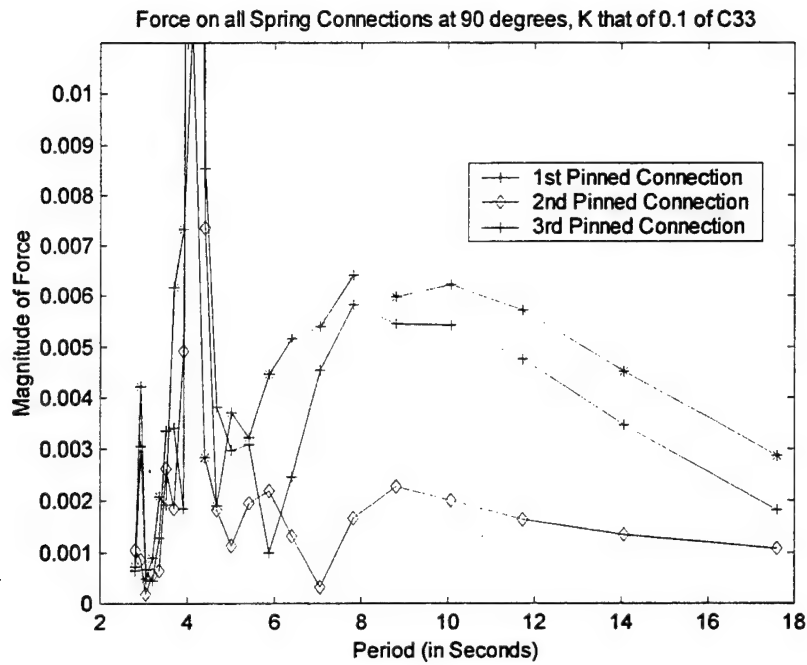


Figure 116a. Plot of Ramp Exciting Force on all Three Pinned Connections at a Wave Angle of 90 Degrees with a Spring Constant of 0.1.

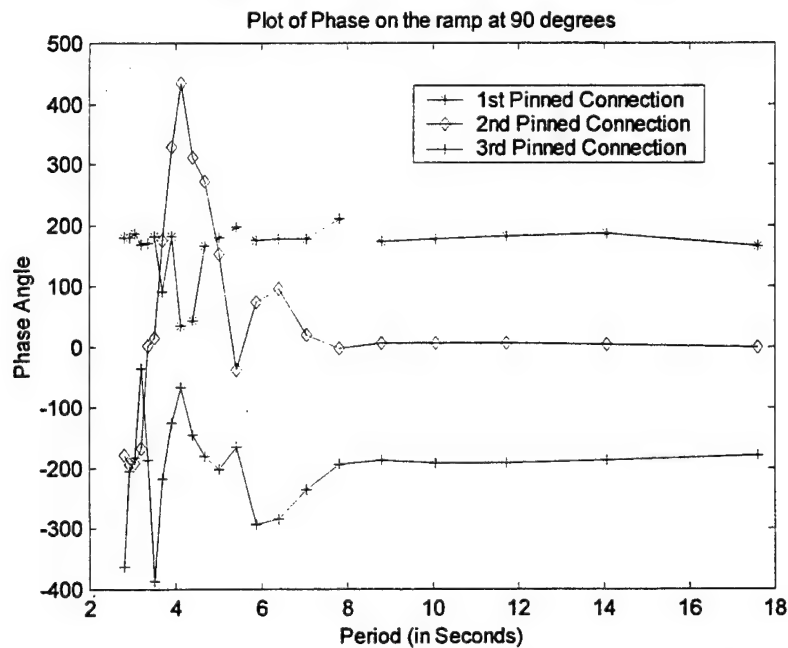


Figure 117. Plot of Ramp Exciting Force Phase Angle on all Three Pinned Connections at a Wave Angle of 90 Degrees with a Spring Constant of 0.1.

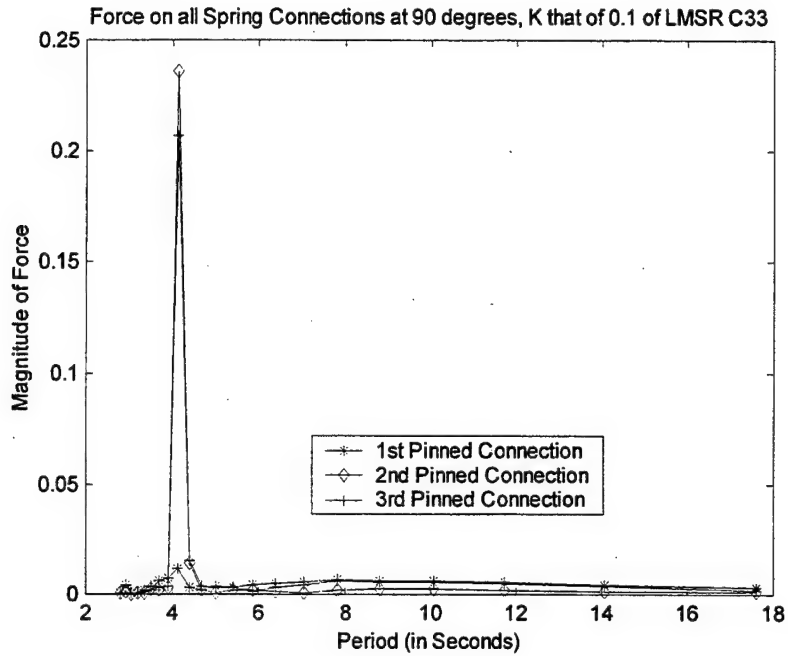


Figure 118. Plot of Ramp Exciting Force on all Pinned Connections at a Wave Angle of 90 Degrees with all Spring Constants 0.1 of the LMSR Stiffness.

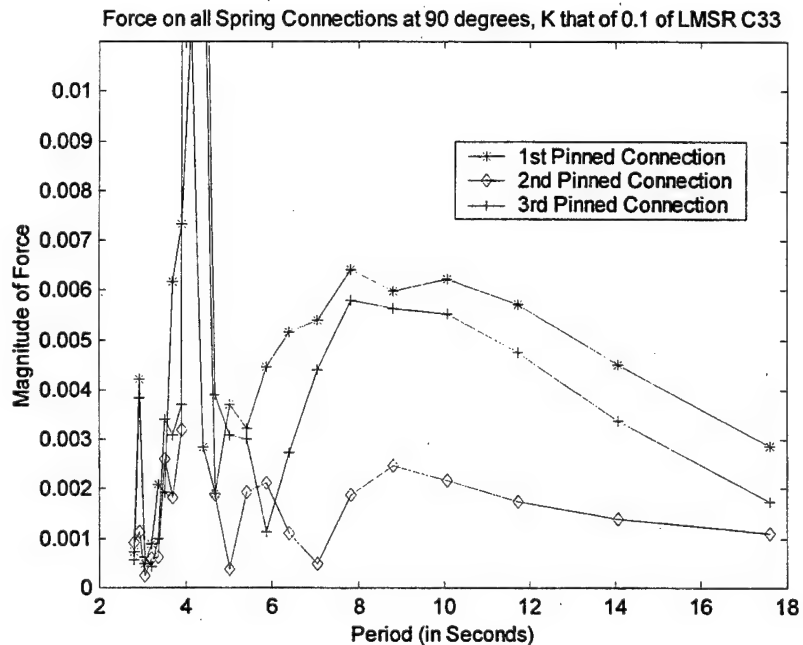


Figure 118a. Plot of Ramp Exciting Force on all Pinned Connections at a Wave Angle of 90 Degrees with all Spring Constants 0.1 of the LMSR Stiffness.

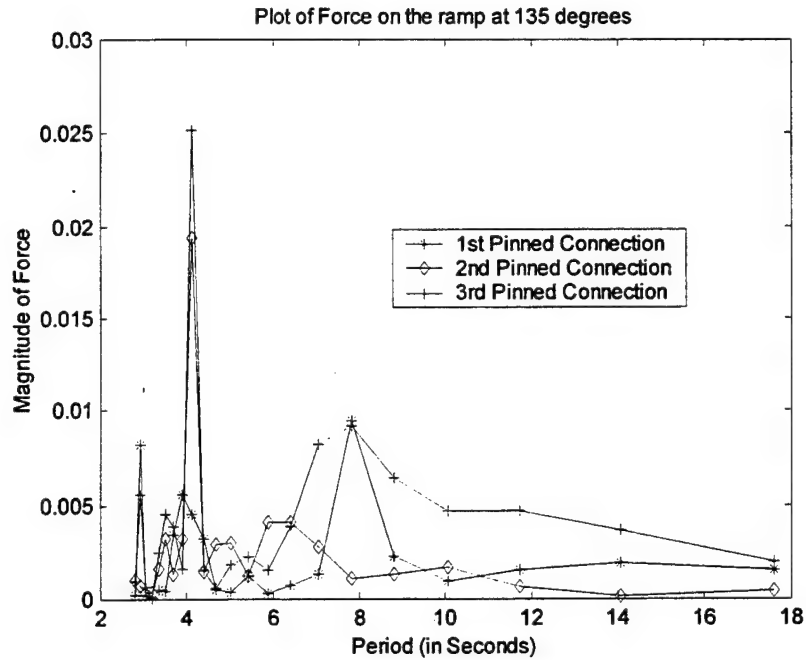


Figure 119. Plot of Ramp Exciting Force on all Three Pinned Connections at a Wave Angle of 135 Degrees with a Spring Constant of 0.1.

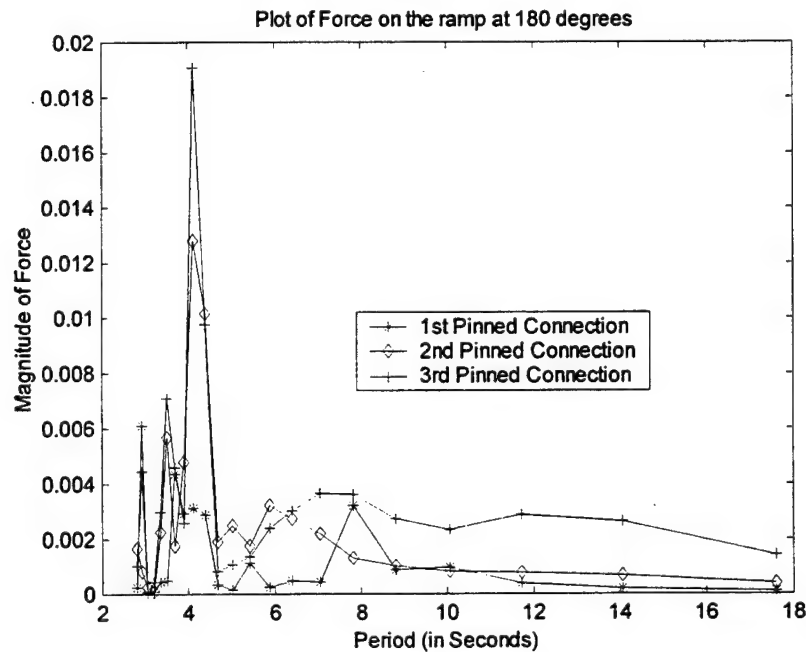


Figure 120. Plot of Ramp Exciting Force on all Three Pinned Connections at a Wave Angle of 180 Degrees with a Spring Constant of 0.1.

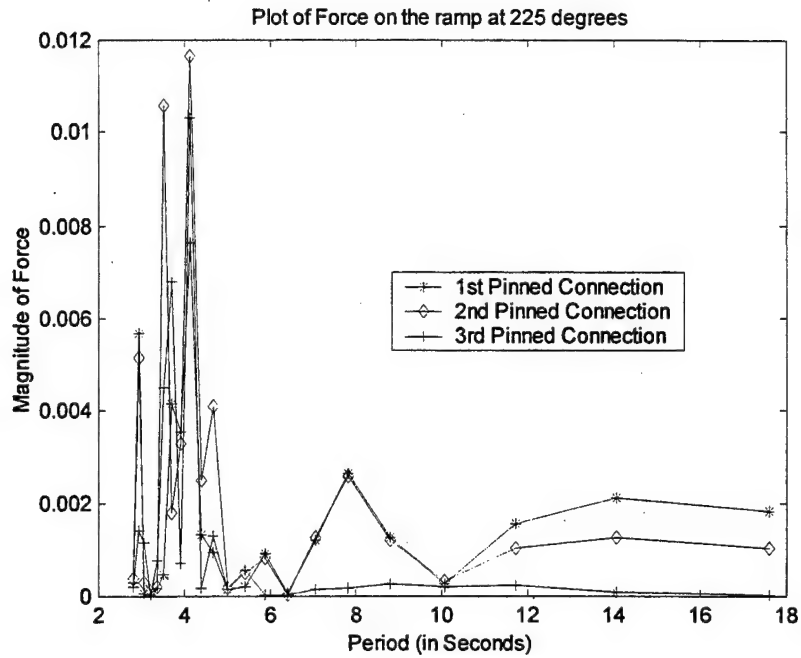


Figure 121. Plot of Ramp Exciting Force on all Three Pinned Connections at a Wave Angle of 225 Degrees with a Spring Constant of 0.1.

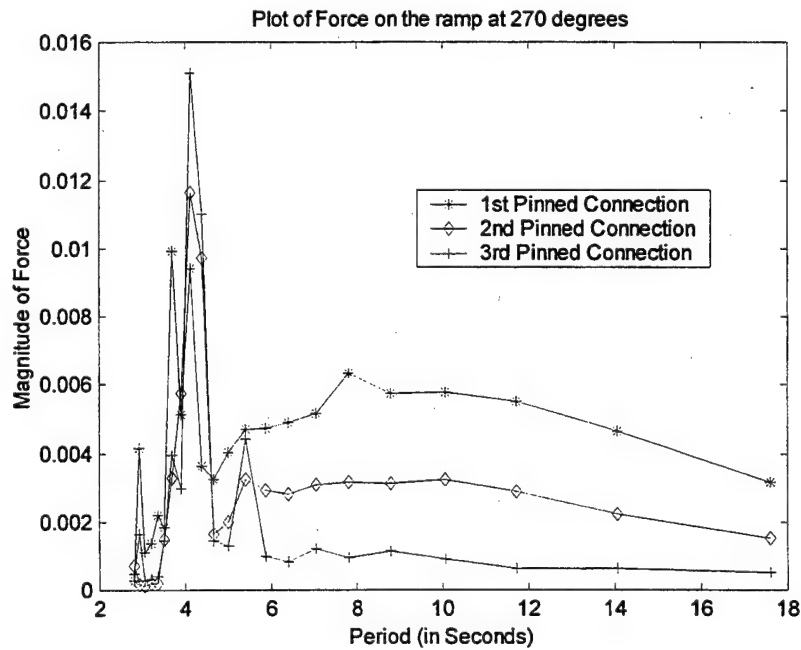


Figure 122. Plot of Ramp Exciting Force on all Three Pinned Connections at a Wave Angle of 270 Degrees with a Spring Constant of 0.1.

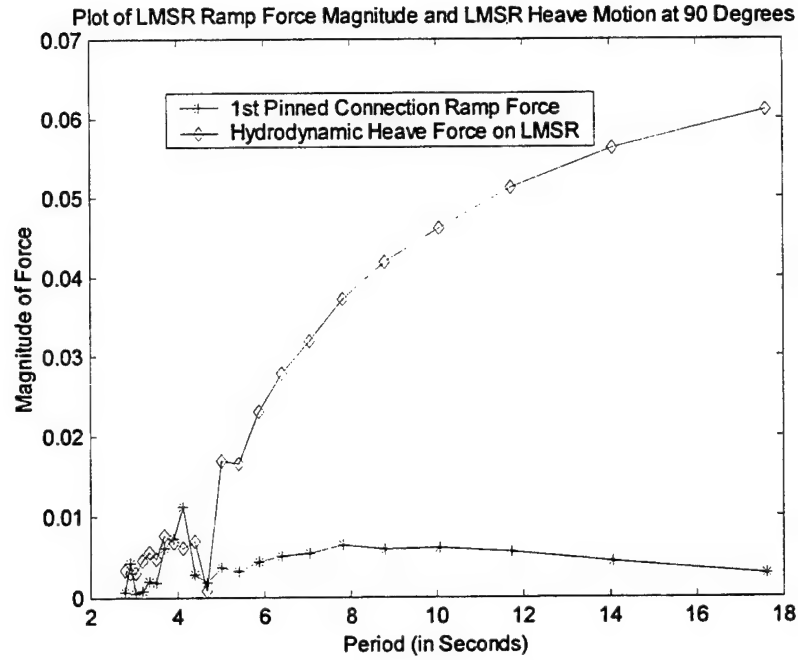


Figure 123. Plot of Ramp Exciting Force on the First Pinned Connection and Ship Heave Motion at a Wave Angle of 90 Degrees with a Spring Constant of 0.1.

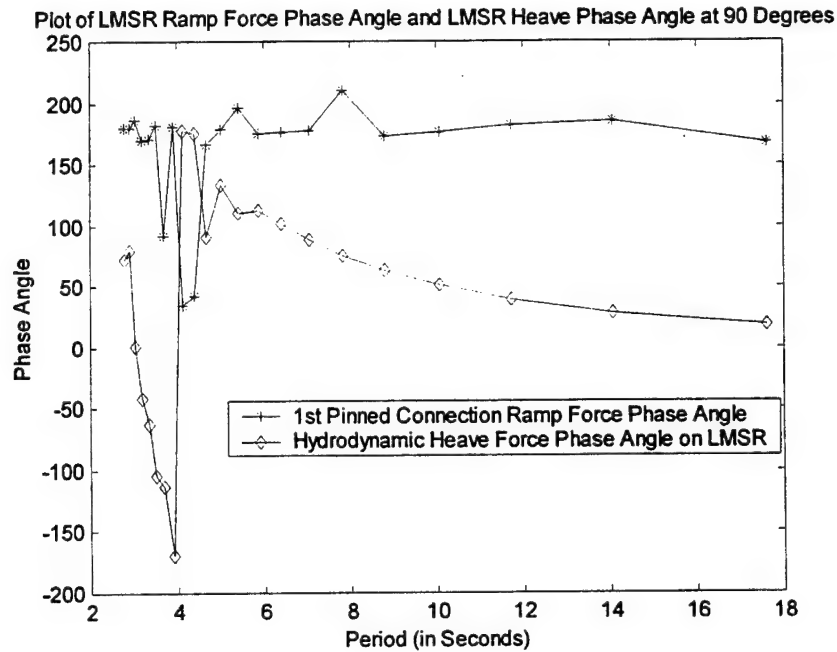


Figure 124. Plot of Ramp Exciting Force on the First Pinned Connection and Ship Heave Motion Phase Angles at a Wave Angle of 90 Degrees with a Spring Constant of 0.1.

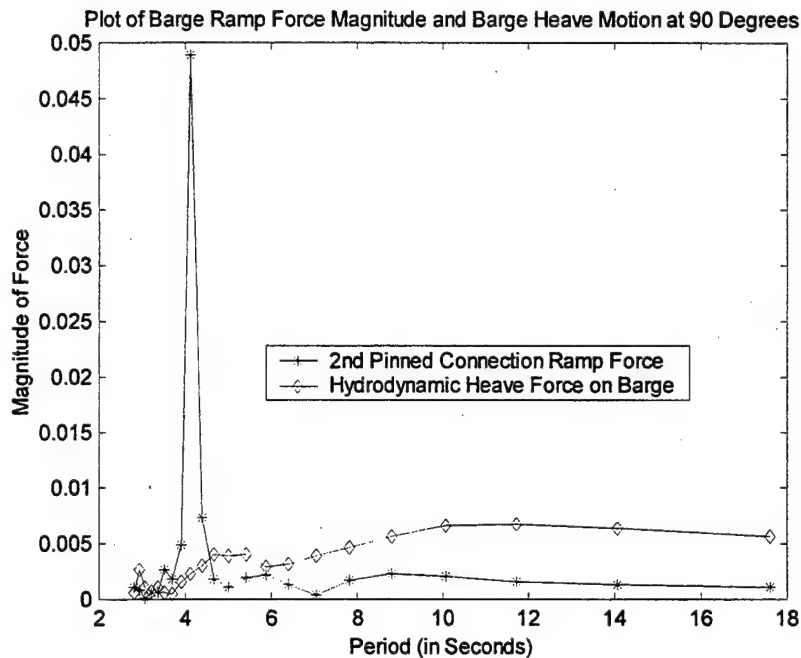


Figure 125. Plot of Ramp Exciting Force on the Second Pinned Connection and Ship Heave Motion at a Wave Angle of 90 Degrees with a Spring Constant of 0.1.

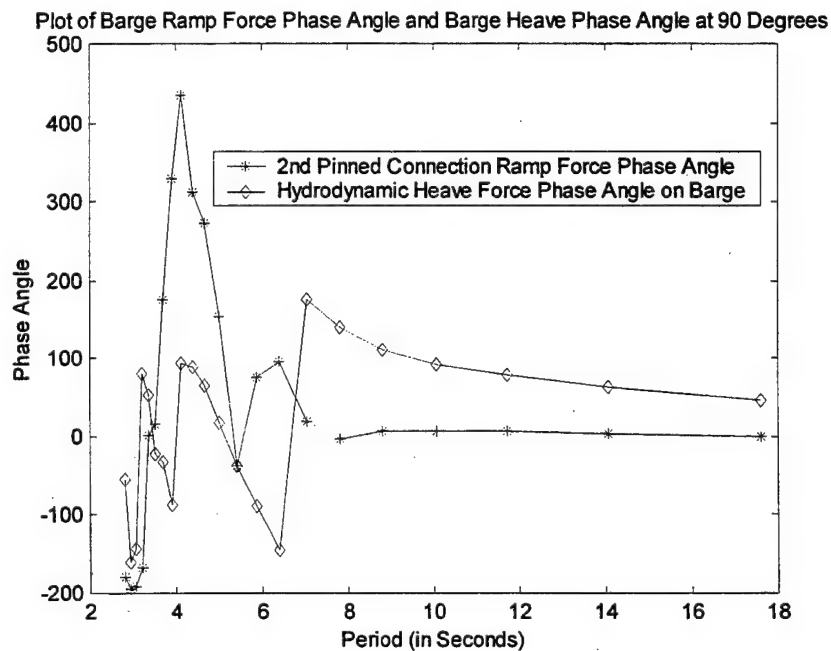


Figure 126. Plot of Ramp Exciting Force on the Second Pinned Connection and Ship Heave Motion Phase Angles at a Wave Angle of 90 Degrees with a Spring Constant of 0.1.

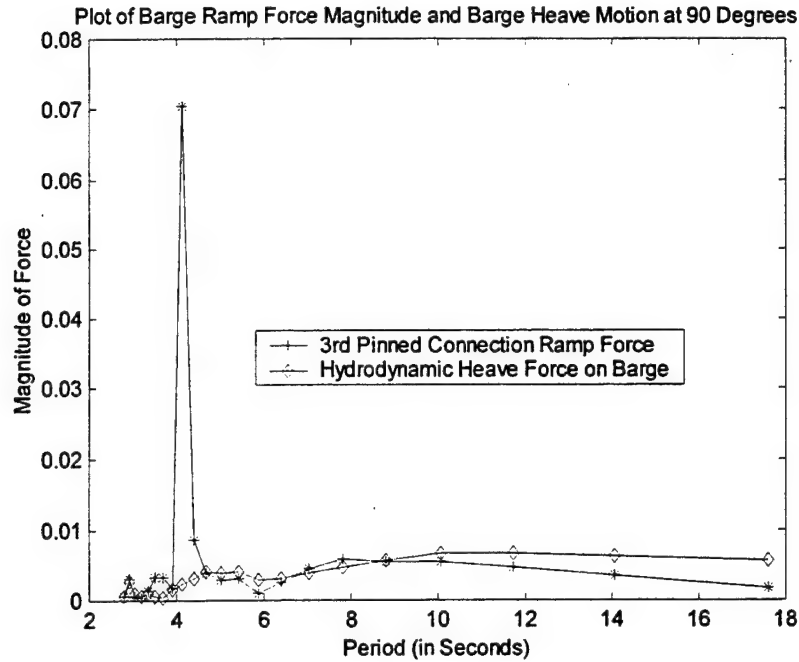


Figure 127. Plot of Ramp Exciting Force on the Third Pinned Connection and Ship Heave Motion at a Wave Angle of 90 Degrees with a Spring Constant of 0.1.

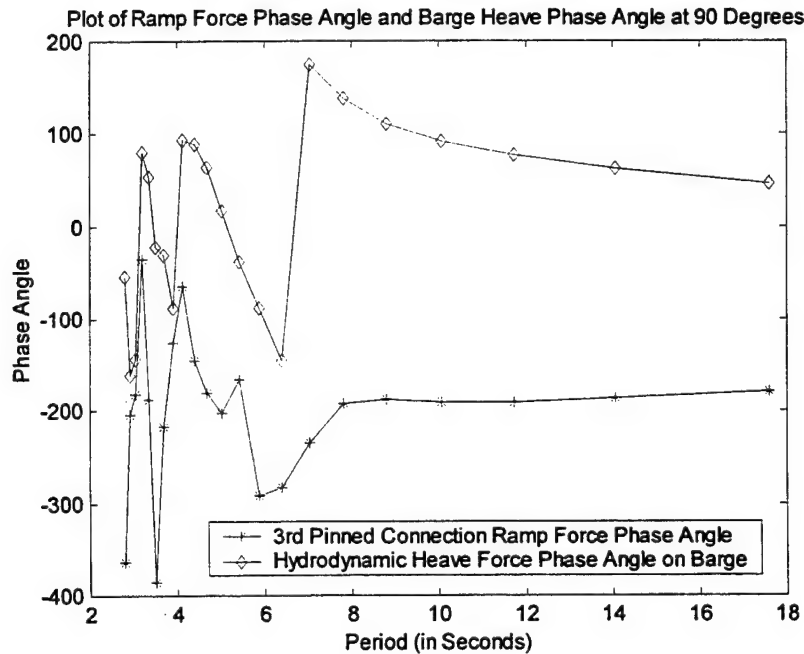


Figure 128. Plot of Ramp Exciting Force on the Third Pinned Connection and Ship Heave Motion Phase Angles at a Wave Angle of 90 Degrees with a Spring Constant of 0.1.

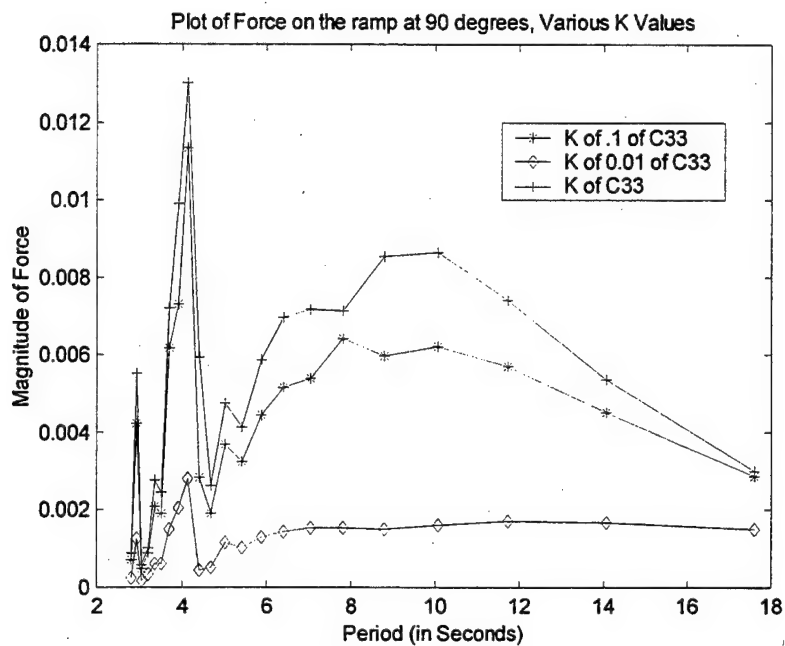


Figure 129. Plot of Ramp Exciting Force on the First Pinned Connection at a Wave Angle of 90 Degrees with Various Spring Constants.

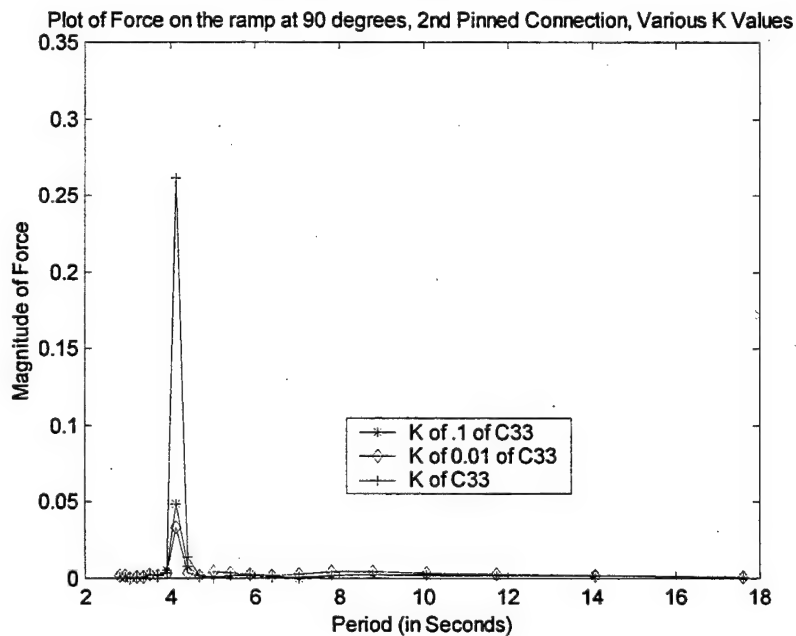


Figure 130. Plot of Ramp Exciting Force on the Second Pinned Connection at a Wave Angle of 90 Degrees with Various Spring Constants.

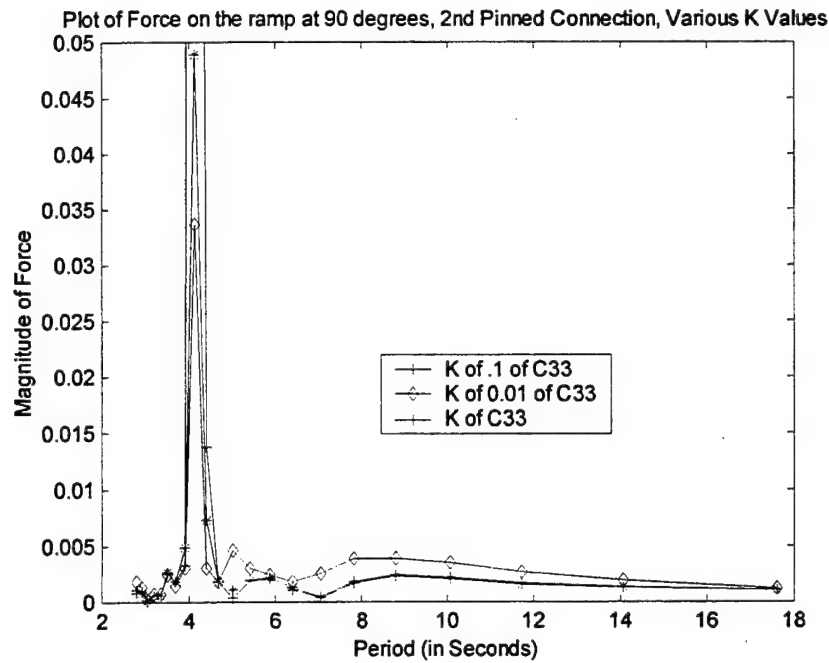


Figure 130a. Plot of Ramp Exciting Force on the Second Pinned Connection at a Wave Angle of 90 Degrees with Various Spring Constants.

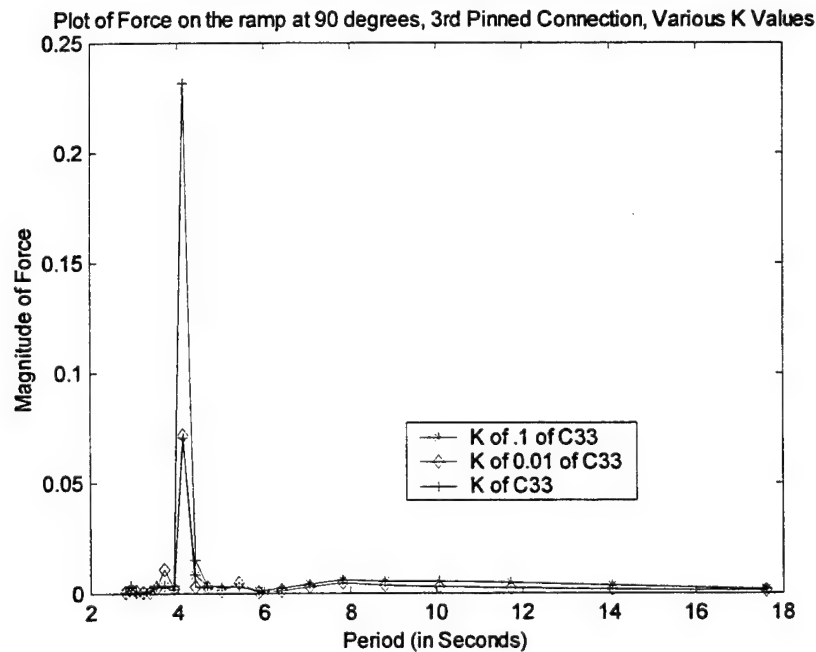


Figure 131. Plot of Ramp Exciting Force on the Third Pinned Connections at a Wave Angle of 90 Degrees with Various Spring Constants.

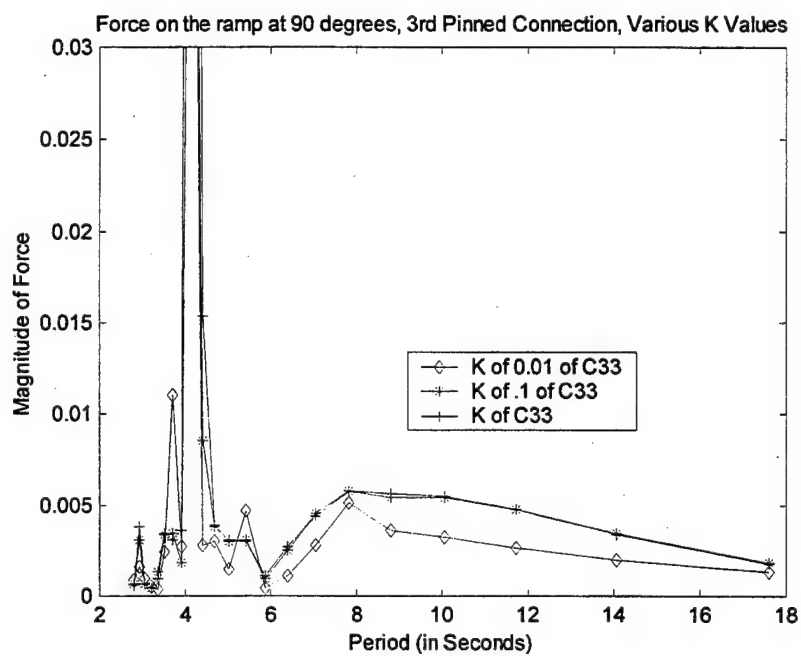


Figure 131a. Plot of Ramp Exciting Force on the Third Pinned Connections at a Wave Angle of 90 Degrees with Various Spring Constants.

THIS PAGE INTENTIONALLY LEFT BLANK

V. CONCLUSIONS

The main conclusions from this work are summarized below:

1. The comparison between a panel based three-dimensional hydrodynamic solver and a two-dimensional strip theory solver showed excellent agreement when modeling the LMSR. When the LMSR was modeled with the barges attached, although the strip theory solver was unable to account for the wave interaction effects, the added mass and damping coefficients as well as the wave exciting forces for the LMSR were still predicted fairly well.
2. The use of the strip theory solver is more economical in that it requires significantly less computational time. Therefore, it may be effectively used to model the LMSR. A combination of two-dimensional and three-dimensional hydrodynamic solvers is the most efficient method to obtain the added mass and damping values for the LMSR/barge system.
3. The strip theory solver was unable to accurately predict the hydrodynamic effects of the LMSR on the barge. This was attributed mainly to the irregular frequencies.
4. Exciting forces that are induced due to proximity produce a pitching moment on the barges attached to the LMSR in beam seas. This moment causes the barges to pitch when they would naturally not exhibit any pitch motion. This results in larger barge motion than would be expected in beam seas and thus produces a large force on the pinned connections in beam seas.

5. A sheltering and magnification effect produces a dramatically lowered total force on the barges when seas are from 270 degrees and a significantly larger force when the wave direction is from 90 degrees.

6. The king pin on the LMSR is the point where the most force is exhibited. This point is anywhere from 2 to 3 times larger than the connection on the barge. At higher frequencies, this force may be higher than the hydrodynamic forces which the ship experiences.

7. With larger spring constants, the force acting on the pinned connections is significantly greater.

VI. RECOMMENDATIONS

Based upon the data and conclusions, the following recommendations are made:

1. Reformulate the problem as a four degree of freedom system. This would require modeling the ramp as non-rigid body. Preliminary studies indicate that the first torsional mode of the ramp is the most significant, so this would need to be incorporated first in the analysis.
2. Utilize the transfer functions that were developed in this work to select the proper isolator properties. The minimization index would be the maximum stress in the ramp.
3. Analyze all six motions of the LMSR and barges to verify that other motions are negligible as assumed in this problem.

THIS PAGE INTENTIONALLY LEFT BLANK

APPENDIX A

FIGURE OF LMSR/BARGE CONNECTION:

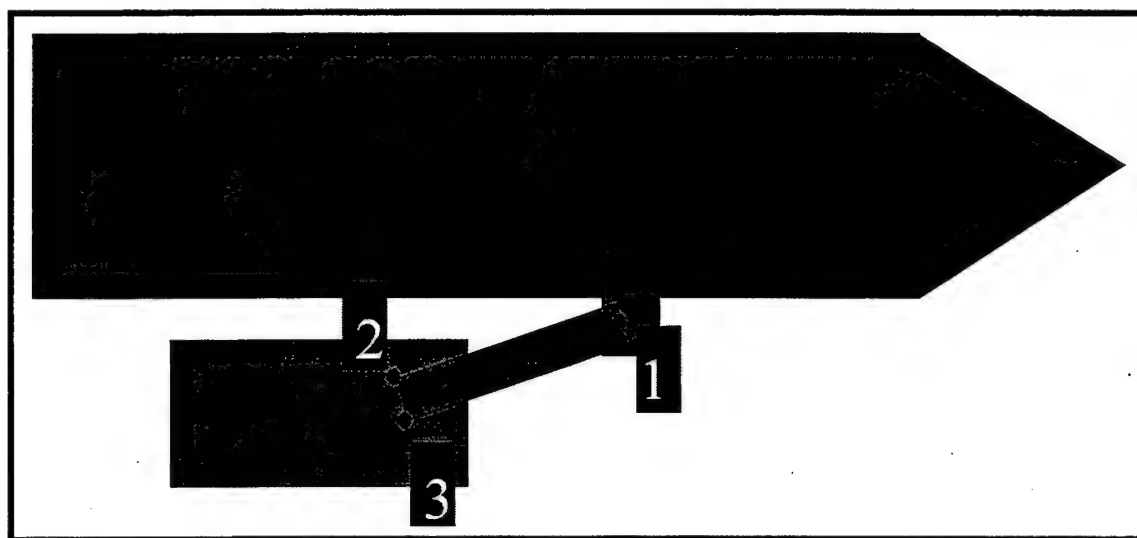


Figure A. Basic Drawing of LMSR and Roll-On, Roll-Off Discharge Facility Connected together by Ramp. Black Dots Indicate the Locations and Number of the Pinned Connections.

THIS PAGE INTENTIONALLY LEFT BLANK

1

LIST OF REFERENCES

1. K. Kokkinowrachos and H.G. Zibell, "Wave Interaction With Multiple Cross-Sections in Finite Water Depth", *Proceedings of the Third International Offshore Mechanics and Arctic Engineering Symposium*, Volume 1, 1984, pp. 144-155.
2. N. Kodan, "The Motions of Adjacent Floating Structures in Oblique Waves", *Proceedings of the Third International Offshore Mechanics and Arctic Engineering Symposium*, Volume 1, 1984, pp. 206-213.
3. S. Chen and O. Mahrenholtz, "Interaction of Water Waves and Floating Twin Cylinders in Beam Waves", *Applied Ocean Research*, Volume 14, 1992, pp. 371-379.
4. U. Bjorkenstam and X. Lei, "Wave Loading on Multiple Floating Bodies", *International Shipbuilder's Program*, Volume 38, Number 416, 1991, pp. 361-391.
5. P. Krishnankutty, "Analysis of Diffraction-Radiation Problem of a Twin-Hull Barge System", *International Shipbuilder's Program*, Volume 42, Number 432, 1995, pp. 357-379.
6. Yoshiyuki Inoue, Xuangang Zhang, and Shigeru Tabeta, "Numerical Study of the Hydrodynamic Forces on Huge Floating Structures in Waves and Ocean Currents", *Proceedings of the Seventh (1997) International Offshore and Polar Engineering Conference*, Volume 1, 1997, pp. 221-228.
7. Erick T. Huang, "Motional Dynamics of Coupled Pontoons in Seaways", *Proceedings of the Seventh (1997) International Offshore and Polar Engineering Conference*, Volume 3, 1997, pp. 596-601.
8. A. Nobakhti, G.J. Lyons, and D. T. Brown, "The Effects of Binding Hinge Connections in Multipli-Connected Pontoon Arrays", *Proceedings of the Seventh (1997) International Offshore and Polar Engineering Conference*, Volume 3, 1997, pp. 564-572.
9. G. Van Oortmerssen, "Some Hydrodynamic Aspects of Multi-Body Systems", *Hydrodynamics in Ocean Engineering*, The Norwegian Institute of Technology, Volume 2, 1981, pp. 725-744.
10. Arne Edvin Loken, "Hydrodynamic Interaction Between Several Floating Bodies of Arbitrary Form in Waves", *Hydrodynamics in Ocean Engineering*, The Norwegian Institute of Technology, Volume 2, 1981, pp. 745-780.
11. P. Sayer and R. Spencer, "The Wave-Induced Motions of Adjacent Floating Vessels", *Hydrodynamics in Ocean Engineering*, The Norwegian Institute of Technology, Volume 2, 1981, pp. 781-798.

12. Makoto Ohkusu, "Ship Motions in Vicinity of a Structure", *First International Conference on Behaviour of Off-Shore Structures*, The Norwegian Institute of Technology, Volume 1, 1976, pp. 284-306.
13. G. Van Oortmerssen, "Hydrodynamic Interaction Between Two Structures, Floating in Waves", *Second International Conference on Behaviour of Off-Shore Structures*, The Norwegian Institute of Technology, 1979, pp. 339-356.
14. Edward V. Lewis, Editor, *Principles of Naval Architecture, Volume III, Motions in Waves and Controllability*, The Society of Naval Architects and Marine Engineers, 1989, pp. 1-125.
15. Terrence Applebee, Dan Hayden, Richard Bishop, and Timothy Smith, "T-AKR 296/RRDF Ramp Model Test", *Carderock Division, Naval Surface Warfare Center*, CRDKNSWC/HD-1421-05 March 1997, Hydromechanics Directorate, Research and Development Report.

INITIAL DISTRIBUTION LIST

1. Defense Technical Information Center2
8725 John J. Kingman Rd., STE 0944
Ft. Belvoir, Virginia 22060-6218

2. Dudley Knox Library2
Naval Postgraduate School
411 Dyer Rd.
Monterey, CA 93943-5101

3. Professor Fotis A. Papoulias, Code ME/PA.....3
Department of Mechanical Engineering
Naval Postgraduate School
Monterey, CA 93943

4. Engineering & Technology Curricular Office (Code 34)1
Naval Postgraduate School
Monterey, CA 93943

5. Department of Mechanical Engineering1
Naval Postgraduate School
Monterey, CA 93943

6. LT Scott R. Barry3
100 C. Street
Port Hadlock, WA 98339

7. Mr. Frank Leban, Code 2931
c/o Commander Carderock Division NSWC
9500 MacArthur Blvd
West Bethesda, MD 20817-5700

8. Professor Josh Gordis, Code ME/GO1
Department of Mechanical Engineering
Naval Postgraduate School
Monterey, CA 93943

9. Professor William Spencer1
Department of Civil Engineering
University of Notre Dame
South Bend, IN 46556